DEVELOPMENT OF NONDESTRUCTIVE TESTING TECHNIQUES FOR HONEYCOMB HEAT SHIELDS

ANNUAL REPORT

1 July 1965 - 31 May 1966

By J. F. Moore, George Martin

July 1966

Prepared under Contract No. NAS 8-11733 by

NORTH AMERICAN AVIATION, INC/ LOS ANGELES DIVISION
Los Angeles, California

for

NATIONAL AERONAUTICS AND SPACE ADMINISTRATION

FOREWORD

This report was prepared by North American Aviation, Inc, Los Angeles Division under Contract NAS8-11733 for the George C. Marshall Space Flight Center, NASA. The work was administered under the direction of the Contracting Officer, Mr. W. J. McKinney, and the Contracting Officer Representative, Mr. Wayman Clotfelter, Propulsion and Vehicle Engineering Laboratory, Materials Division, George C. Marshall Space Flight Center.

The development program is supervised by Mr. J. Moore, Program Engineer, under the direction of Mr. N. Klimmek, Manager, Materials and Producibility, and Dr. George Martin, Program Manager. The research described in this report and its preparation was carried out by Dr. George Martin, Mr. J. Moore, Mr. H. Varney, Dr. S. Tsang, Mr. J. W. Rocke, and with Dr. D. O. Thompson, NAA Science Center, and Mr. D. C. Erdman as technical consultants and advisors.

The studies described in this Annual Program Report were made during the period from 1 July 1965 through 31 May 1966.

The report was issued by North American Aviation, Inc/Los Angeles Division under report number NA-66-638. This report was approved and released for distribution in August 1966.

ABSTRACT

This report describes the work accomplished during a developmental research program to provide nondestructive testing techniques for the Saturn honeycomb heat shields. The objectives of the program were twofold. The further adaption of the NAA Sonic Resonator to the design stage for a production inspection system for the Saturn composites. This development has resulted in two improved systems which are in the process of being characterized. Performance was increased to 10-100 volt signal sensitivity for disbonds. The second objective was the development of a technique for determining the adhesive bond strength of the honeycomb composites. A fundamental vibration analysis is reported describing the relationship between the composite bond strength and the damping characteristics. Experimental evidence of this mechanism is reported and analyzed in terms of the Saturn composites. An experimental breadboard system was developed, called "DOT", which showed a capability of discrimination between various strength bonds. Recommendations are presented for the further development of this system for both near and far side bond strength measurements in honeycomb composites.

In addition to these main objectives, methods for preparation of honeycomb specimens for use as defect standards were developed and a literature survey was continued to include the amplified scope of the program.

TABLE OF CONTENTS

LIST OF ILLUSTRATIONS

LIST OF TABLES

SUMMARY

The literature and industrial survey was continued through the reporting period. Survey results are reported in terms of ultrasonic inspection standards and specifications, and Saturn honeycomb defect characterization. In general, it was concluded that although adequate direction and reference standards are available in many fields of nondestructive testing, standards for honeycomb composites must be prepared from actual vehicle components with prescribed defects designed from performance design allowables. A survey was conducted to determine the factors affecting the strength of an adhesive bond and the mechanisms that weaken or fail in an adhesively bonded joint. The survey included theory of adhesion, and adhesion testing. It is concluded that cohesive bond failures were representative of the majority of composite failures. Further, that a means of realistically simulating a degraded bond condition must be developed for specific adhesives.

A number of adhesive bonded lap shear and honeycomb composite specimens were fabricated representative of the Saturn materials and a wide range of defects. The specimens included 0.8 inch mylar honeycomb, 1/16 to 4-3/4 inch HRP honeycomb, and tedlar 1.6 inch insulation honeycomb type specimens. The simulated defects ranged from various degrees of degraded adhesive bond strength to disbonds ranging in size from a unit cell to three inch square areas located at the various composite adhesive interfaces.

A limited number of ultrasonic property tests were conducted to establish a significant adhesive bond strength relationship. The tests in general were nonconclusive. Detection sensitivity levels available were too low to obtain even a qualitative bond strength correlation.

Experimental vibration tests on degraded honeycomb adhesive bonds showed a qualitative relationship between vibrational response and adhesive bond strength. The relationship was based on the mechanical vibration analysis of the bonded adhesive lap shear specimens and the identification and measurement of a relaxation mechanism. This mechanism in turn established a difference in expected response between high and low strength adhesive bonds. The low strength bond has a higher amplitude and lower frequency vibrational response than a high strength bond. This hypothesis was proven on different adhesive strength Saturn honeycomb composites. The vibrational response of the various adhesive bonds showed a direct correlation with fracture stress. Recommendations are presented for a development program to establish this technique as a nondestructive inspection process.

The impedance system evaluation included significant sensitivity improvement by impedance matching the crystal to the composites. Optimum elevation tests proved an increase sensitivity by a factor of 100. Based on these tests the crystal transducer was mounted in a Sperry prototype wheel used to successfully inspect the 4-3/4 inch Saturn common bulkhead composite. Characterization of crystal transducer was defined in terms of dynamic coupling mechanical Q. The electrical system was evaluated and significant improvement was achieved by two techniques. The complex bridge circuit was replaced with a series tuned circuit with a single adjustment control. The new technique utilized a self driven crystal which proved successful in identifying the adhesive layer in which disbonds were found. The technique also has the potential of determining the damping characteristics of the adhesive bond, a factor which was shown to be related to bond strength.

INTRODUCTION

Advanced aerospace vehicle systems have dictated the development of materials and structures capable of meeting increased structural and thermal requirements. Recent advancements in the design of honeycomb composite materials have demonstrated their superior structural and thermal properties over conventional materials. However, coupled with this advancement is the need for improved nondestructive testing techniques to ensure the safety and reliability of the aerospace mission. An assembled vehicle of the Saturn type contains numerous bulkheads and superstructures which limit test access to a single side. Inspection of such structures, therefore, prompts the need for techniques suitable from one side of the structure.

The prime purposes of this program are (1) the development of an ultrasonic inspection technique for composite materials in which all instrumentation, probes, detectors, etc, are located on one side of the material only, and (2) the development of a portable scanning device with remote instrumentation for the inspection and recording of composite material quality.

Two ultrasonic inspection systems developed under the first year's contract have proved capable of detecting disbonds in the Saturn adhesive bonded composites. The scope of this program has been extended to include the development of nondestructive methods for determining the quality of the adhesive bonds. The following program was planned for accomplishing this objective:

PHASE I

Survey of Bond Parameters and Tests
Bond Quality Study
Lap-shear and Honeycomb Specimens
Nondestructive Tests
Correlation Analysis

PHASE II

Equipment Standardization
Material Standardization
Calibration Procedures

PHASE III

Defect Characterization
Equipment Characterization

Section I

LITERATURE AND INDUSTRIAL SURVEY

A literature and industrial survey of pertinent nondestructive testing techniques and equipment was conducted throughout the report period. A partially annotated bibliography (1) covering major subject areas relating to nondestructive testing, and listing approximately 700 references, was prepared and published. In addition to ensuring a continuing awareness of current state of the art developments, subsequent survey effort was directed toward information regarding ultrasonic equipment characterization, standards, and characterization of honeycomb defect mechanisms. Results of these efforts were presented in detail in the Quarterly Program Reports and are included in Appendix A of this report.

ULTRASONIC SYSTEM CHARACTERIZATION

Literature relating to equipment characterization was surveyed, to determine if a common denominator existed among the various types of ultrasonic equipment in present use. Several approaches to equipment characterization are evident, but each relates to specific equipment and/or application(s). Predominant is information relating to transducer characteristics, based on evaluation of the transducer(s) alone rather than as an integral part of a system. Transducer sensitivity in a system, versus flaw detection capability appears as a significant factor for consideration. It has been demonstrated that two apparently identical transducers will not necessarily produce the same response when scan speed and distance (measured from search unit to specimen surface) are varied. Transducer size and frequency have been shown to affect the Fresnel zone, affecting the extent of the close field. Preparation of amplitude versus distance plots, based on the use of standard specimens and test conditions, is suggested by one author as a means of compensating for variables of this type. However, of significance is the fact that regardless of the basic characteristics of the transducer, the inspection system must eventually be characterized as an integrated system.

It has been demonstrated that in some cases the signal bandwidth influences the amplitude of the indications obtained from test blocks used for instrument calibration. The effect is not as pronounced in cases where the defect diameter is in the same order of magnitude as the ultrasonic wavelength. Therefore, to avoid variation in equipment calibration, it is important that bandwidth effects be considered and noted in equipment calibration procedures. Flaws of the same order of magnitude or smaller than the beam width are not readily detected by a single frequency detection unit.

The effectiveness of pulse echo testing can be improved by the use of multi-frequency signals. These factors, representative of those brought out by the literature reviewed, point up the need for definitive system frequency characteristics as opposed to a broad characterization of the equipment frequency range.

Optimum efficiency of the ultrasonic inspection system is dependent upon not only the transducer, but the means of coupling used to transmit the energy into the test article. Coupling methods range from direct contact to the use of elaborate fluid coupling devices or other materials such as Knox gelatine. While the purpose served by the couplant is of prime importance, the restrictions are many and varied. The relationship between couplant or coupling means, the material, conditions of inspection, and system efficiency thus become a significant factor in system characterization.

Parameters are easily established for electronic power supplies, and the efficiency is readily measureable. However, these factors are basic and do not provide a true representation of equipment performance. Studies indicate the need for a practical means of measuring transducer sonic power input, to establish transducer performance and attain maximum power levels under various mechanical loading conditions. There is also a need for reliable instrumentation capable of measuring power levels during system operation. The primary characterization parameters, in one author's opinion, as regards pulsed transmitter and receiving equipment used for measuring ultrasonic attenuation, are given as (1) receiver signal-to-noise ratio, (2) maximum transducer excitation, and (3) receiver recovery time. Here again, are factors which relate to operation of the system as a whole rather than as individual parts.

The foregoing discussion touches only briefly on the wide range of factors which are significant in the characterization of an ultrasonic inspection system. There is little evidence of so called standardized characterization parameters as in most cases the research relates to a specific application, problem, or system. As a result of this survey, it is concluded that accurate and representative characterization of an ultrasonic inspection system as a whole must be accomplished on a specific equipment-application basis. In this manner, all significant factors can be evaluated under actual operating conditions. Variables can be identified and optimum operating parameters established. While characterization of a single system for a given application would at first appear to be a relatively simple task, the possible combinations of operating conditions are of considerable magnitude. This task could best be accomplished by detailed documentation of test conditions and results over a period of time.

ULTRASONIC INSPECTION STANDARDS

Literature surveyed to date indicates that ultrasonic standards encompass three primary areas, as follows:

1. Reference standards for equipment calibration

2. Specifications defining equipment calibration and application

3. Inspection standards defining acceptance-rejection parameters.

Reference standard blocks are universally used for equipment calibration and as an inspection reference in ultrasonic inspection. While fabrication of the blocks (from solid metal billets) is an intricate task, the major problem is in attaining proper ultrasonic response from the flat bottom hole used as a reference. Considerable research has been done regarding the fabrication and use of reference blocks, but the majority of this effort has been directed toward a specific application or purpose. Various approaches have been used in attempts to improve fabrication methods, and technique in the application and response from, reference blocks. While the results offer merit for consideration, their use is usually limited to specific equipment and/or application. The concensus of opinion tends to favor the need for two sets of reference blocks; one set for use in calibrating the equipment and the other to serve as a material inspection standard.

Tests have shown that the material used for fabrication of the reference blocks need not necessarily be the same as the material to be tested as long as the ultrasonic response is the same. However, the use of aluminum or steel predominates in the fabrication of reference blocks. Reference standards have been fabricated from plastic and composite materials, again with a specific application in view. A major problem in the fabrication of reference blocks from composite materials and nonmetallics is that of achieving representative defect simulation. This is usually accomplished by introduction of a secondary material, to represent a disbond or void. The problem is in achieving a condition which provides a representative simulation, and subsequent response, of the actual defect.

The importance of clear, definitive specifications is frequently mentioned in relation to ultrasonic standards. All too often, the ultrasonic inspection specification deals in general rather than specific terms. As a consequence, the burden of interpretation and application is left to the technician responsible for conducting the inspection. This not only opens the door to misinterpretation, but leads to either under- or over-inspection, often with high rejection rates as the result. This condition has emphasized the need for well trained, experienced equipment operators where the final inspection results are dependent upon operator skill and judgement.

Of equal importance in the specification is the need for conscise acceptance-rejection criteria. This poses questions such as: When is an indicated defect not a defect in terms of article reliability and performance? What type of indicated defects are negligible as opposed to critical? Where can minor defects be tolerated or repaired as opposed to complete rejection? The answers to these typical questions must be clearly defined if high operator rejection rates or substandard articles are to be avoided. Responsibility does not end with the development of equipment capable of locating a defect; the significance and identification of the defect subsequently becomes a prime factor in the complete inspection cycle.

It becomes evident that specific inspection standards and criteria are a vital element in a nondestructive testing program, regardless of the inspection method used. As regards ultrasonic inspection, it was noted that less than 20 recognized ultrasonic reference specifications were listed in a comprehensive tabulation of specifications covering all types of nondestructive testing techniques. Nearly all the ultrasonic references related to metals or metal products.

HRP FAILURE MECHANISMS AND CHARACTERIZATION

To establish a basis for honeycomb defect identification and interpretation, an extensive search was made for literature relating to failure mechanisms and defect characterization. The results evidence a paucity of information relating to defect characterization. Hexell Products Corporation of Berkeley, California have conducted extensive studies regarding the design, loading and strength properties of honeycomb materials. Forest Products Laboratories have published several reports concerning various aspects of stress-strain relationship and analysis for sandwich and composite materials. In this respect, literature concerning theoretical studies of various strength properties of sandwich and honeycomb materials are more common than information regarding actual failure and defect charcterization.

The Space and Information Division of North American Aviation (NAA/S&ID) was contacted as a possible source of information concerning failure mechanisms in honeycomb structures. In relation to its Apollo and Saturn program effort, NAA/S&ID has gained extensive experience with many types of honeycomb materials including the HRP core combinations. Specifications defining a variety of defects and the related repair have been prepared, or are in various stages of preparation. Basic criteria for determining panel repairability include defect type, size and location. Detailed repair methods are given; verification of repair strength is accomplished by destructively testing a specimen prepared from the repair materials.

The NAA/S&ID Seal Beach Division was also contacted regarding potential damage during honeycomb composite installation and subsequent handling operations. Strict precautionary measures are employed to avoid damage during these operations. However, the possibility of accidental damage is always present, especially during the lifting of vehicular sections and during transport of the vehicle itself. Damage of this nature is considered to be of two basic types, namely (1) crushed core due to impact loads, and (2) core fracture due to load shifting.

The Los Angeles Division (NAA) has prepared a comprehensive Structural Repair Manual for metallic honeycomb core structures. This manual was reviewed to obtain guidelines as to factors involved in establishing criteria for honeycomb repair parameters. Information of this nature is necessary to the development of ultrasonic inspection techniques applicable to structural repairs.

Biaxial load tests of common bulkhead type specimens are currently being conducted by the NAA/LAD Structures Laboratory. The objective is to determine acceptance criteria for adhesive disbonds. Preliminary tests appear to indicate that relatively small disbond areas have a substantial effect on the limit load, however, as the tests are still in progress, complete data were not available at the close of the reporting period.

Section II

ADHESIVE BONDED SPECIMENS

DESIGN CRITERIA

The evaluation of nondestructive test techniques for the Saturn honeycomb composites requires a knowledge of the composite failure mechanisms and the characterization of corresponding test response. The previous years' effort (1964-65) was concerned with composite defects characterized by a complete lact of adhesive bond and included unbond simulation by precuring the adhesive, undercutting the honeycomb core, and inserting teflon shims at the adhesive interfaces. These defects were deliberately introduced in composite specimens and formed the basis for evaluating five breadboard ultrasonic inspection systems. This current report describes the further use of these specimens for development of the Impedance Inspection System.

The second year's effort (1965-66) also included the evaluation of nondestructive inspection systems for the determination of adhesive bond strength. A literature and industrial survey was conducted (Appendix A) to determine the parameters that affect bond strength, and the nature of adhesive bond failures. Based on this survey, a program was initiated to simulate degraded strength bonds by deliberately exceeding the manufacturer's cure time and temperature conditions. The program included fabrication and evaluation of adhesive bonded lap shear and honeycomb specimens using the Bloomingdale HT-424 and Minnesota Mining AF-111 adhesives. A number of specimens were prepared under varying cure condition in order to provide a basis for statistical correlation with bond strength.

LAP SHEAR SPECIMENS

The lap shear specimens were fabricated from commercially available military standard MIL-A-5090E coupons thereby permitting four specimens to be made at one time and be individually separated without affecting the adhesive bond. The coupons (Figure 1) were prepared from 0.063-inch thick, clad 2024-T3 aluminum alloy, Specification QQ-4-362. The coupons were cleaned according to NAA Process Specification MA-0106-002, paragraph 3.2, which includes vapor degrease, acid etch, rinse and air drying.

Test coupons were prepared for use in determining the correlation between bond strength and bond conditions using a degraded bond. Both HT-424 and AF-111 adhesives were used in preparation of the coupons. Preparation was in accordance to the respective manufacturer's recommendations except for variations in cure time-temperature. The adhesive

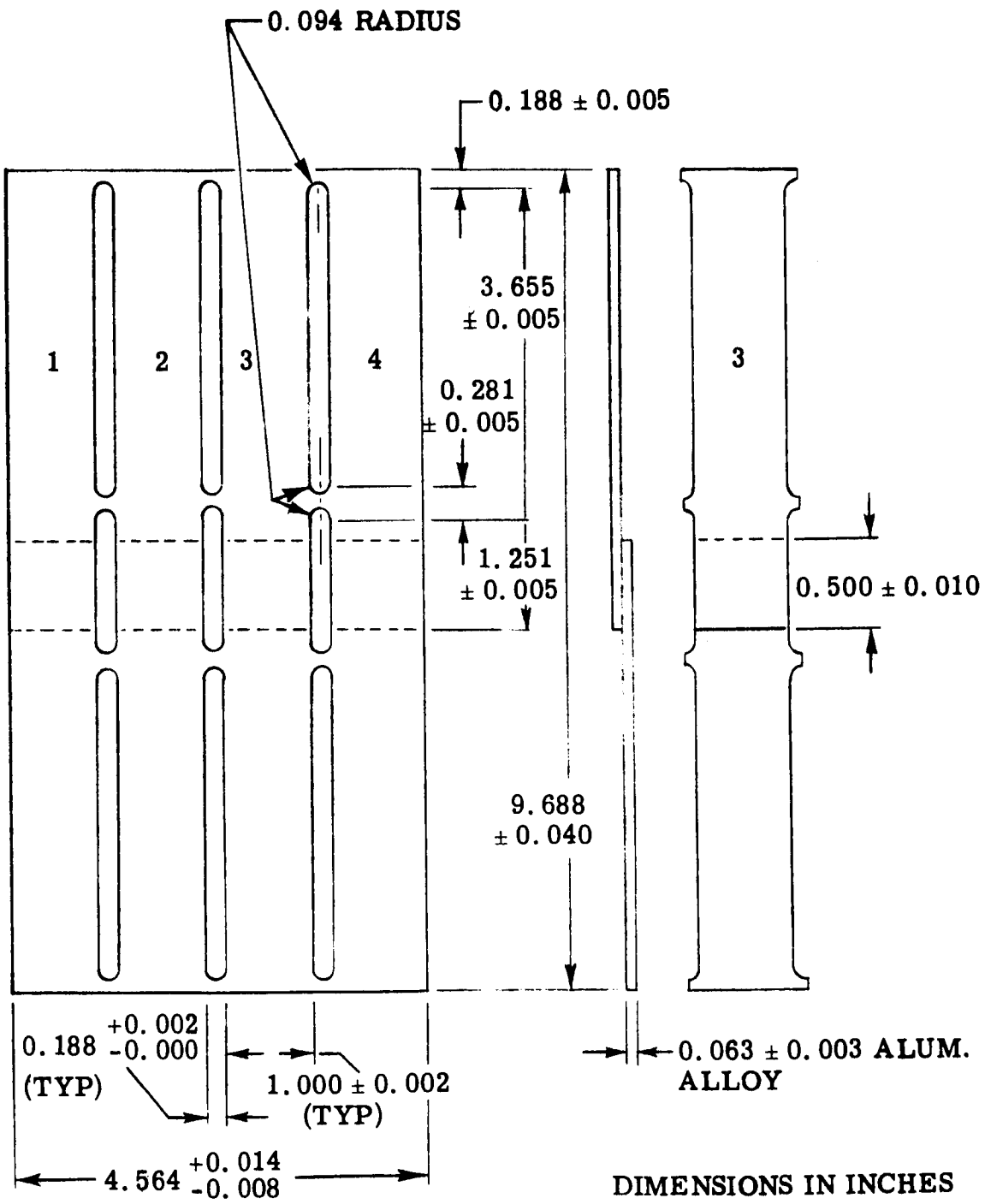

Figure 1. Lap-shear Test Specimen

cure cycle is shown in Table I. All test coupons were subsequently subjected to flatwise tensile tests. Significant changes on bond strength were obtained. Comparative bond cure-strength data for all the test coupons is summarized in Table II.

Lap shear specimens were subsequently fabricated, using the significant time-temperature cure conditions determined from the initial tests used for bond strength evaluation by the nondestructive test systems.

HONEYCOMB SPECIMENS

Four single layer honeycomb specimens were fabricated, incorporating Mylar honeycomb and the applicable adhesives as follows:

	2 ea HRP Specimens	2 ea Mylar Specimens
Core:	4-3/4 inch-thick	0.8 inch-thick
Adhesive:	Bloomingdale HT-424, Type IV	Minnesota Mining AF-111
Face sheets:	1/4 x 18 x 18 inch aluminum	1/4 x 18 x 18 inch aluminum

The 1/4 inch face sheet thickness was based on flatwise tensile testing requirements. Specimen preparation was in accordance with Specifications MIL-A-5090D and MIL-A-401A, "Military Standard Sandwich Constructions and Core Materials; General Test Methods," paragraph 5.2.3, "Sandwich Tension."

Table I. ADHESIVE CURE CYCLE

	HT-424	AF-111
Time-to-cure temperature	within 40-110 min	10°F/min rate
Controlled pressure applied prior to heating:	50 psi	10 psi
Pressure maintained until temperature reduced to:	150°F	200°F
Cure temperature monitor	Thermocouple attached to coupon immediately adjacent to glue line	

Table II

DATA SUMMARY FOR LAP SHEAR SPECIMENS

Adhesive	Cure		Average Failing Stress ($lb/in.^2$)
	Time (min.)	Temperature (°F)	
HT-424 Run No. 1	20 50 80	300	3009 3264 2892
	20 50 80	340	3103 3021 * 2773
	20 50 80	375	2839 2856 2914
HT-424 Run No. 2	20 50 80	200	226 618 829
	20 50 80	250	711 1541 2355
	40	350	2994 *
AF-111	15 30 60	190	473 472 398
	15 30 60	250	1915 3952 4400 *
	15 30 60	225	296 2841 4261

* Manufacturer's recommended cure

One specimen of each type was cured according to the manufacturer's recommendations and one specimen of each type was cured at reduced time and temperature conditions as determined by the lap shear specimen degradation tests. The specimens were cut into 2 x 2 inch-square tensile test specimens (Figure 2) and flatwise tensile tested per Specification MIL-A-401A. The test system included a Baldwin-Tate-Emery testing machine Type UNIV and a special tensile test specimen fixture (Figure 3).

Destructive testing of the six properly bonded and six degraded-bond specimens of each honeycomb type was done to determine the relationship between the respective bonds. Photographs of the specimens after test are shown in Figure 4. The Mylar test data established a degradation value of approximately 68 percent. Initial HRP test data were considered inconclusive and additional degradation tests were conducted at lower time-temperature cure conditions. Therefore, a specimen measuring 4-3/4 x 18 x 18 inches with 0.040 inch aluminum face sheets was fabricated with a degraded bond zone measuring 9 x 18 inches at one adhesive layer. Bond degradation was accomplished by exposing the 9 x 18 inch adhesive layer at 120°F temperature for fifteen minutes. Destructive tests showed an average bond degradation of 94 percent of full bond strength. A second and identical specimen was fabricated with an average degraded bond of 14 percent of full bond strength.

Another set of 4-3/4 inch thick honeycomb specimens of similar size were fabricated according to the same process but with 0.032 inch thick aluminum face sheets. The specimens were bonded using two cure cycles. The low strength bond was degraded to 26 percent of the good bond.

The three sets of standard and degraded adhesive bonded HRP specimens using HT-424 adhesive with facing sheet thicknesses of 0.032, 0.040, and 0.250 inch, respectively, were used for the evaluation of the DOT vibration system. Test results for the degraded bond specimen fabrication are summarized in Table III.

TAPERED HONEYCOMB SPECIMENS

The four HRP specimens bonded with HT-424 adhesive were fabricated in 9 x 18 inch rectangular form with the thickness tapering from 1/16 to 1-1/8, 5/8 to 2-3/8, 1-7/8 to 3-1/2, and 3 to 4-3/4 inches, respectively. The specimens were designed for evaluation of the sensitivity of the impedance system and contained a three inch wide simulated disbond section located at one adhesive layer of the composites. Figure 5 shows the relative

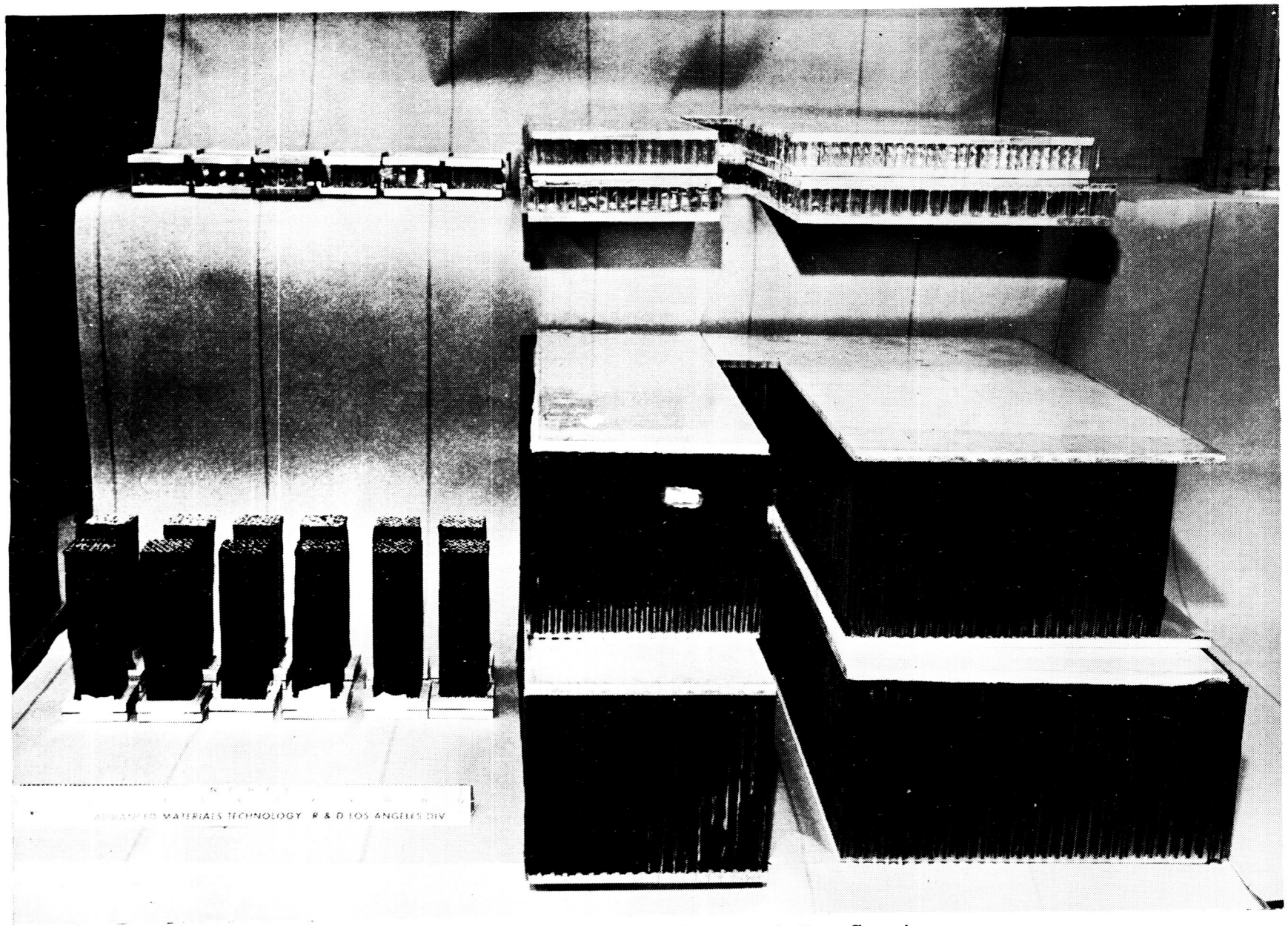

Figure 2. Honeycomb Bond Degradation Specimens

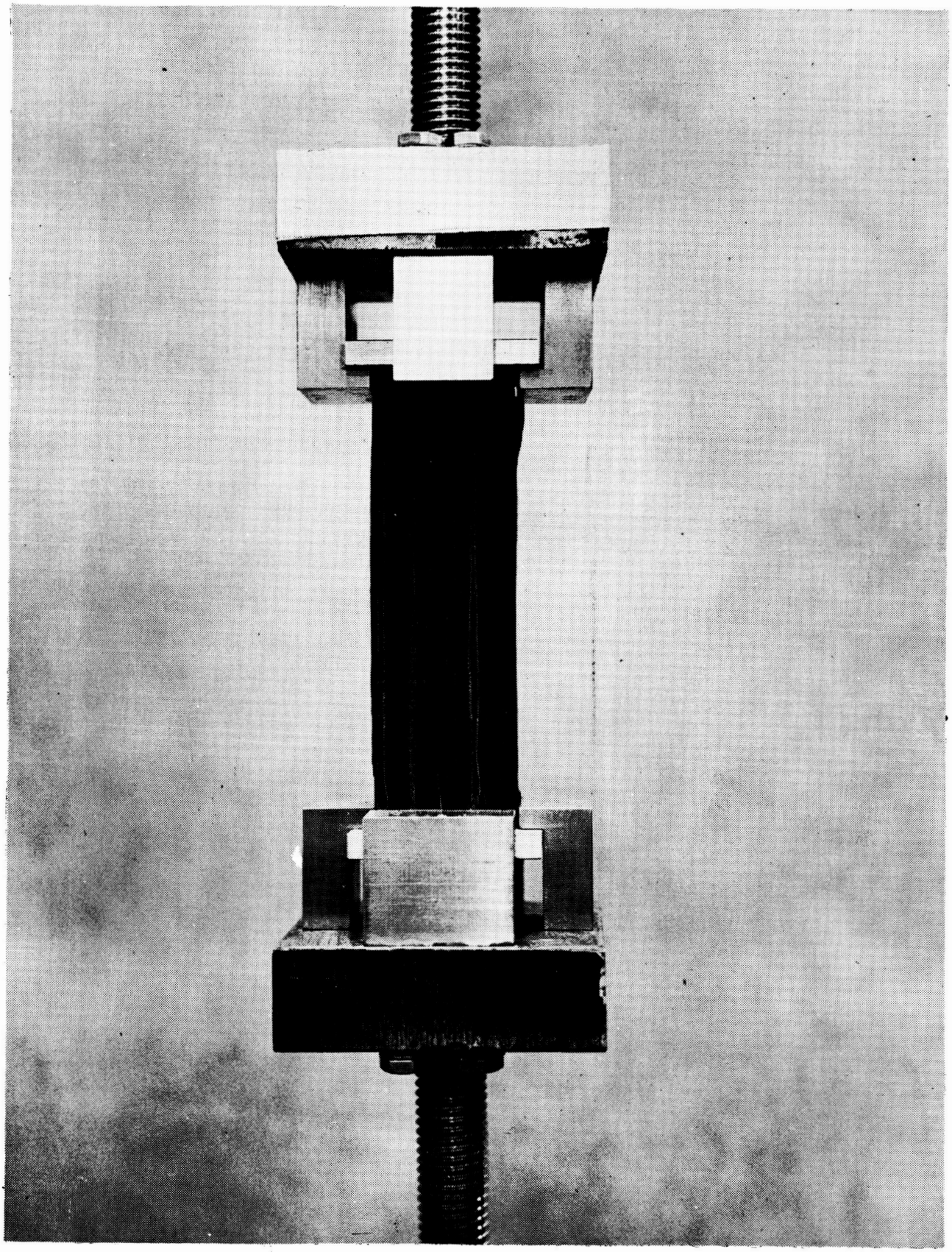

Figure 3. Flatwise Tensile Specimen and Holder

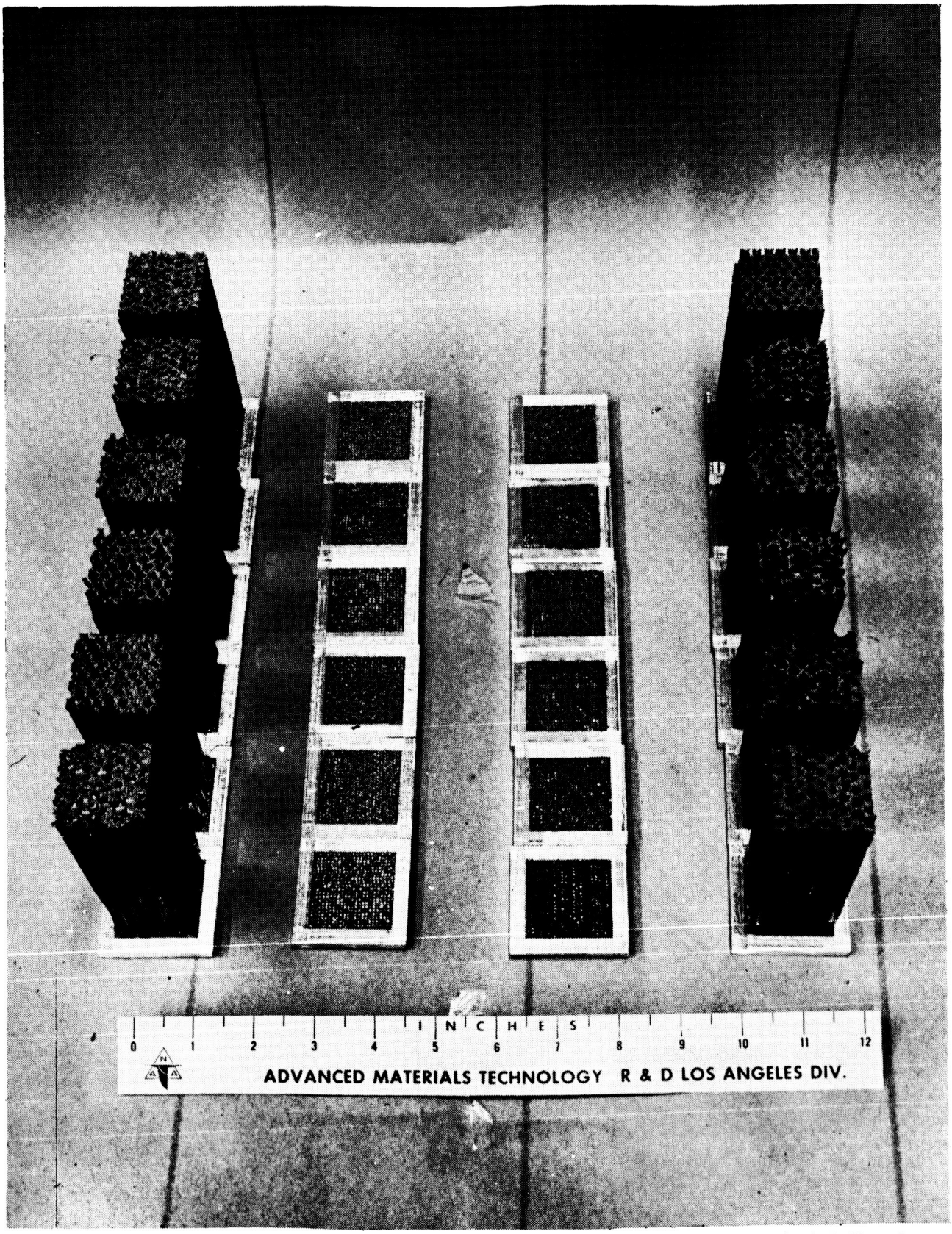

Figure 4. HRP Honeycomb Flatwise Tensile Specimens - HT424 Adhesive

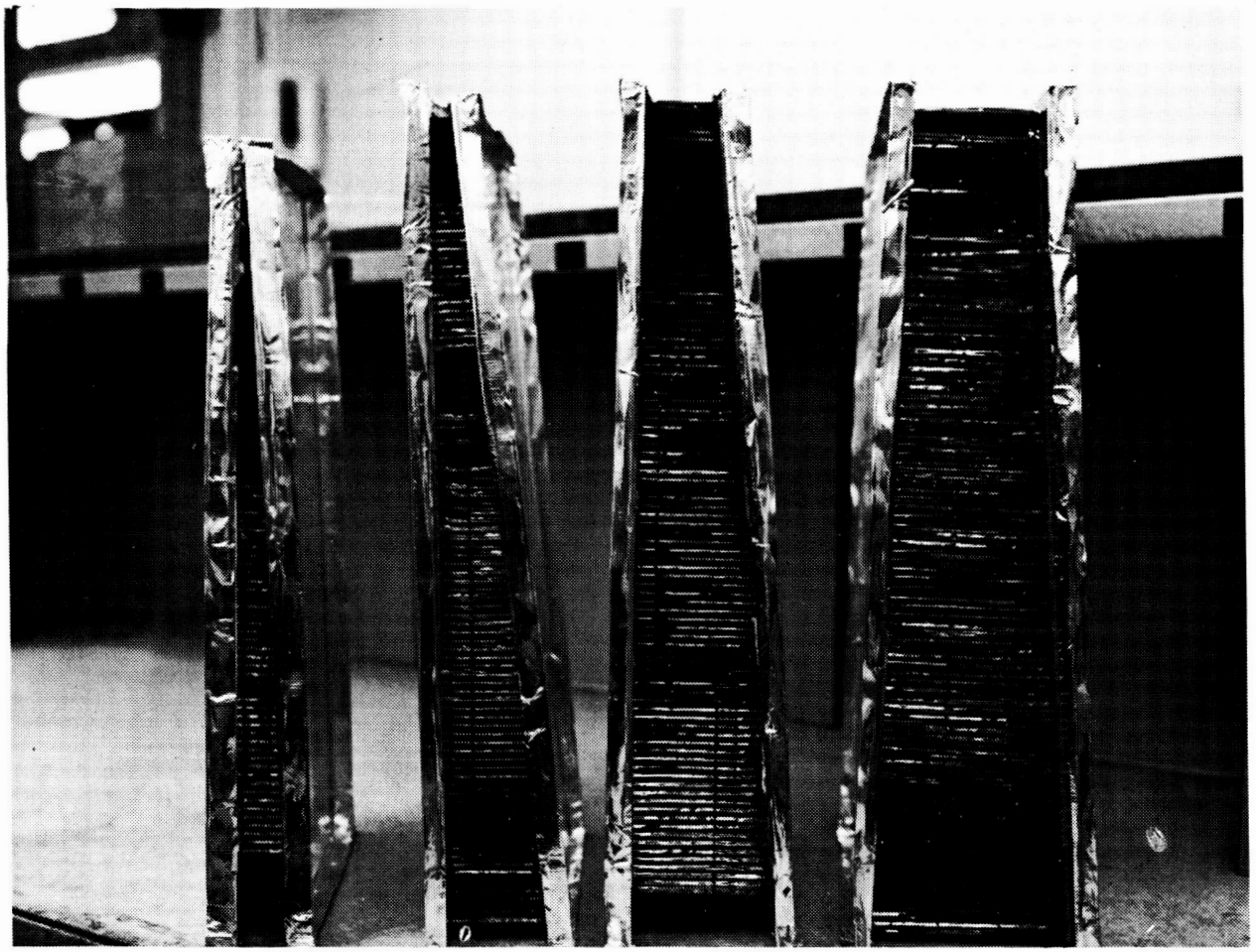

Figure 5. Tapered Honeycomb Specimens Ranging From 1/16 to 4-3/4 inch Thickness

Table III. BOND DEGRADATION SUMMARY FOR HRP HONEYCOME WITH HT-424 ADHESIVE

Specimen	Face Sheet Thickness (In.)	Quantity of Tensile Specimens	Average Stress (PSI)	NDT Specimen Size (In.)	Percent Bond Strength
HRP-1	0.250	6	486	(1) 4 3/4 x 18 x 24	100
HRP-2	0.250	6	462	(1) 4 3/4 x 18 x 24	95
HRP-3	0.040	3	610	(1) 4 3/4 x 18 x 18	100
HRP-4	0.040	3	577		94
HRP-5	0.040	3	86	(1) 4 3/4 x 9 x 18	36
HRP-6	0.032	3	500	(1) 4 3/4 x 9 x 18	100
HRP-7	0.032	3	130	(1) 4 3/4 x 9 x 18	26

taper of specimens fitted with aluminum tape for immersion impedance inspection. Ends of the specimens were designed to give comparable thicknesses to preclude edge effects during transition from one specimen size to the next. The disbond zone within the specimen was identified and test stations were measured to ensure repeatability of sensitivity tests.

INSULATION 1.6 INCH HONEYCOMB SPECIMEN

An additional type of honeycomb composite was constructed in accordance with the recent redirection regarding the Saturn insulation honeycomb material. This composite, referred to as the 1.6 inch honeycomb is shown diagramatically in Figure 6. Construction of the specimen for nondestructive testing followed current NAA/S&ID Process Specification. Deliberate adhesive disbonds were included for detection testing. Figure 7 shows the specimen and the relative location of the disbonds. The disbonds were fabricated at each of four adhesive interfaces and in the following sizes: 2-inch square, one cell (3/4-inch), two adjacent cells, and two end cells.

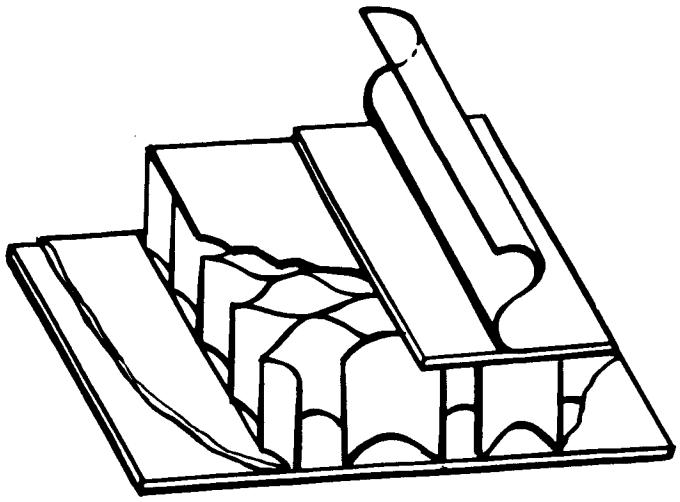

	RAW MATERIAL	NAA SPECIFICATION	NOMINAL THK IN.
1	TEDLAR GAS BARRIER FILM	MB 0130-024	0.002
2	NYLON-PHENOLIC PREIMPREGNATED	MB 0130-023	0.005
3	EPOXY-PHENOLIC ADHESIVE TAPE	MB 0120-048	0.008
4	GLASS FABRIC REINFORCED PHENOLIC RESIN HONEYCOMB CORE	MB 0130-014	1.600
5	POLYURETHANE FOAM	MB 0130-15	1.600
6	EPOXY-PHENOLIC ADHESIVE TAPE	MB 0120-048	0.010
7	2014 T6 ALUMINUM	N A	0.160

Figure 6. Insulation 1.6-inch Honeycomb Composite

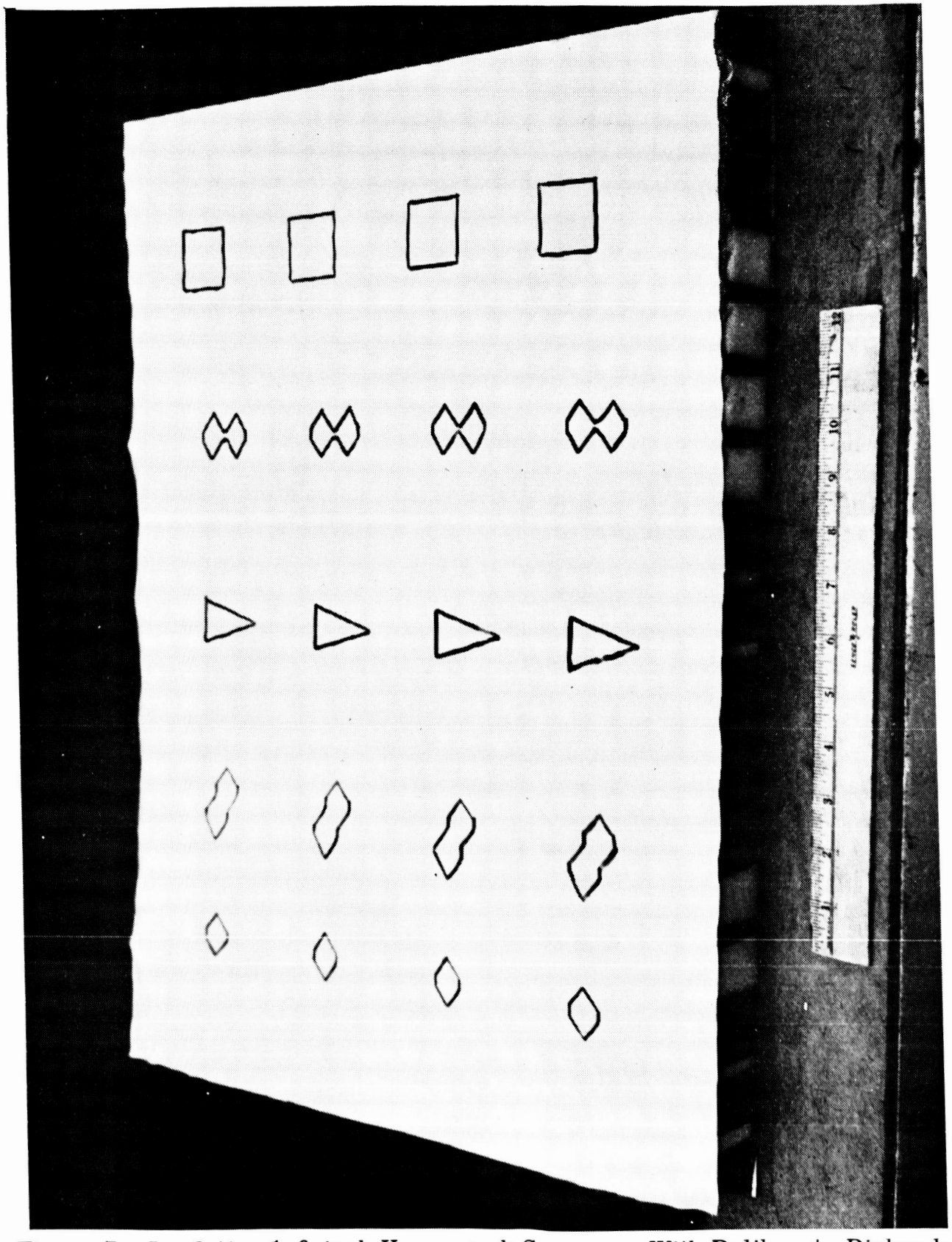

Figure 7. Insulation 1.6-inch Honeycomb Specimen With Deliberate Disbonds

The S-4B-type honeycomb composites used in the Saturn common bulkhead fabricated during the first years' program were also utilized for the additional development effort. The specimens were composed of two aluminum facing sheets adhesive-bonded to HRP honeycomb core. The specimens ranged from 1, 1-3/4, and 4-3/4 inch thick flat specimens, 12 x 12 inches and 24 x 36 inches. Deliberate disbonds (100 percent lack of bond) were installed at each adhesive interface i.e., between the facing sheet and adhesive (1/2), adhesive to core (2/3), core to adhesive (3/4) and adhesive to facesheet (4/5). The disbonds included precured adhesive, under cut core, and teflon film disbonds. The disbonds ranged in size from one inch triangles up to three inch squares.

Section III

ULTRASONIC PROPERTY TESTS

TECHNICAL APPROACH

The objective of this phase of program effort was to determine the effectiveness of ultrasonic techniques in determining adhesive bond strength. The ultrasonic parameters potentially related to bond strength include attenuation, impedance, velocity, power absorption, resonance, reflectivity, phase shift, and possible combinations thereof. To determine the feasibility of utilizing ultrasonic systems as a technique for the evaluation of bond quality, it is necessary to determine which ultrasonic parameter(s) and method(s) are best suited to achieving the objective.

Ultrasonic tests were conducted on adhesive bonded lap shear test coupons fabricated with varying bond strengths. The purpose of the tests was to (1) determine which, if any, of the ultrasonic parameters showed a correlation to bond strength with the HT-424 and AF-111 adhesives, and (2) which ultrasonic system(s) appeared best suited to evidencing the parameter(s).

Ultrasonic inspection systems were evaluated to determine the existence of qualitative indications of ultrasonic parameter-bond strength relationships. The systems included (1) Pulse Echo Reflection, (2) Pulse Echo Through Transmission, (3) Lamb Wave, (4) Impedance Technique, and (5) Shear Wave Techniques.

The inspection of the small bond area in the lap shear specimens (1/2 x 1 inch) required a precise scanning control with minimum hysteresis. A surplus two-axis radar antenna positioner was adapted for scanning the lap shear specimens. The total scan length was adjustable from 1/16 to 6 inches, and scanned at a constant rate regardless of scan length with index adjustments from 0.007 to 1.8 inches per scan. The existing recorder trigger circuit was fitted with a trigger level and recordings were made on a Mosely Model 4S X-Y recorder.

PULSE-ECHO REFLECTION TECHNIQUE

A high resolution flaw detector capable of resolving echo multiples in 0.010 inch stainless steel was used on the adhesive bonded lap shear specimens. The pulse echo system was mechanically scanned and the echo signal recorded on an X-Y recorder. The difference in echo amplitude is an indication of acoustic loading on the surface of the top face sheet. When

the transducer was over water-backed metal, stronger echoes were noted as opposed to those obtained when the transducer was positioned over an adhesively bonded area. Minor variation in second rear surface echo strength was noted as the transducer was scanned over water-backed metal; greater variation was noted over bonded areas. Figure 8 shows an X-Y recording starting with water-backed metal and ending with bonded metal. A periodicity in the pattern, especially over the bonded area is noticeable; this matched the threads in the adhesive scrim cloth.

This system appears capable of resolving gross differences of attenuation as seen in bonded and unbonded sections of the specimens. However, quantitative measurements of attenuation variations within adhesive did not prove feasible due to high background noise.

PULSE-ECHO THROUGH-TRANSMISSION TECHNIQUE

Through-transmission tests were conducted using the transmitter system described above and a narrow band receiver. The transmitting and receiving transducers were immersed, aligned, and fixed within a small tank. The transducers have a 1.7-inch focal length and were spaced approximately 2.5 inches apart, short of the optimum focus position so that the broadened beam would reduce the effect of minor attenuation variations within the adhesives. The specimens were wiped with a wetting agent to ensure good acoustical contact, and positioned between the transducers. An unbonded portion of the specimen was positioned in the ultrasonic beam and the attenuator adjusted to provide a reference level on the oscilloscope. With the same alloy and thickness, this level varied approximately 0.5 db (voltage). The bonded section of specimen was next inspected, being careful to exclude diffraction effects from the specimen edges. The attenuator was again adjusted to bring the received signal to reference level. The reduction in attenuation is the comparative attenuation value for the bonded joint. Measurements were made with a repeatability of ±1db. These measurements were conducted at both one and four MHz. This technique showed a capability of qualitative attenuation measurements of gross bond strength differences.

The method of least squares was used to fit attentuation, adhesive thickness, and lap-shear strength results to various assumed relationships. The results, expressed in the form of correlation coefficients are given in Table IV. The correlation coefficients are quite small; a value between 0.9 to 1.0 is desirable. The main problem is that of properly introducing the lap shear strength value into the thickness - attenuation relationship. The analysis of trial 3 (shown in Figure 9) gave the best results. However, none of the correlations are really significant.

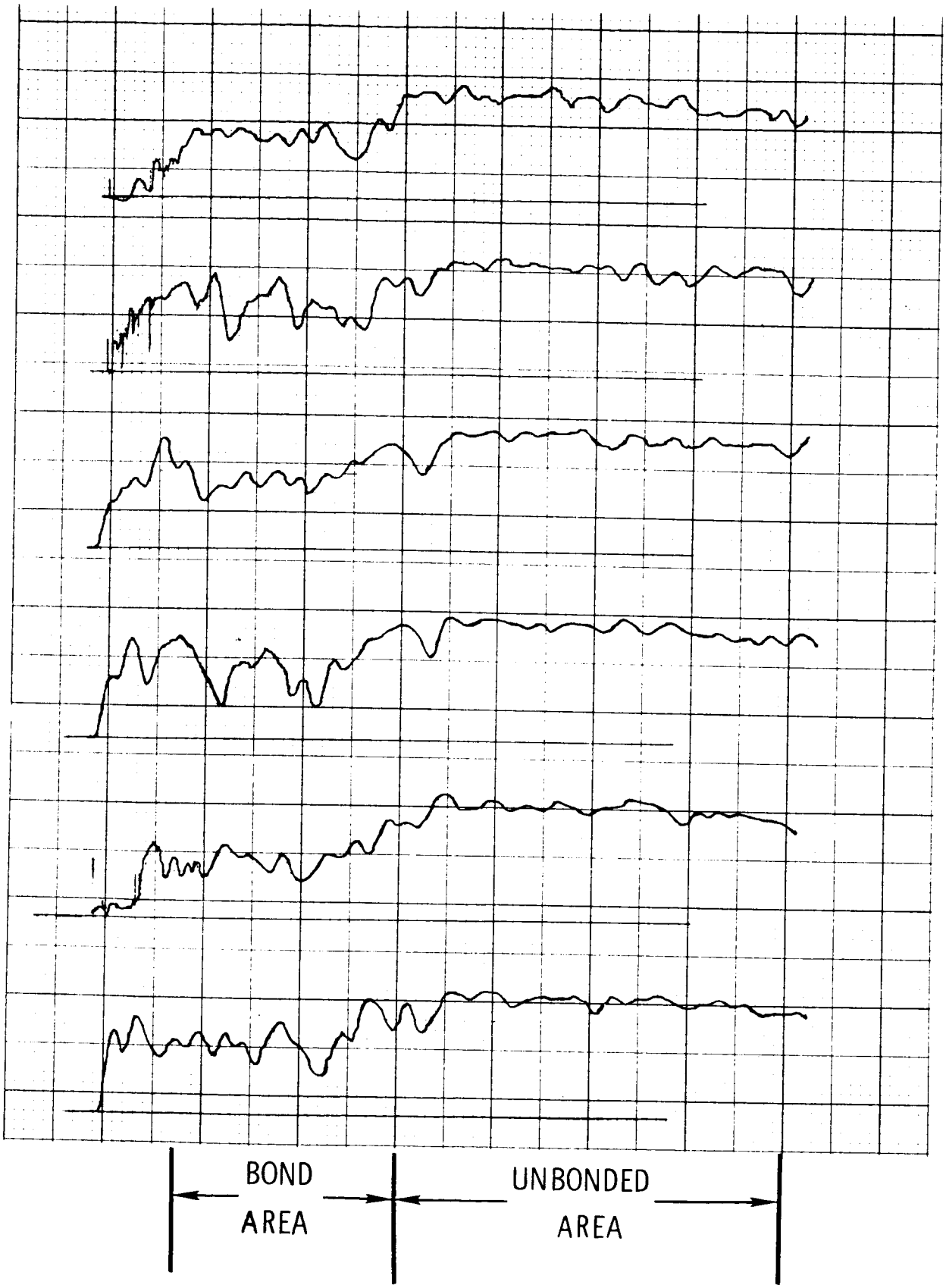

Figure 8. Pulse-Echo Scan of Lap-Shear Specimen at 1/8-inch Increments

Table IV

STATISTICAL CORRELATION DATA

ULTRASONIC THROUGH TRANSMISSION TESTS

Trial No.	Resin *	Condition	Assumed Relation-ship	Ni Alloy		1 MHz/sec Titanium		Steel		Ni Alloy		4 MHz/sec		Steel	
				No.	R	No.	R	No.	R	No.	R	No.	R	No.	R
1	A	Exposed	(a)	18	0.320	18	0.609	17	0.205	18	0.010	16	0.132	18	0.272
2	A	Exposed	(b)	18	0.358	18	0.398	17	0.040	18	0.155	16	0.025	18	0.240
3	A	Exposed	(b)	17	0.354	18	0.516	17	0.518	18	0.065	16	0.383	18	0.421
4	A	Exposed	(c)	14	0.071	15	0.018	--	- - -	14	0.153	15	0.460	--	- - -
5	B	Exposed	(c)	9	0.288	12	0.230	8	0.028	9	0.747	12	0.199	9	0.046
6	A	Unexposed	(d)	20	0.142	12	0.239	19	0.071	20	0.332	8	0.394	19	0.020
7	A	Exposed	(d)	14	0.148	15	0.043	13	0.245	14	0.271	15	0.057	14	0.055
8	B	Unexposed	(d)	13	0.051	--	- - -	6	0.591	13	0.139	--	- - -	5	0.689
9	B	Exposed	(d)	9	0.346	12	0.064	8	0.058	19	0.221	12	0.587	9	0.502
10	A	Exposed	(e)	18	0.176	18	0.443	17	0.248	18	0.070	16	0.271	18	0.013
11	A	Exposed	(f)	18	0.080	18	0.258	17	0.213	18	0.155	16	0.093	18	0.088

Assumed Relationship

(a) $A_x/A_o = K_{exp}(Bt)$

(b) $A_x/A_o = K_{exp}(BT)/S$

(c) $A_o - A_x = Mt + N$

(d) $S = M(A_o - A_x) + N$

(e) $A_x/A_o = K_{exp}(BtS)$

(f) $A_x/A_o = KS_{exp}(Bt)$

where

S = Lap shear strength
t = Glue line thickness
A_x = Attenuation difference (dB), exposed
A_o = Attenuation difference (dB), unexposed
R = Correlation coefficient
K, M, N, = Constants
No. = Number of specimens in each batch

*Resin type A and B are identified under Air Force Contract No. AF33(615)-2848

COLUMN 1 VS COLUMN 5
AS SPECIMENS TESTED AT ROOM TEMPERATURE - ALL EXPOSURES

•15337000E-05	•72727000E+00	•69644736E+00
•21097000E-05	•70454000E+00	•65126984E+00
•15337000E-05	•76744000E+00	•69644736E+00
•21201000E-05	•76744000E+00	•65048167E+00
•13085000E-05	•70454000E+00	•71495099E+00
•15673000E-05	•61111000E+00	•69372796E+00
•19230000E-05	•50000000E+00	•66558276E+00
•31250000E-05	•64705000E+00	•57865406E+00
•26666000E-05	•66666000E+00	•61037888E+00
•86206000E-06	•70000000E+00	•75309883E+00
•25862000E-05	•67500000E+00	•61611983E+00
•29268000E-05	•64705000E+00	•59216350E+00
•47945000E-05	•28571001E+00	•47642580E+00
•27322000E-05	•50000000E+00	•60573437E+00
•23584000E-05	•56250000E+00	•63268078E+00
•41322000E-05	•75471000E+00	•51461997E+00
•39603000E-05	•62500000E+00	•52502420E+00
-•18318249E+00	-•11643775E+06	•44921350E-01
•51404594E-01	•49669096E+05	•92069005E+00

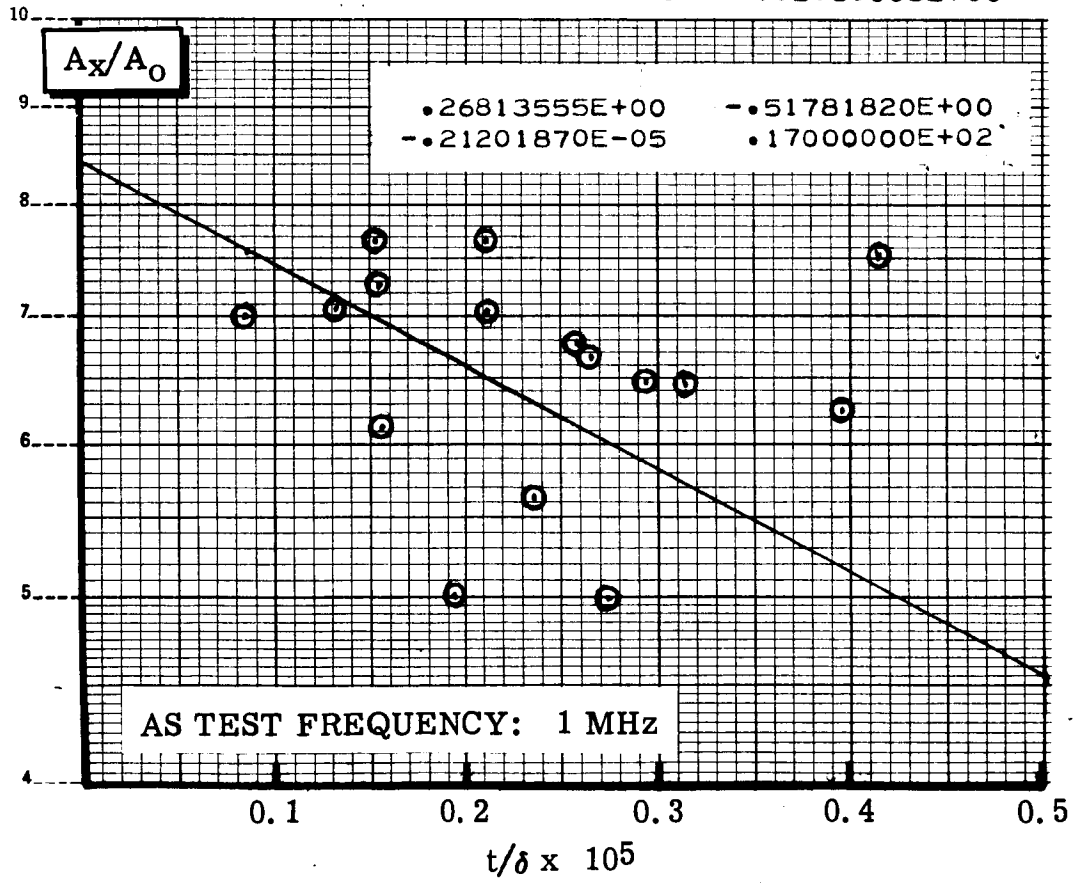

Figure 9 . Statistical Correlation Showing Computer Data and Data Plot - Trial No. 3

Based on results of these experimental tests, additional confirmatory tests appeared warranted. These were conducted in conjunction with a concurrent Air Force adhesive development program. Through-transmission attenuation tests were conducted on the specimens as fabricated, and subsequent to environmental aging. Approximately 260 specimens were tested at 1 and 4 MHz, and the ultrasonic attenuation and tensile shear test data were correlated by computer analysis.

LAMB WAVE TECHNIQUE

Lamb wave transmission tests were conducted on the lap-shear specimens using the pulse echo reflection system described previously. A special transducer positioning device was fabricated to accurately vary the launch angle (Figure 10). At 33 degrees, evidence of Lamb wave propagation with variations in the bond areas was noted. Since Lamb wave formation is a function of frequency, the two frequency pulser-receiver was employed. The well bonded specimens were tested, and without apparent differences in through transmission and pulse echo signal amplitude, phase or echoes. The signal levels were too low to differentiate between good or degraded bond strength.

IMPEDANCE TECHNIQUE

An impedance measuring system was breadboarded per the block diagram which shows the basic system and the equipment used for the precision measurements. The transducer uses a PZT-5 crystal, 1/4 inch diameter by 3/4 inch long, bonded to a 1/8 inch thick plexiglass shoe. The crystal was mounted in an aluminum tube to facilitate handling. A plexiglass template and calibrated arbor press were used to align and hold the transducer on the lap-shear specimen. A glycerine-wetting agent fluid was applied to the specimen for coupling.

The following test procedure was observed:

1. The transducer was removed from the specimen and the bridge oscillator tuned to the crystal mechanical resonance point as shown by a null on the VTVM.

2. The transducer was located on the specimen with the plexiglass template, coupled, and held with a constant force.

3. The bridge was nulled by adjusting the external capacitor and resistance instruments.

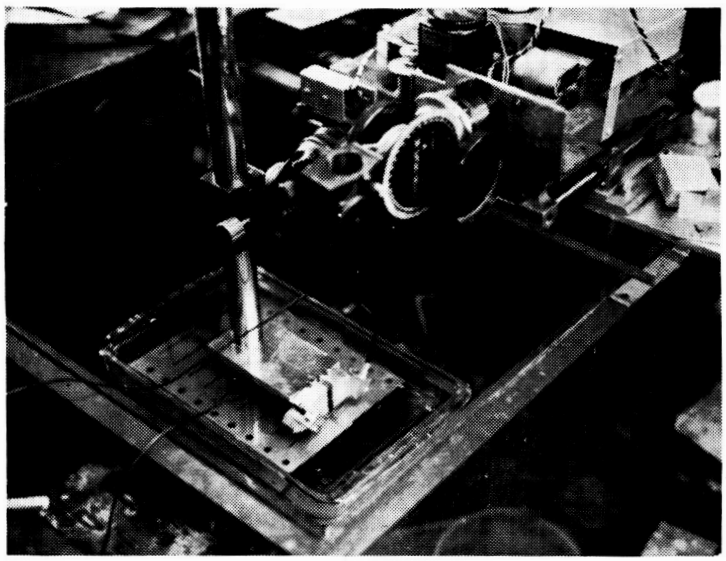

LAMB WAVE TEST SYSTEM

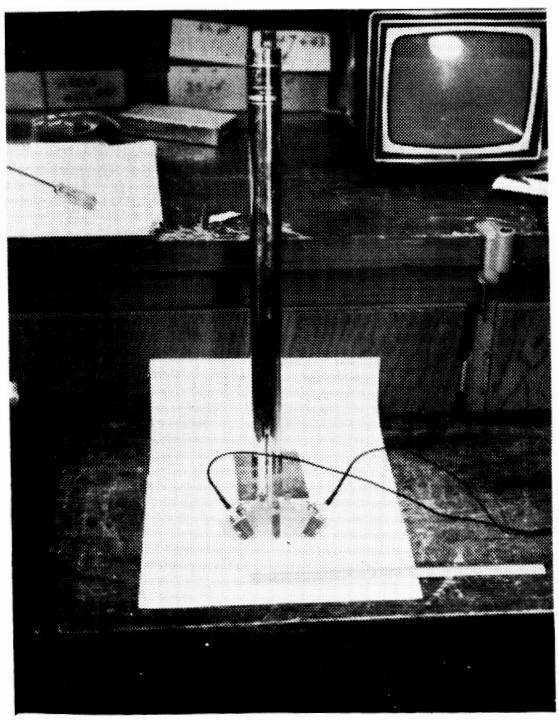

POSITIONING PROBE ASSEMBLY

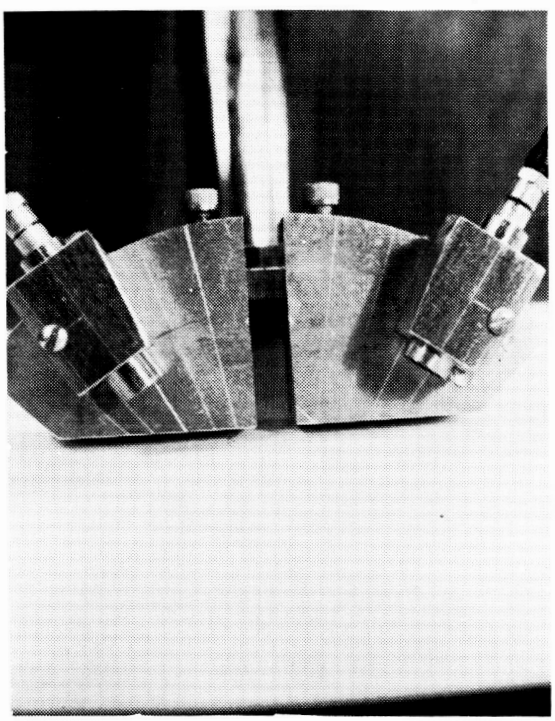

ADJUSTABLE PROBE HEAD

Figure 10. Lamb Wave Testing

4. Capacitance was read directly from the precision capacitor dial. The resistance is switched from the circuit to reduce frequency effects, and indicated on the digital ohmmeter.

Qualitative test data have shown repeatability and a fair range of impedance values between bonded and unbonded adhesive specimens.

SHEAR WAVE TECHNIQUE

Shear wave measurements were conducted with a Sperry UW (0.2 - 25 MHz) and UM 700 (1 - 5 MHz) Reflectoscope. The specimen was oriented at an angle to produce shear wave propagation through the bond area. The two transducers are fixed while the specimen is moved to give a scan-mode node. Initial tests showed significant changes due to variations in the adhesive glue line thickness. However, the repeatability of attenuation data varied up to one hundred percent. Positioning of the specimen between the transducers was accomplished by a relatively large drive mechanism which contributed some hysteresis and instability in the scanning mode. However, static tests failed to show repeatability.

Photographs and diagrams of the respective systems used in these tests are included in the Quarterly Program Reports prepared during the reporting period.

CONCLUSIONS

The conventional ultrasonic test techniques evaluated during this program were not successful in reliably differentiating between gross differences in adhesive bond strength. Of all the techniques, the through transmission attenuation measurements demonstrated the greatest potential for correlation with bond strength. Two specific conclusions appear warranted. First, additional test specimens may have shown a relationship. Data were taken for three to five specimens at each degraded bond strength condition and perhaps additional data points would have reduced the data scatter. Second, the specimen bond area was quite small, (1/2 by 1 inch) and controlled wave propagation was extremely difficult. Additional tests on larger specimens would also have reduced the data scatter.

Section IV

ADHESIVE BOND DETERMINATION BY VIBRATION ANALYSIS

TECHNICAL APPROACH

General tests on organic adhesives indicate that the adhesives act under stress as visco-elastic solids, and that their response to an applied stress is time dependent. This effect is characterized by the maximum in the internal friction according to the relation

$$\tan \delta = K f t/(1 + f^2 t^2)$$

The internal friction is also proportional to the energy dissipated per cycle of vibration. It is clear that the maximum occurs when ft = 1. A curve plotting tan δ against f will peak at this point (Figure 11). From the shape of these curves and the frequency dependency, it can be considered that the underlying hypothesis of a Zener relaxation process is applicable. It was therefore considered that the vibration tests should show non-destructively a relationship between the adhesive bond strength of an adhesive and its internal friction. A series of experiments were designed to evaluate the applicability of this hypothesis as a measure of adhesive bond strength for the Saturn adhesive bonded composite. The initial tests were conducted on lap shear specimens to verify the hypothesis, included the development of a test system. Subsequent tests verified the system for use on the Saturn honeycomb composites. Finally, tests were conducted on various strength adhesive bonded honeycomb composites.

LAP SHEAR SPECIMEN TEST

A series of vibration tests were conducted on adhesive bonded lap shear specimens of various bond strengths to determine whether the vibratory properties could be qualitatively correlated with bond quality. The initial test system utilized two 28 KHz piezoelectric crystals, one for excitation and the other for detection. The specimens were preloaded between the crystals and driven with a swept frequency (20Hz to 200KHz) oscillator. The bandwidth for half amplitude at resonant frequency was compared with the lap shear fracture stress. The peak width at half amplitude is directly proportional to the internal friction. The data

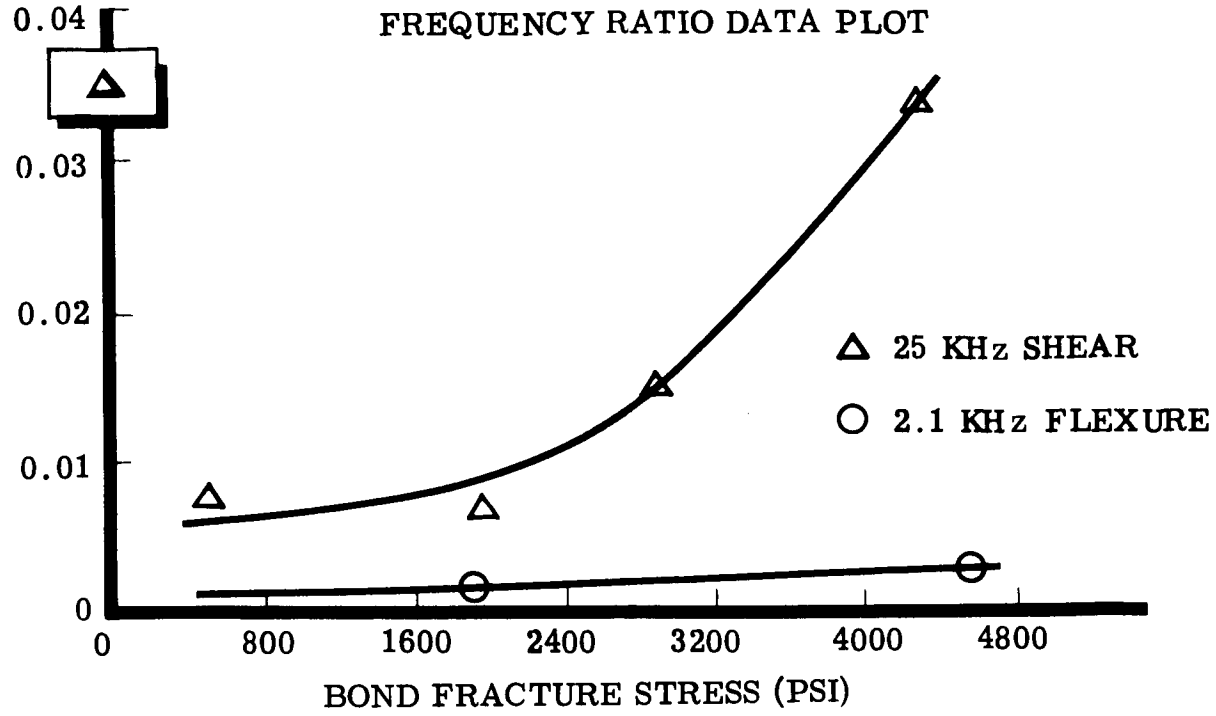

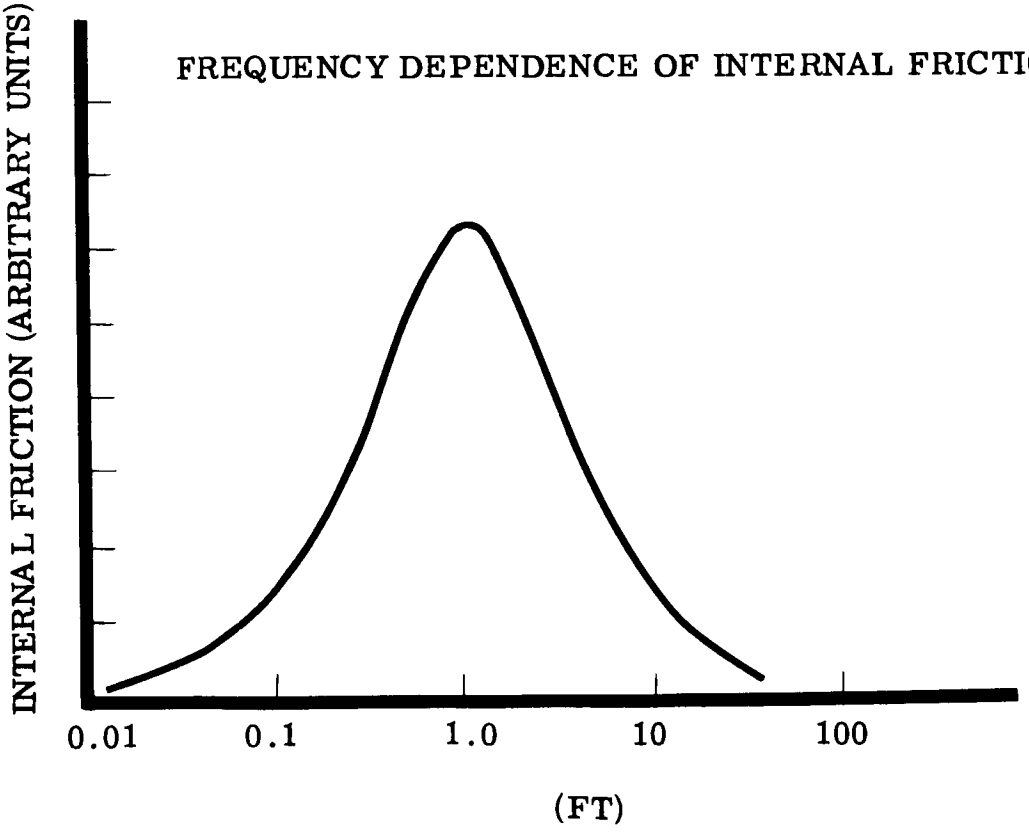

Figure 11. Internal Friction Relationships Including Test Data (Top) and Zener Mechanism (Bottom).

compilation and reduction is shown in Table V. The half-width data were plotted and a definite relationship was evident. This is shown by the upper curve in Figure 11. Additional vibratory tests were conducted with the lap shear specimen clamped to a vibration fixture and driven to the first mechanical resonance (see Appendix B for calculated specimen resonances). The resonance occurred at approximately 2.1 KHz. The test system used a proximity probe for displacement measurement over the bond area. The autocollimator provided gross vibrational data and preliminary indication of vibratory modes. The specimen was driven at the first mechanical resonance, and the excitation frequency was then varied to one-half resonance amplitude points above and below resonance. A plot of the damping results for these data are shown in Figure 11 (lower curve), and may be compared with the shear data for the same specimens.

It was concluded from these results that bond strength can be related to a relaxation mechanism. Further, these results show that a shorter relaxation time occurs with a low strength bond. It was considered highly significant that the damping characteristics were frequency dependent. Damping is also temperature dependent. To check this dependence, tests were conducted using a low strength bonded specimen at varying temperatures. If the hypothesis was correct, a peaking would occur in the damping curve at lower temperatures for a well bonded specimen. A proportional shift in temperature should occur for low strength adhesive bonds. The damping-temperature dependency tests were conducted in a test system in a liquid nitrogen cooled supplied chamber. An electromagnetic driver driven by an HP201 oscillator and 55 watt Heathkit power amplifier was used for excitation. Displacement was detected by a Bently Model 15 type H-1 Proximity Probe monitored with a vacuum tube voltmeter and oscilloscope. Figure 12 shows three temperature cycles and the damping-temperature relationships. Test run number one showed a peaking in the +20 to -40°F temperature range; test run number two shows a gradual peaking at approximately $+30^{\circ}$F. The peak at -320°F is attributed to a mechanism other than the relaxation mechanism. Test run number 3 specifically defines the peak at approximately $+5^{\circ}$F.

The low temperature tests indicate some anomalies which may be due to material variations but support the assumption of a bond strength related damping mechanism based on relaxation phenomena.

Based on the above tests which demonstrated the mechanisms of frequency dependent damping, several types of potential inspection system designs were considered. Of these, two had a greater apparent feasibility. First, the Driver-Displacement Oriented Transducer (DOT) system was conceived wherein an electromagnetic driver and displacement measuring system were incorporated into a single unit. The DOT system

Table V

ELASTIC CONSTANT CALCULATION

Specimen No.	Calibration		Peak Output		Half-peak Output		Full Width of Curve at Half-peak Voltage Output, Δf (cps)	First Peak Freq, f_o (cps)	Half-width, $\delta = \frac{\Delta f}{f_o}$	$\delta - \delta'$ (Notes 1 and 3)	% Change (Note 2)	Fracture Stress lb/in.^{2}
	db	v	db	v	db	v						
B-97	17.5	0.10	49.5	3.98	43.5	1.99	26800-25000 =1800	25900	0.0694	0.0338	5.7	4261
B-88	17.4	0.10	49.0	3.80	43.0	1.90	27200-25900 =1300	26300	0.0494	0.0138	9.9	2841
B-47	15.7	0.10	44.0	2.60	38.7	1.30	26400-25320 =1080	25900	0.0417	0.0061	38.3	1915
B-17	15.9	0.10	41.9	2.00	35.9	1.00	26360-25270 =1090	25800	0.0423	0.0067	52.6	473
	25.5	0.10	50.6	1.80	34.6	0.90	28500-26100 =2400	27300	0.0878	0.0522	57.2	473
Solid Al	17.5	0.10	50.0	4.22	44.0	2.11	25900-25000 =900	25300	0.0356	-	-	-

Note 1: δ = half-width of solid aluminum (Δf is determined from the db-f curve at an ordinate in db units equal to one-half the half-peak voltage output).

Note 2: % change of peak voltage output equals $\frac{\text{Peak Voltage Output of Solid Al} - \text{Peak Voltage Output Specimen}}{\text{Peak Voltage Output of Solid Al}}$ multiplied by 100.

Note 3: The superposition rule ($\delta = \delta_1 + \delta_2 + \ldots$) is applicable to a composite material to determine its specific damping energy if this energy is expressed in in. lb in.^{3} cycle and if the interface damping is small.

Note 4: The half-width δ defined in the table is not directly related to the logarithmic decrement ($\frac{\pi}{\sqrt{3}} \cdot \frac{\Delta f}{f_o}$) because the sinusoidal driving force for the amplitude readings above, below, and at resonance was not the same when a constant excitation voltage (10 v) was imposed throughout the test.

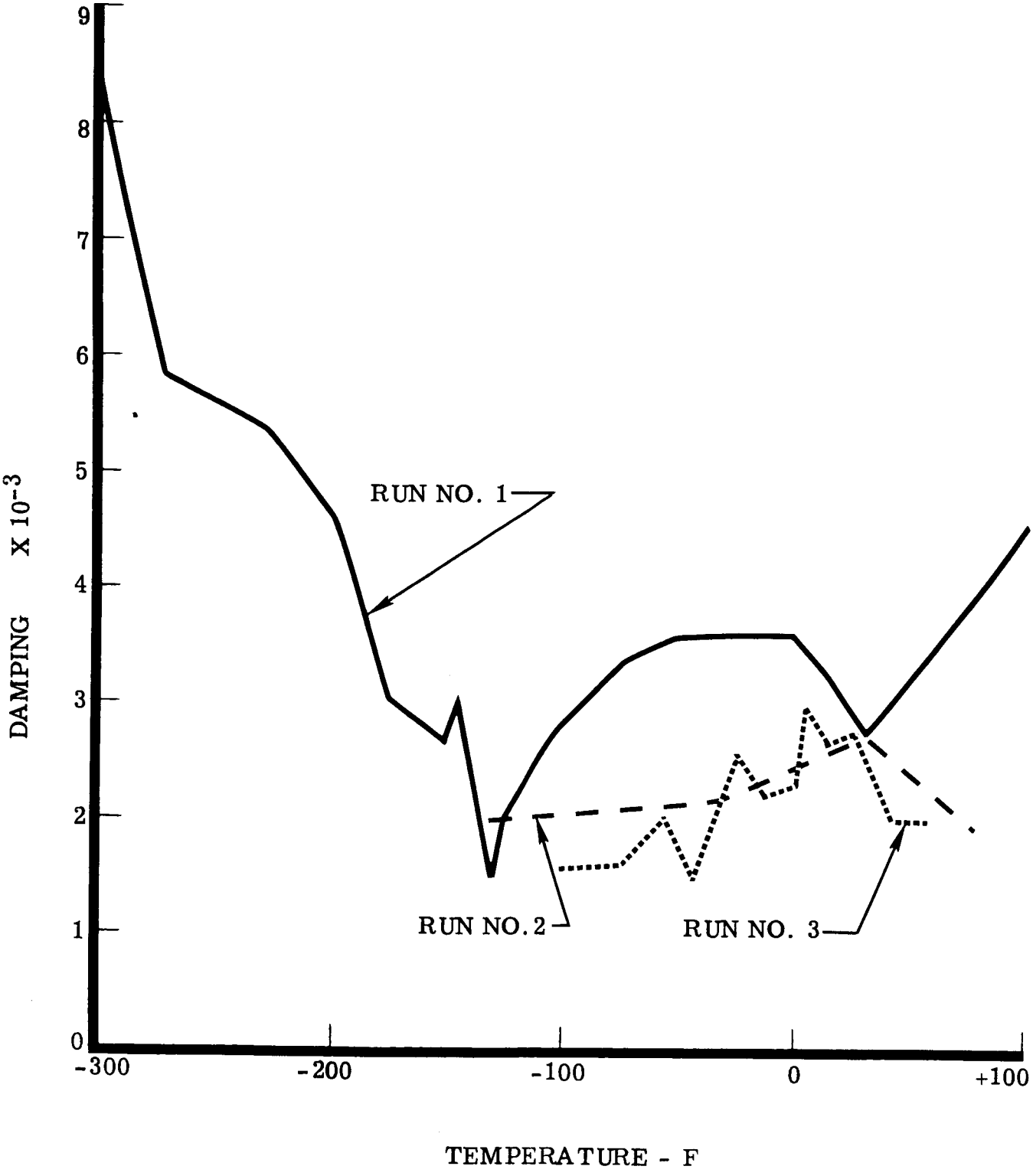

Figure 12. Graph Showing Temperature Versus Damping Relationship for AF-111 Adhesive

makes use of the measurement of the displacement of the honeycomb composite face sheet at a given resonant frequency. The displacement can be directly related to the "spring constant" of the adhesive joint and the damping characteristics which are in turn indicative of adhesive bond strength. This concept was further enhanced by the fact that for frequencies below approximately 30KHz, it appears that the damping decreases with decreasing adhesive bond strength. Therefore, the amplitude response of the composite face sheet should also be increased by the damping as well as by the weaker "spring constant."

An alternate system makes direct use of the damping mechanism and includes an oscillating system at approximately 30KHz wherein the adhesive bond damping becomes part of the oscillator circuit Q. This frequency is indicated by the fact that damping appears to go through a large change at this frequency in going from poor to good bonds. Here, increased damping would be indicated by a greater load on the oscillator. By designing a feedback system so that oscillation is sustained at preset amplitude, changes due to damping (load) become a measure of adhesive bond strength.

The first (DOT) system was initially selected for evaluation because more detailed damping information could be acquired. The existing Eddy-Sonic electromagnetic driver was modified by shielding the excitation driver and addition of a capacitance sensing probe for displacement measurements at the center of the driver. The probe was initially fabricated from a 7/8-inch diameter copper plated nylon disk sized to measure face sheet displacements greater than a single honeycomb cell. This reduces positioning problems, and yet maintains a sensitivity for low strength bonds in the order of several 3/16 inch honeycomb cells. A single cell measurement would have entailed difficult positioning problems.

The DOT transducer (Figure 13) was checked initially to determine the drive characteristics and displacement measurement range. The transducer was mounted on the lap shear vibration drive system (Figure 14) and connected to a B&K Spectrometer for displacement indication. With a 0.020-inch spacing between the lap shear beam and the capacitance probe, a displacement signal indication of 300 millivolts was measured at beam resonance; second harmonic (approximately 2 Hz) and half amplitude measurements gave a band-width of 4 Hz. This is approximately the same half width obtained in the other experiments at this frequency. The DOT coil was then energized for drive, however, the displacement indication at beam resonance was indeterminate on the Spectrometer. Using a Panoramic Spectrum Analyzer, the second harmonic displacement signal

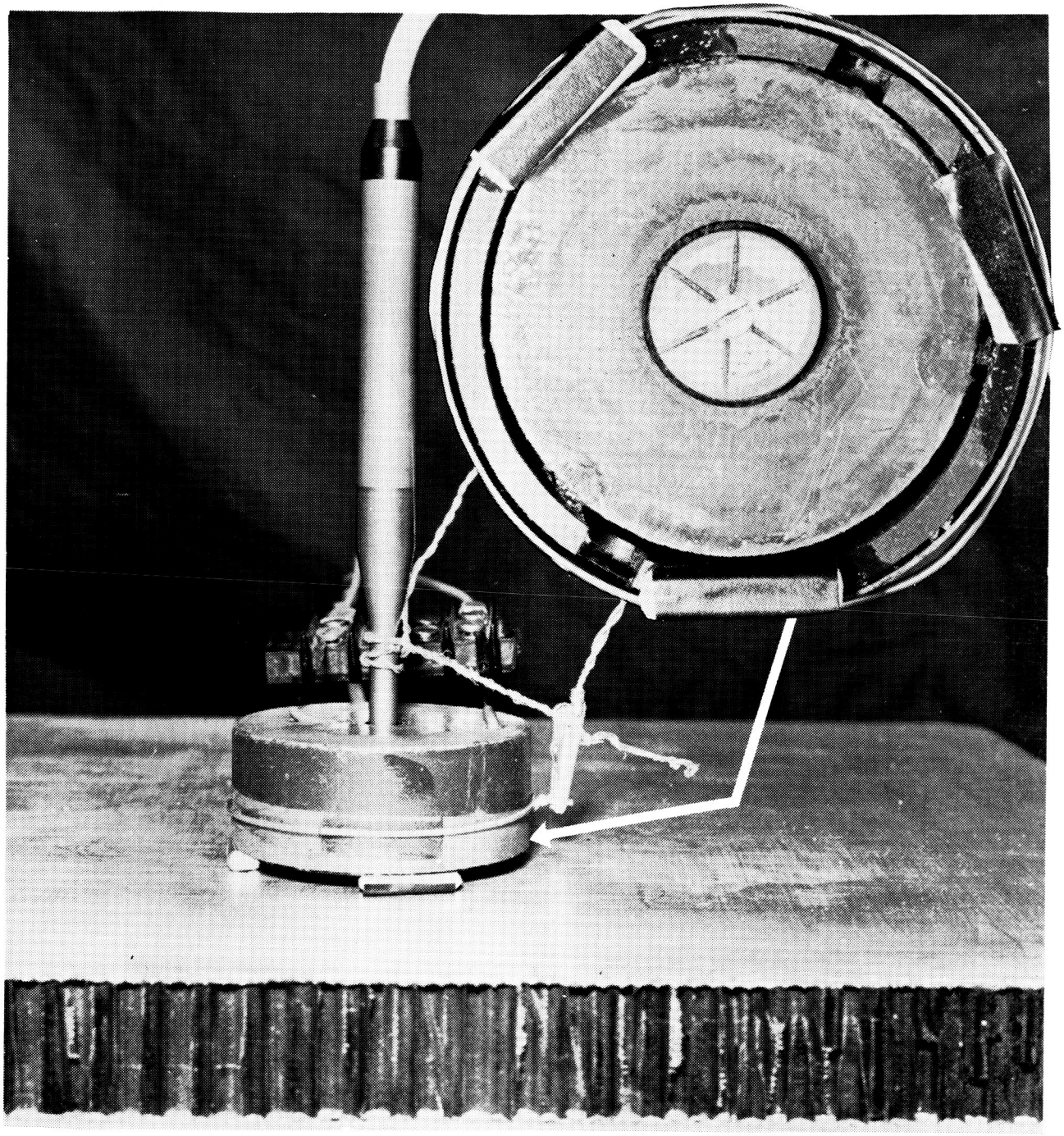

Figure 13. DOT Transducer, Side View, Showing Ferrite Cup and Microphone Probe, Bottom View, Showing Slotted Capacitance Detector

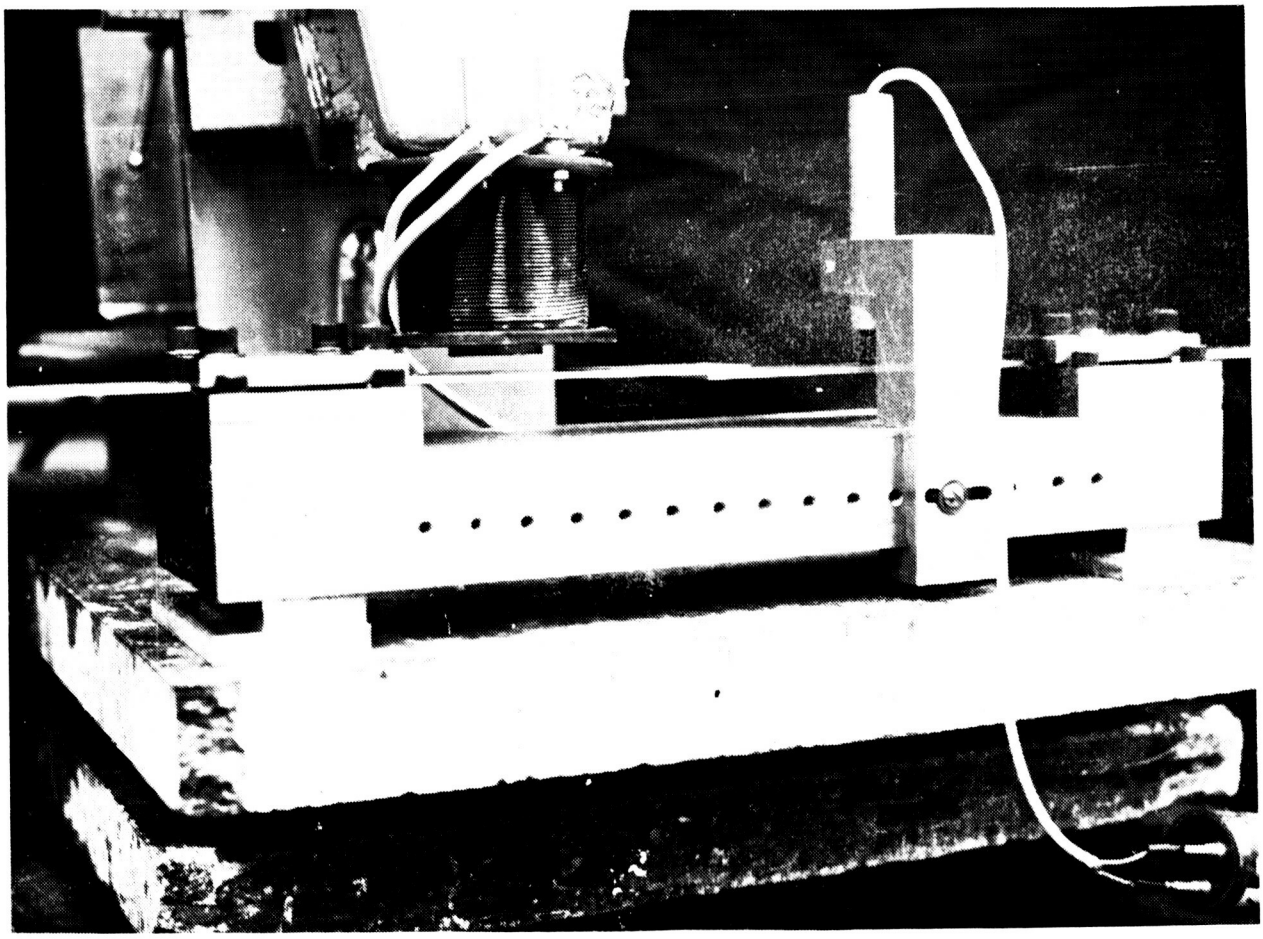

Figure 14. Lap Shear Specimen Fixture, Driver, and Displacement Transducer

was measureable. The calculated band-width checked again at 4 Hz. The following response relationship was used for calculation of bandwidth. The idealized response of a simple beam is:

$$A = \frac{KF(v)}{\sqrt{f^2 - f_n^2\, t}}$$

where

A = vibration amplitude
F(v) = Driving force
f = Frequency
f_n = Resonant frequency
Δ = Logarithmic decrement
K = Constant

and according to ASTM METHOD C-215:

$$\Delta = K\frac{\Delta f}{f_n}$$

where

f = frequency bandwidth at half amplitude points.

HONEYCOMB SPECIMEN TESTS

The DOT transducer was next evaluated on a properly bonded specimen representing the Saturn common bulkhead. A constant current of 0.63 ampere was used to permit comparison of relative vibratory modes. The displacement probe was partially shielded to reduce noise and a Wagoner ground system was employed to reduce or balance out ground currents. The transducer was placed on the composite at an approximate 0.003-inch spacing and the total displacement was indicated by a 9-millivolt signal. The noise level was high, evidently due to electrostatic coupling. By further isolating the cathode follower, the displacement signal-to-noise ratio was improved by a factor of three. It was shown that second harmonic signal response was caused by face sheet displacement because if the transducer was lifted 0.01 inch above the composite, the second harmonic signal disappears. The adjustment of the Wagoner ground greatly affected the second harmonic response. With the ground adjusted for

minimum fundamental drive, the second harmonic response was not a function of the composite since the signal was evident when the transducer was elevated. A check was made of the transducer electromagnetic field at 10 KHz by using a small six-turn pick-up coil. The field was rich in harmonics, and showed a second harmonic drive signal with an amplitude approximately one-third of the fundamental drive frequency. In order to further reduce the second harmonic drive, a guard circuit was installed to surround the displacement probe. The maximum noise reduction at 10 KHz was achieved with a grounded guard. From 100 Hz to 7. 5 KHz excitation, the ground or driven guard reduced the noise level by a factor of 3. A frequency scan was made and the relationship between the displacement of the composite facing sheet as measured at the second harmonic and frequency was determined. The second harmonic displacement measurements were not possible above 15 KHz due to excessive harmonic generation by the transducer.

A plot of the frequency response of the honeycomb showed a number of peaks that proved repeatable and appeared characteristic of the specimen. However, the copper plated teflon probe was not considered sufficiently rigid and was replaced by glass plate silver coated to form the capacitance electrode. The opposite side of the glass was silver coated to provide a grounded guard circuit. The internal surfaces of the ferrite cup were also silver coated to further shield the drive system and provide a connection to a common ground. The improved DOT transducer (Figure 15) was evaluated on several aluminum sheet and plate surfaces; these tests proved highly repeatable with second harmonic responses indicated up to 8 KHz drive frequency without significant interference. An analysis of the honeycomb response to the vibration showed that the amplitude of vibration of the top sheet on a honeycomb in response to an external driving force is a function of the elastic properties of the sheet itself and by the stress/strain/time relationship of the bonds underneath the area being driven. If the elastic response of the unbonded sheet is known, then the bond strength which is determined by this relationship could be measured by the amplitude of vibration over a range of driving frequencies. A transducer which acts on an area encompassing several honeycomb cells will see evidence of very weak bonds in the form of a large amplitude (resonant) response at low frequencies as compared to the lowest resonant frequency of a single honeycomb cell. As the bonds get stronger, this low frequency resonance will disappear, and the response should have small amplitude and move toward higher frequencies.

The determination of bond strength by this technique hinges on an accurate description of the behavior of the unbonded sheet and on the development of a method for analyzing the frequency response in terms

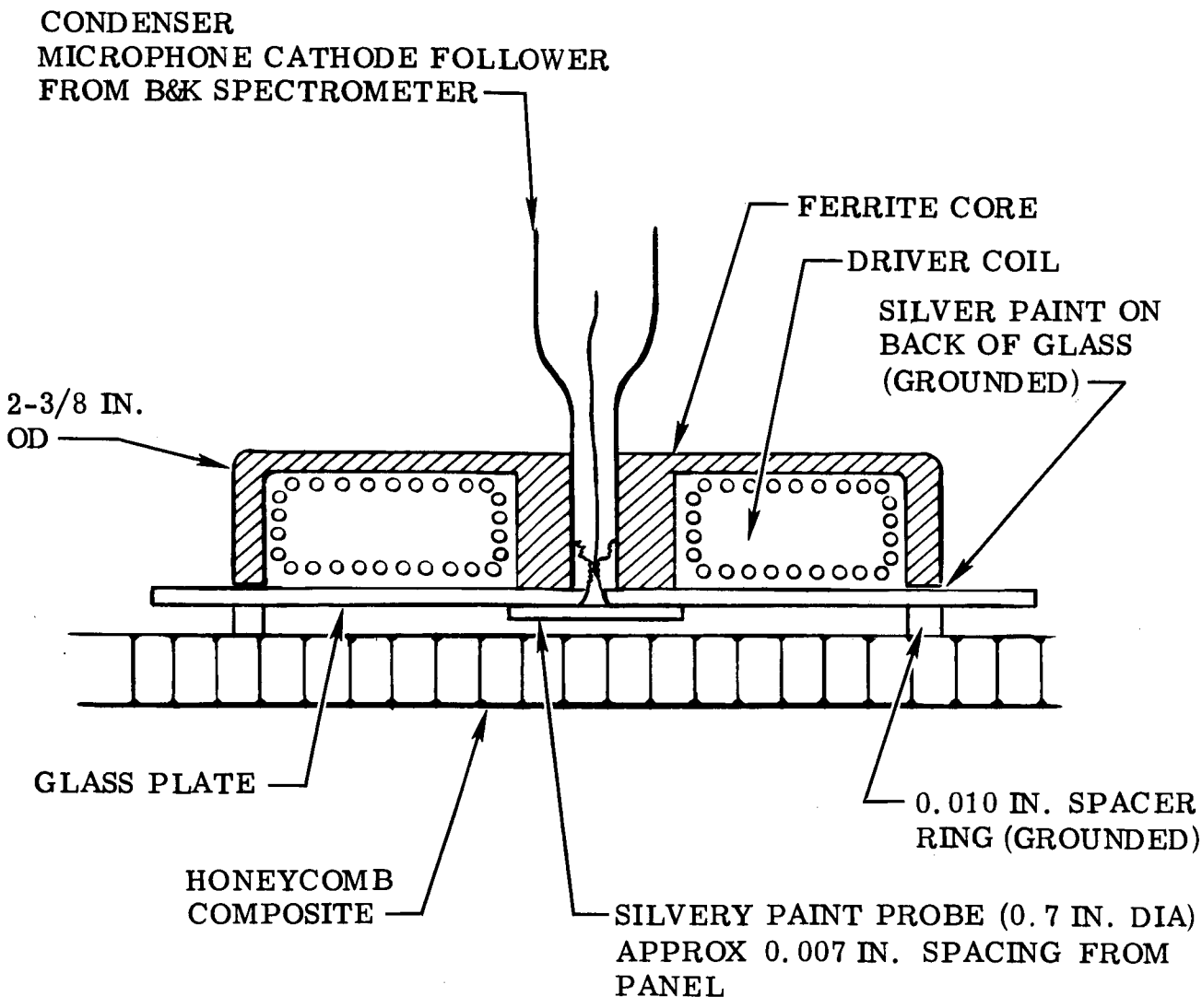

Figure 15. Improved DOT Transducer With Grounded Guard

of the character of the bonds. The first requirement can be met by direct measurement on unbonded sheets of the same thickness and composition. The second requirement is best satisfied by a mathematical analysis of the dynamics of a bonded sheet. In fact, this analysis can be carried out in terms of the much simpler dynamic response of an unbonded sheet through the application of Green's function techniques to the differential equations describing the vibration of the surface. Appendix B discusses the mathematical analysis establishing this response.

A series of experimental tests were conducted to evaluate the dynamic response of Saturn honeycomb composites of varying bond strengths. The specimens (described in Section II) ranged from composites with areas of the core and one facing sheet removed, leaving only the top facing sheet, triangular under cut core disbonds, and varying degrees of bond degradation ranging from 5 to 80 percent. The procedures followed in performing the tests with the DOT test system (Figures 16 and 17) are described in the following paragraph.

The DOT transducer was positioned on the honeycomb panel; the drive oscillator was then set at a lower frequency and adjusted to a preselected drive level of 0.63 amperes RMS. A frequency scan was made up to 8 KHz at 100 or 500 Hz increments, with readjustments as required for constant drive excitation. The spectrum analyzer was useful for preliminary frequency scans; however, the harmonic wave analyzer was necessary for quantitative data. Checks were made during each test to confirm second harmonic response indications by lifting the transducer. At the completion of the frequency scan, the data were analyzed to determine adequate definition of displacement peaks. Additional data points were added as required to accurately define the responses. The background noise of the DOT transducer system, due to electrical interference, varied from 0.01 to 10 millivolts depending on the test frequency. Since the displacement response of the honeycomb composites varied from only two to five times this amount, a measurement was made before and after each test, and the noise magnitude was subtracted at each test frequency. This standardization was performed by mounting the DOT transducer on a plexiglass disk, silver coated to simulate the ground effect from the top aluminum face sheet.

In order to obtain data, the vibratory response of the honeycomb facesheet with a complete absence of adhesive bond was determined. The first specimen evaluated was the S-4B-1 composite with 0.055 inch face sheets and undercut core triangular disbonds. A second defect was simulated by cutting a 3 inch diameter hole from the reverse side of the composite and removing the core and adhesive so that only the top face sheet was left. Vibration responses from a good bond area and the two defect areas was measured and plotted. Figure 18 shows these responses with minimal low frequency response in the good bond area, and high amplitude response - low

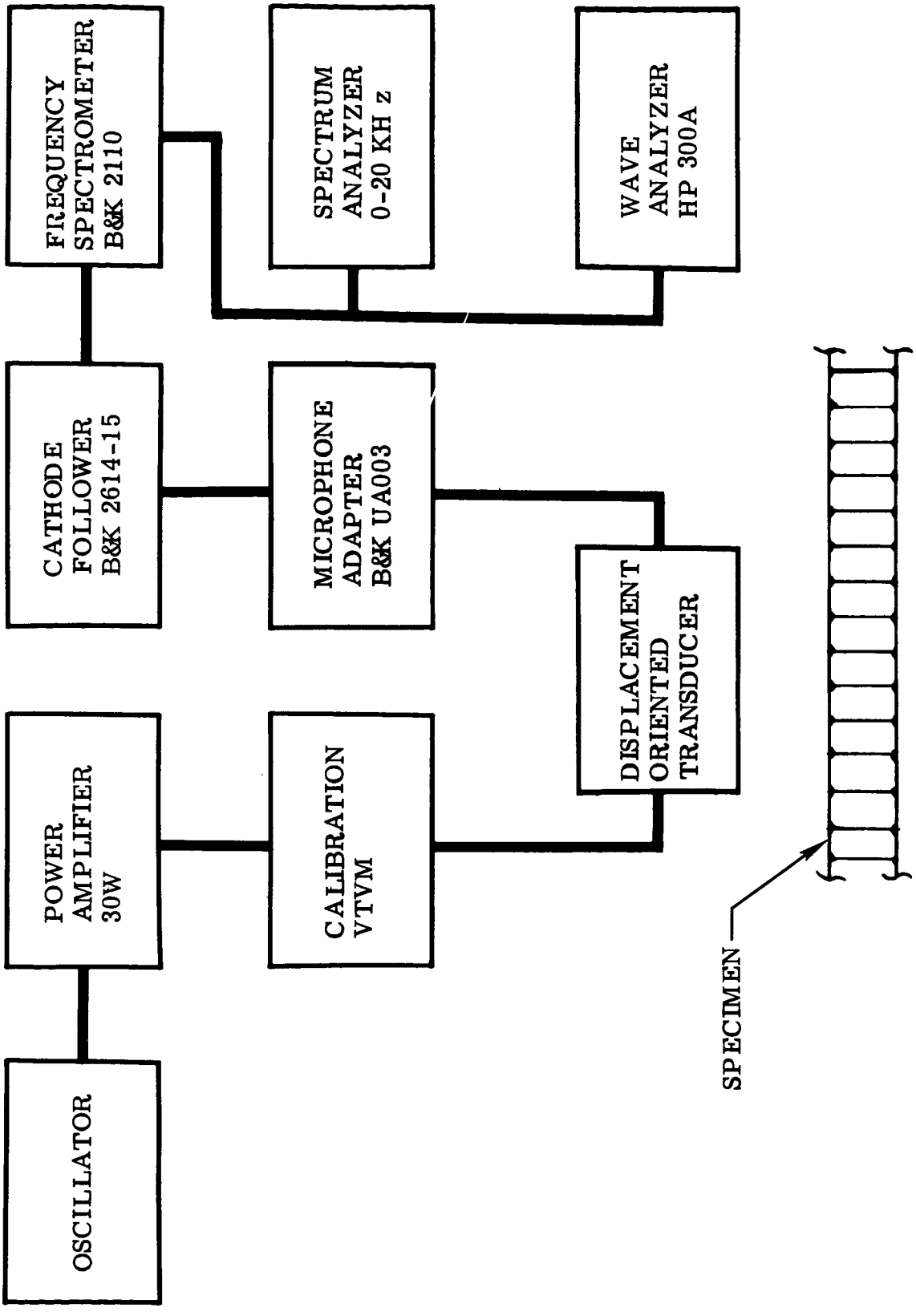

Figure 16. Block Diagram of Adhesive Bond Strength Test System

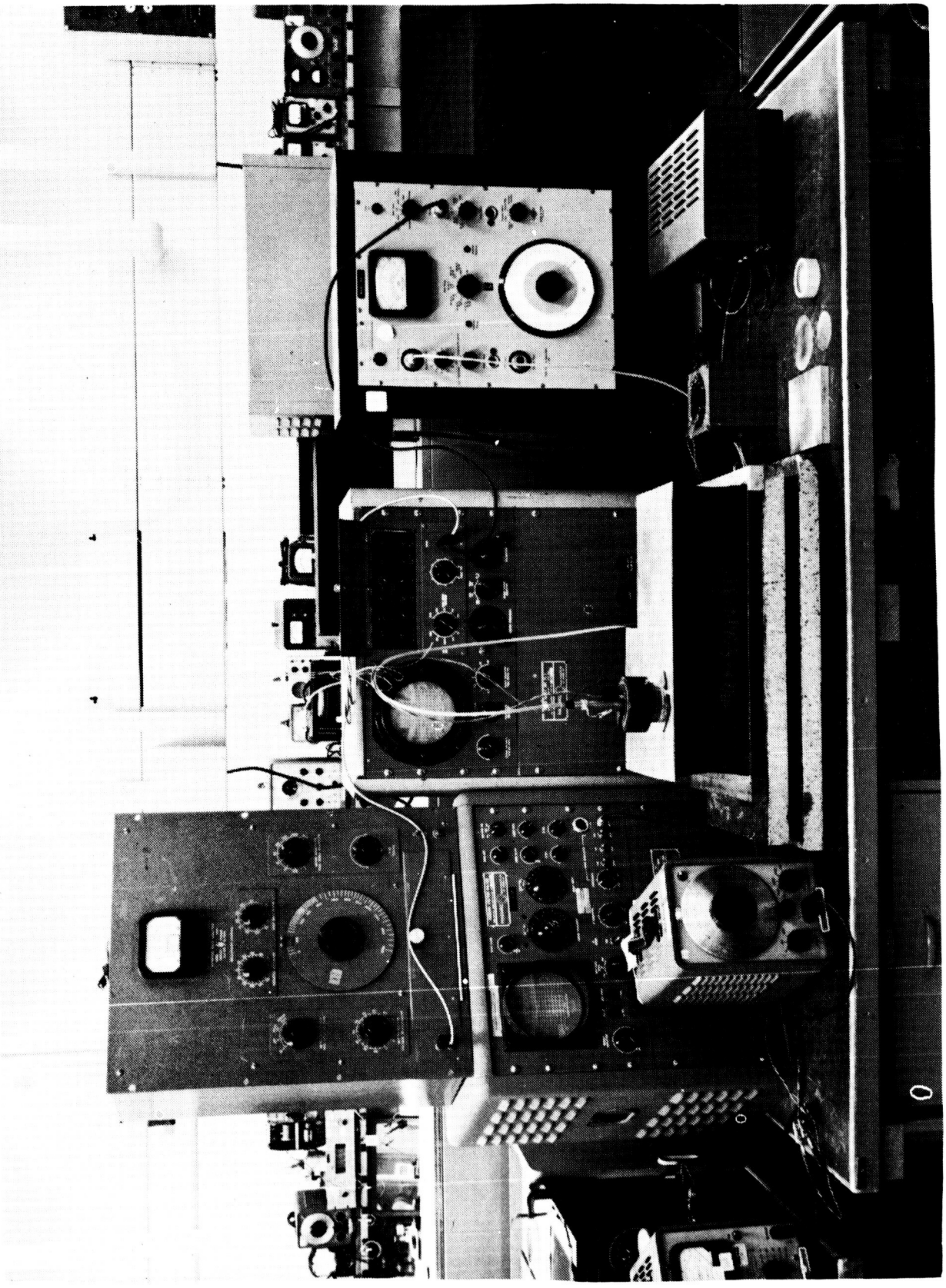

Figure 17. Adhesive Bond Strength Test System With DOT Transducer

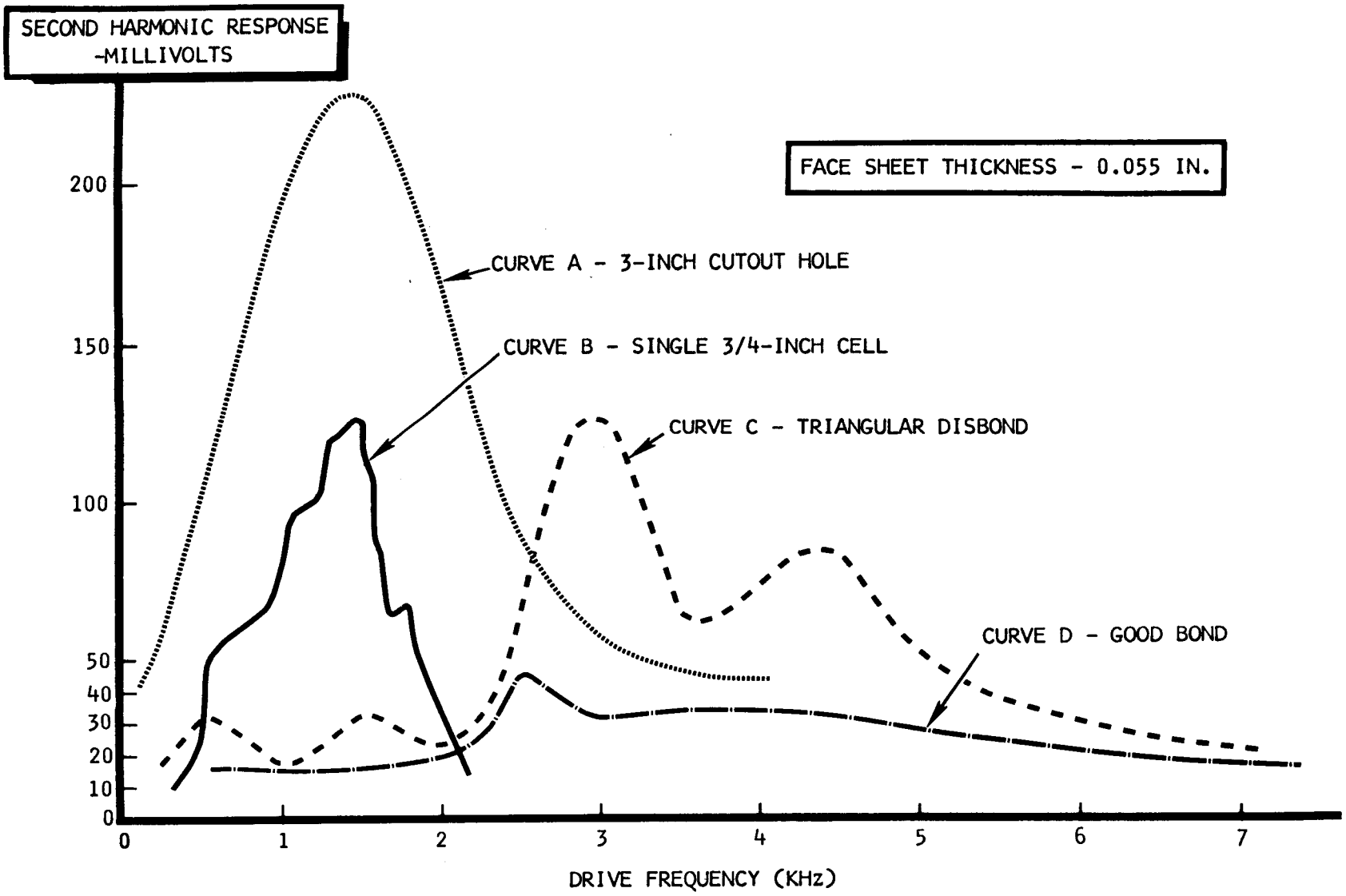

Figure 18. Vibration Response of Saturn One-inch Honeycomb Composite Measured With DOT System

frequency response for the removed core area. This is in agreement with the hypothesis for extreme cases of bond strength. Both the frequency range and amplitude of the response are significant. The low frequency response of the removed core area agrees with the predicted response based on face sheet vibration formulas for a sheet 0.055 inches thick with an unsupported area as defined by the diameter of hole.

The response plot indicates that the edges of the transducer act like artificial boundaries on the face sheet. The well bonded honeycomb area response did not show low frequency activity response and indicates that displacement is negligible in this frequency range.

Frequency response tests were subsequently conducted on a single 3/4 inch (nominal) HRP honeycomb cell to determine if the good bonding of the cell walls created a vibration boundary conditions. The response graph (Figure 18) shows that the cell does in fact form a boundary condition and response frequency that scales favorably with the peak frequency response of the 2-1/2 inch diameter hole. The scaling was accomplished by comparing the largest dimension of the nominal 3/4 inch cell with the 2-1/2 inch diameter hole, and by correcting for the thickness differences between facing sheets (0.040 and 0.055 inch).

Further evidence of this response relationship is shown (Figure 18) where a 1 x 2 inch isoceles triangular disbond was evaluated by the DOT system. The response referenced to the frequency scale shows evidence of at least two major vibratory modes and indicates that the response is at an intermediate frequency as compared to the honeycomb boundaried sheet hole and the well bonded honeycomb composite.

VIBRATION TESTS FOR HONEYCOMB BOND STRENGTH RESPONSE

A series of Saturn 4-3/4-inch thick honeycomb composites with various degraded adhesive bond strengths were tested with the DOT system. Correlation of the measured responses and corresponding flatwise tensile test data is given in Figures 19 and 20 for specimens with 0.032 and 0.040-inch thick facing sheets, respectively. A significant difference is noted in the responses with qualitative agreement with the expected behavior, i.e., the lower strength bond gives a greater response. The repeatability shown in Figure 20 is better than the differences between destructive test data from specimens taken from honeycomb composites. The second significant point is the apparent lack of expected frequency shift with bond strength. It was generally concluded that the response data were definitely correlatable with the differences in measured adhesive bond strength. A series

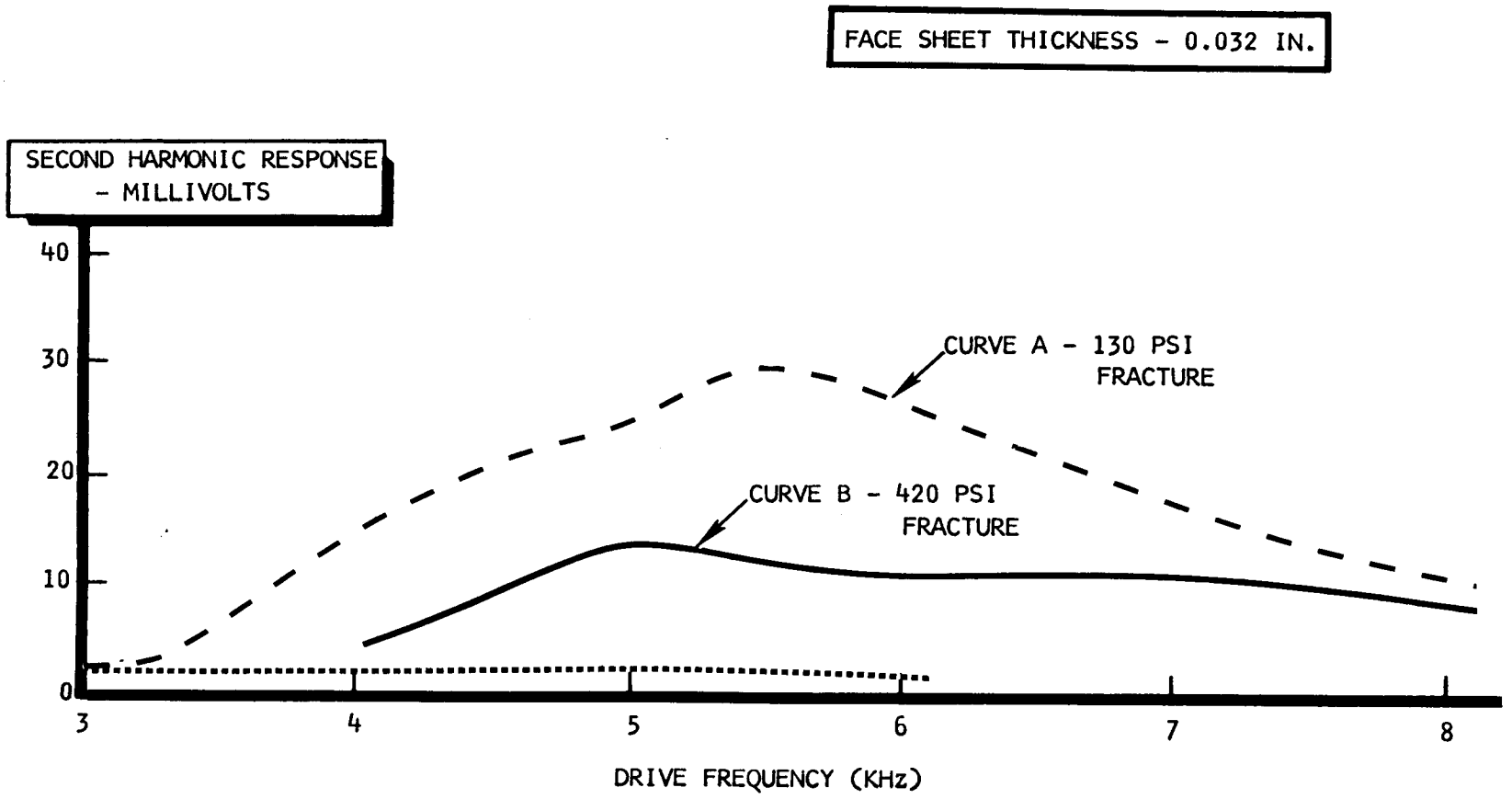

Figure 19. Vibration Response of Saturn 4-3/4 Inch (0.032 inch Face Sheet) Honeycomb Composite Measured With DOT System

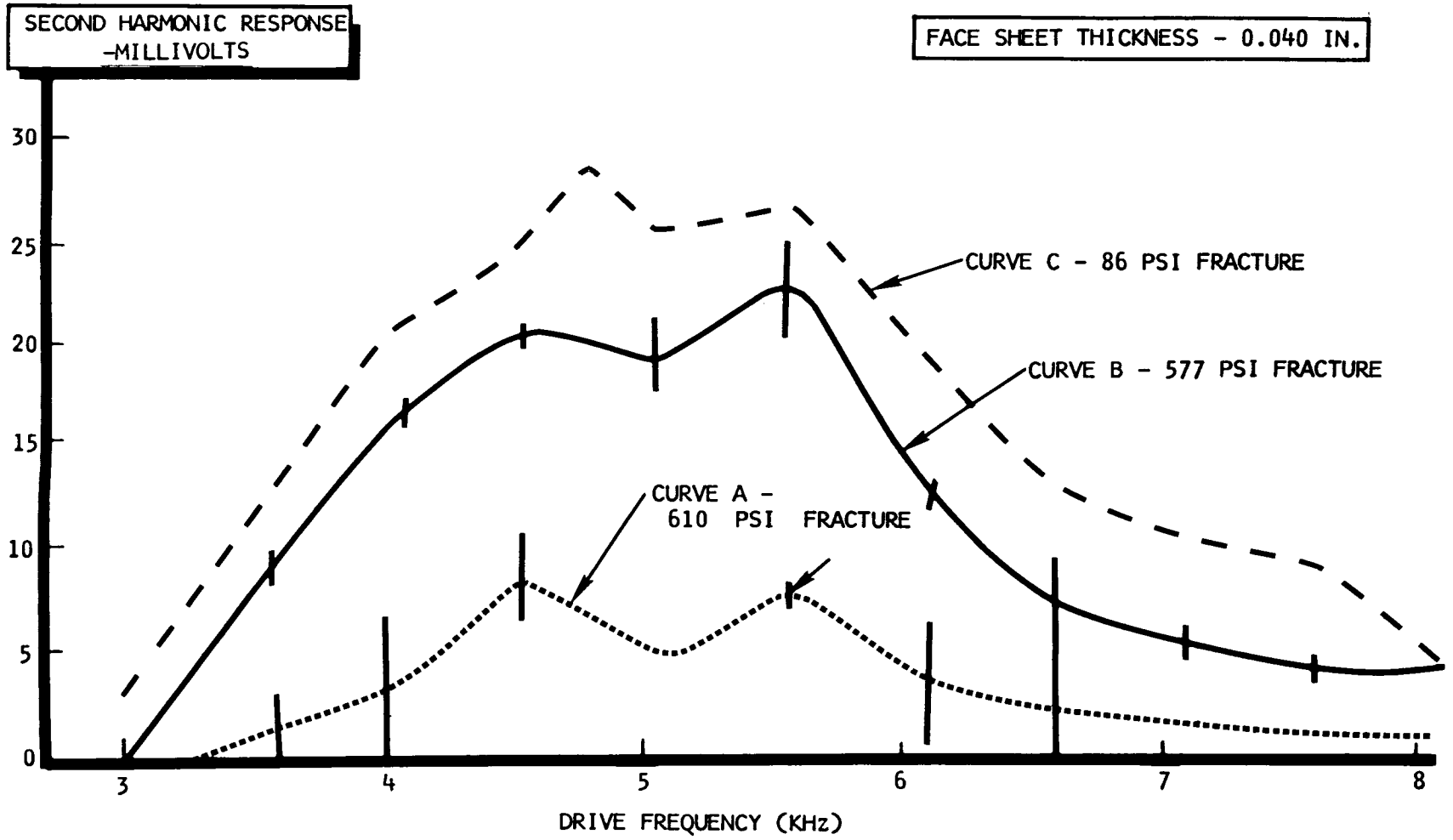

Figure 20. Vibration AC Response of Saturn 4-3/4 Inch Honeycomb (0.040 -inch Face Sheet) Composite Measured With DOT System

of lower frequency response tests were conducted on the same composites; the results are plotted in Figure 21.

DISCUSSION OF RESULTS

Qualitatively, the response data from the varying bond strength composites is in agreement with the expected behavior, i.e. a low strength bond gives a greater response (figure 22). Quantitatively, the results are not completely understood, probably because of the limited number of tests. In particular, two questions are raised and indicate the need for further experimental effort. The first is that the response amplitude does not seem to be directly proportional to the measured bond strengths. However, it is not presently understood whether the flatwise tensile tests are as accurate as the vibration response measurement. It might be that the tensile test, using 2 x 2 x 4-3/4-inch specimens, averages over 5 or 6 times as many honeycomb cells as the DOT transducer, and may reflect the strength of the strongest cells in the bond. Experimental tests could be conducted using one, two, three, etc., honeycomb cells in flatwise tensile tests to establish the width of distribution of honeycomb cell strength about some average value.

The second point is the lack of apparent frequency shift with bond strength. The reason for this deficiency is not completely clear, but may well be associated with the clamping condition imposed on the honeycomb sheet by the DOT transducer dimensions. This result may be related to the appearance of a response at very low frequencies in the low bond strength composite.

CONCLUSIONS AND RECOMMENDATIONS

The adhesive bond strength determination tests performed to date demonstrate a relationship between bond strength and the vibration displacement amplitude for the face sheets of the honeycomb composites. Such a system could be utilized in an automatic inspection system; it has the distinct advantage of providing non-contact bond strength measurements. Experimental transducer-to-composite spacings were varied from 7 to 10 mils; but an improved driver may be able to operate with spacings up to 50 mils. The response of the DOT system will decrease inversely as a function of transducer spacing; this response can be compensated by driver improvements.

The tests reported measured the near-side adhesive bond damping. It is reasonable to expect that variation in far-side bond strength will also affect the response of the transducer by virtue of the rigidity of the core material and far-side adhesive joint. Some far-side response has been

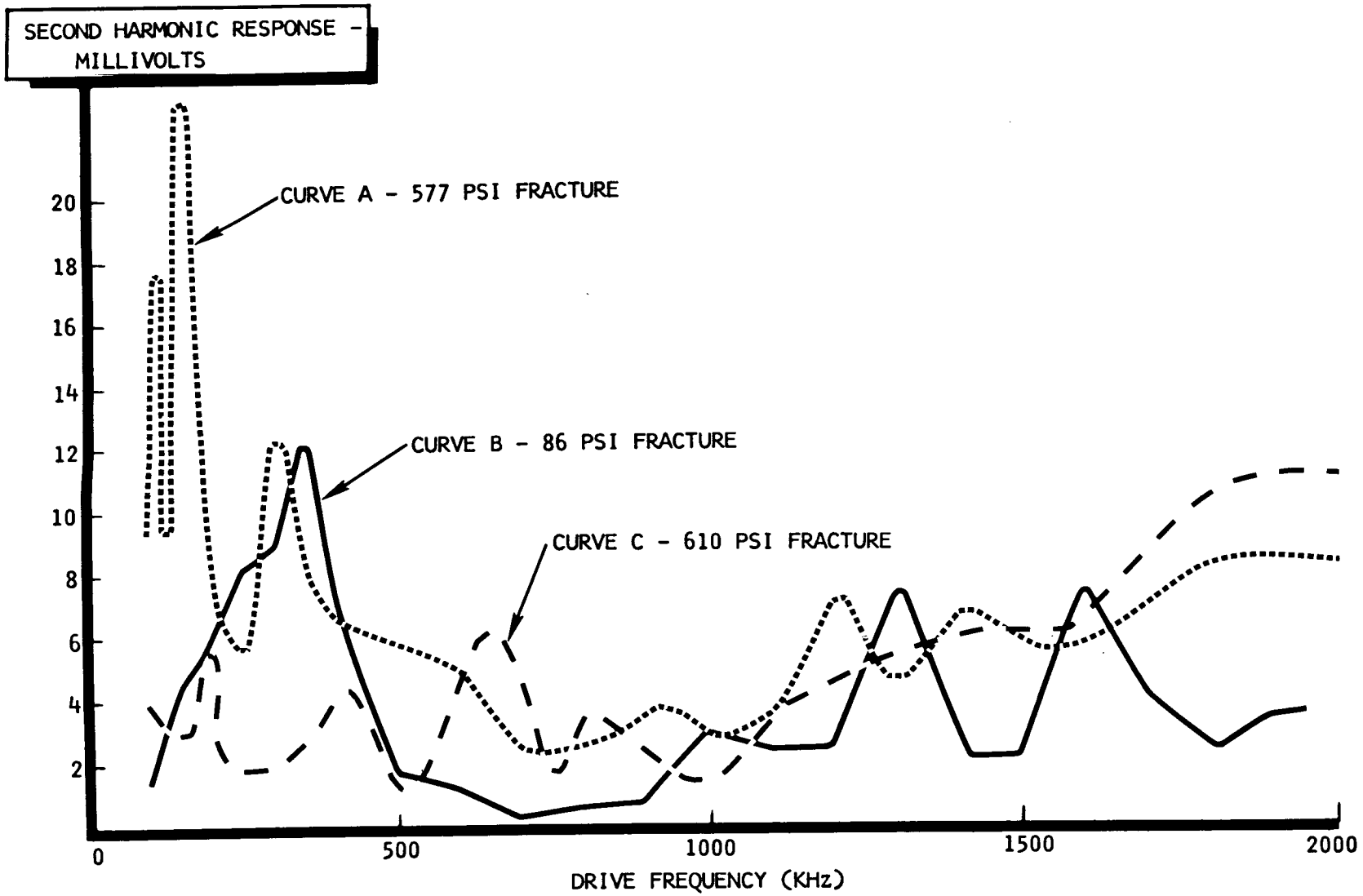

Figure 21. Vibration Response of Saturn 4-3/4 Inch Honeycomb Composite With DOT System - Low Frequency

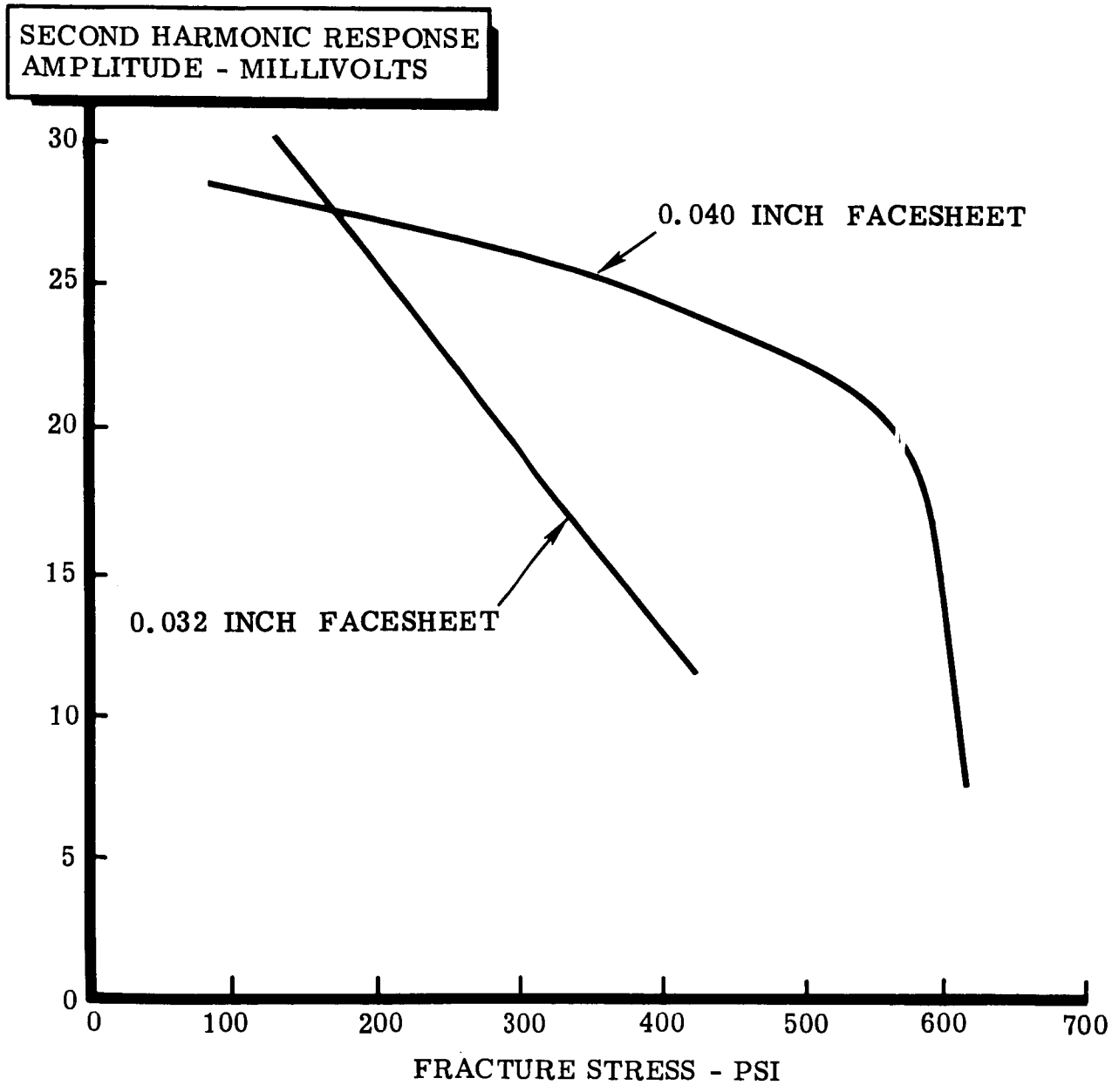

Figure 22. Relationship of Vibration Response Versus Fracture Stress for Saturn 4-3/4 Inch Honeycomb Composite

noted during the testing but quantitative data were not measured. Based on the results of measurements, the following recommendations are presented to further develop this system into a practical bond inspection system:

I. Theoretical Analysis of Honeycomb Vibration Response

A beginning has therefore been made to determine the natural resonant vibrational frequency of a honeycomb panel by analytical methods. The approach should start with simple cases and systematically eliminate one assumption after another until reasonably good agreement is obtained between theory and experiment. The following factors are being considered: 1) Honeycomb dimensions; 2) Mechanical properties of facing sheet and core; 3) Bond strength of facing sheet-to-core adhesive; 4) Minimum number of cells which must be tested simultaneously to obtain a statistically reliable result.

The approach plan is illustrated in figure 23. The first case to be studied should be that of the continuous bar supported elastically at many evenly spaced points. From there an extrapolation can be made to a plate under conditions of linear support and of supports spaced out over an area. The elasticity and strength properties of support taken into consideration represent the bond strength. The analysis should then be extended to the case of a single cell with facing sheets at both ends and rigid walls. This represents a drum, where the vibrational properties of the contained air must be taken into considerations. The "drum" case should then be extrapolated to the case of a drum with flexible walls and finally to a number of cells joined together.

II. Experimental Program

A. Variation and optimization of transducer parameters

(1) With respect to boundary conditions transducer size (OD, capacitance pick-up areas, number of cells included, etc.).

(2) Exploration of various means of excitation and detection. These should include electromagnetic and electrostatic drivers with capacity and FM detection techniques.

(3) Extension of the transducer frequency range.

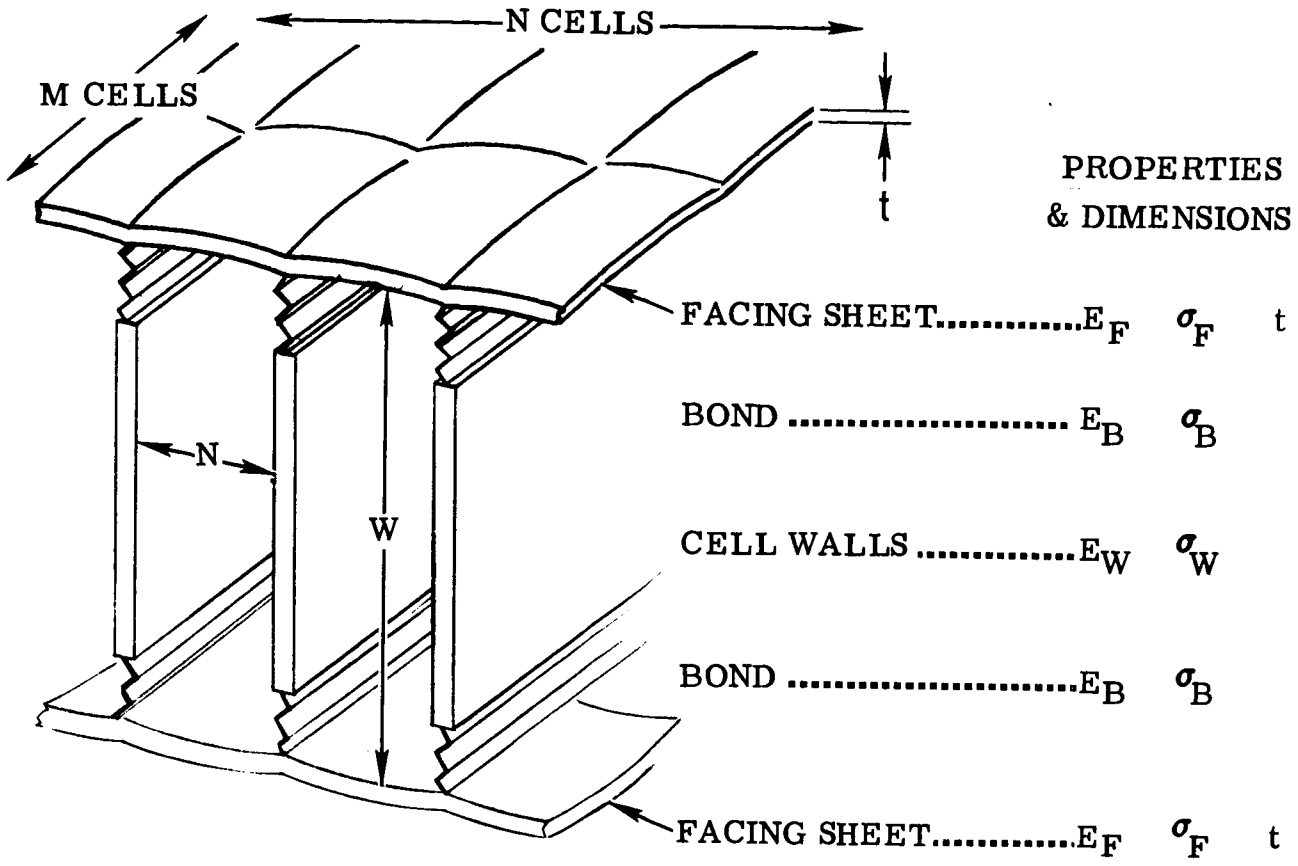

	I	II	III	IV				
	ONE DIMENSIONAL	TWO DIMENSIONAL		DRUM CASES →				
M	0	|	∞	|	|	|	|	∞
N	∞	∞	∞	|	|	∞	∞	∞
BOND	FINITE	L I M I T E D →						
CELLS	0	0	0	RIGID E_W, etc		RIGID E_W, etc		E_W

Figure 23. Schematic Diagram and Analysis Modes for Honeycomb Vibration Study

B. Characterization of optimum transducers with various honeycomb specimens for near and farside bond strength.

(1) Static and dynamic tests (automatic) to determine distribution in strengths of unit cells in honeycomb by destructive and nondestructive tests.

(2) Correlation on, and analysis of results on these panels with transducer responses.

III. Systems Development

A. Frequency Scan System

The basic system would display response of transducers as a function of a swept frequency drive system. Based on the preliminary results, such a display should result in an "anelastic" signature of the honeycomb composite, which is related to bond strengths.

B. Regenerative System

This system mode would employ a feedback system so that the transducer signals would be made a part of a closed loop oscillating system. A measurement of the power necessary to sustain a given amplitude of oscillation (properly phased) should then be proportional to the bond strengths.

In addition, this approach is particularly adaptable to the use of a feedback piezo-electric crystal system in which the damping characteristics of the adhesive are used to alter the Q of the resonant circuit.

IV. Systems Design

A. Based on results of exploratory configurations given in Item III, a final system design could be established for production application.

Section V

IMPEDANCE SYSTEM CHARACTERIZATION

TECHNICAL APPROACH

Ultrasonics has been used in nondestructive testing of honeycomb composite structures, but conventional ultrasonic methods required modification because of the special features of structural geometry and material composition of honeycomb composite. The composite can be acoustically energized throughout its entire thickness, but the overall complex acoustical interactions can be measured at one of its external surfaces as a lumped quantity. Though a change of this lumped quantity measurement indicates the presence of defects in the honeycomb composite, it is very difficult to discriminate between various types of defects.

An idealized solution to this problem is to develop special types of testing techniques, each of which is tailor-made for detecting only one type of defect. The theoretical approach described in the following paragraphs is taken toward this aim. The predominant defect considered is disbond at the adhesive interface between face sheet and honeycomb core.

Each cell of a honeycomb is a drum or tube with closed ends. As a first approximation, the cell walls are assumed rigid and air friction at the cell walls as negligible. A plane wave of sound may be produced in the air confined in each cell through an appropriate source at one of the external surfaces of the honeycomb composite. As the plane wave propagating one end of the cell impinges on the other end, a reflected wave is generated in the cell and a transmitted wave in the face sheet forming that end of the cell. The presence of both incident and reflected waves in the cell produces standing waves. If not all the acoustic energy is reflected, the incident pressure amplitude will differ from the reflected pressure amplitude. The result will be a maximum pressure amplitude at points where the two waves are in time phase, and a minimum pressure amplitude at points where the two waves are 180 degrees out of time phase. The ratio of the maximum value to the minimum value is called standing wave ratio, which is often used for determining acoustic impedance of a material.

Any plane surface normal to the direction of a plane wave propagation in the tube possesses a specific acoustic impedance defined as the complex ratio of the sound pressure at the surface and the particle velocity into the surface

at normal incidence. The terminating impedance at the reflecting surface can be calculated by the following equation:

$$Z_t = Z_o \frac{1 + \frac{Pr}{Pi} \exp(j\psi)}{1 - \frac{Pr}{Pi} \exp(j\psi)} = Z_o [\phi] \qquad (1)$$

where

Z_t = terminating impedance = specific acoustic impedance at the reflecting surface

Z_o = characteristic impedance of the medium for acoustic waves

j = static density of medium x sound velocity in the medium

$\left|\frac{Pr}{Pi}\right|$ = absolute value of $\frac{\text{Pressure amplitude of reflected wave}}{\text{Pressure amplitude of incident wave}}$

$\left|\frac{Pr}{Pi}\right| = \frac{(\text{standing wave ratio})-1}{(\text{standing wave ratio})+1}$

ψ = phase angle between reflected and incident wave. The phase angle is related to the distance x of the first point of minimum pressure from the termination (reflecting surface) by

$$\psi = \pi - \frac{2\omega x}{c}$$

A knowledge of the specific acoustic impedance of the reflecting surface of a honeycomb cell can be utilized to differentiate a bond between core and face sheet and a disbond because values of the terminating impedance due to different boundary conditions affecting the impedance function ϕ of equation (1). Equation (1) has been used to measure the specific acoustic impedance of a material placed at the reflecting end of a tube in which a plane wave propagates, but it is not applicable to a honeycomb structure because both distant x and standing wave ratio cannot be determined without allowing the measuring device to have access to inside of the cell. However, the absolute value of specific acoustic impedance is not necessary for detecting a disbond since its presence can be noticed by a change of impedance. If a piezoelectric transducer is coupled to one of the external faces of a honeycomb panel, good bond and disbond at the interface between core and face sheet will produce a change in impedance of the crystal. This change can be measured by a number of methods. The first year of program effort included development

of an impedance bridge system adapted from the NAA Sonic Resonator, which proved successful in detecting disbonds at all adhesive interfaces in the Saturn common bulkhead and insulation composites. Further development effort was directed towards the evaluation and characterization of the impedance system parameters. For this purpose, the system performance was divided into several major tasks. The first task considered the electrical excitation source and detection signal processing characteristics. The second task considers the electro-acoustic and acoustic-electrical transduction, and the coupling characteristics. The third task considers the honeycomb composite nature and response for selected excitation levels and defects.

ELECTRICAL SYSTEM EVALUATION AND CHARACTERIZATION

The Sonic Resonator was originally designed to measure very small piezoelectric crystal impedance changes caused by composite anomalies. The system measured this impedance change by the use of a bridge technique. However, based on crystal optimization studies, crystal impedance changes in the order of 10 to 1000 are common and corresponding detection signals range from 0.1 to 10 volts. Because of this increased detection sensitivity, a number of alternate and more convenient electrical systems were considered. Four alternate crystal detection systems were evaluated. These included the constant current bridge, constant voltage bridge, a rectified crystal detection system, and a piezoelectric oscillator-self tuned system. The latter system was named POST for identification. Schematics of the four systems is shown in Figure 24. The impedance bridge system is a bridge nulling system wherein the crystal is balanced against an adjustable R-C circuit. Variable loads applied to the bridge affect the bridge balance in terms of impedance and are correlatable to composite anomalies. The constant voltage bridge configuration required maintaining constant crystal voltage at 10 volts and measuring the changes in crystal current with an RF thermocouple milliammeter. The constant current bridge utilized a 55 watt power amplifier to excite the bridge, to maintain a reference voltage of 10 volts on the crystal.

The Rectified Crystal Detector excites the crystal through a series resistance from an oscillator adjusted to the maximum sensitivity frequency for the crystal. The AC voltage across the crystal is rectified, filtered and adjusted by a variable power supply. The honeycomb disbonds cause an impedance change in the crystal which is in turn measured with a DC voltmeter. The advantage of this system over the bridge circuits is that a single nulling adjustment is employed, replacing the two interacting R and C adjustments of the bridge. Further, harmonics generated by the oscillator are readily nulled out with the series R circuit.

1. CONSTANT CURRENT BRIDGE

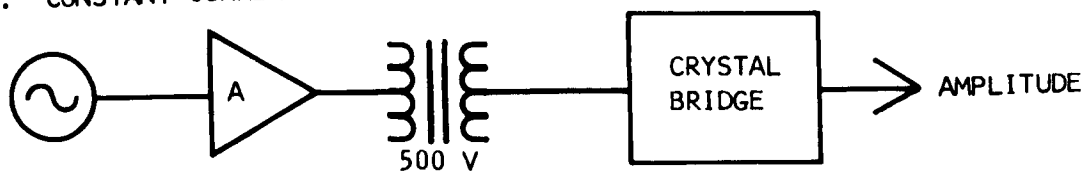

2. CONSTANT VOLTAGE BRIDGE

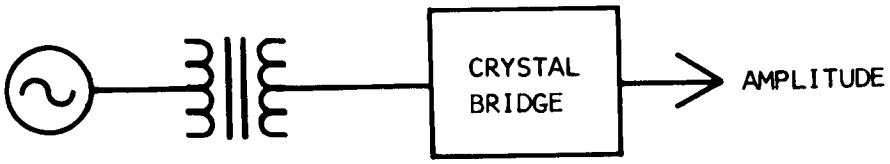

3. RECTIFIED CRYSTAL DETECTOR

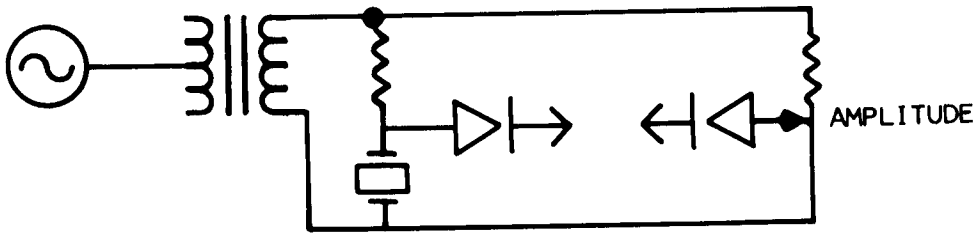

4. PIEZOELECTRIC OSCILLATOR - SELF-TUNED (POST)

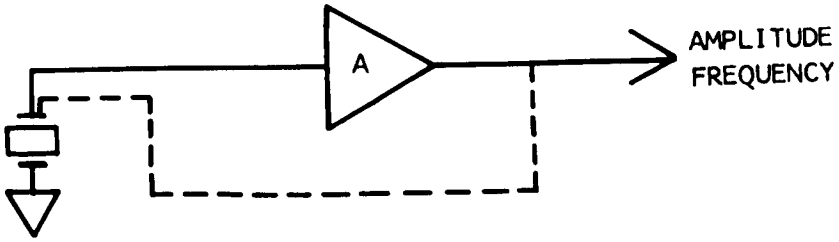

Figure 24. Schematic of Ultrasonic Test Methods

The Piezoelectric Oscillator-Self Tuned (POST) system was designed to self tune the detection crystal (Figure 25) to the composite thereby eliminating the need for frequency scans to determine the optimum sensitivity operating characteristics. This was accomplished by two crystal configurations. The first method consisted of isolating a portion of the crystal's electrode surface for feedback. The second method employed a second small crystal mechanically driven by the detection crystal for feedback. Both methods were tested and proven satisfactory for this system. The pickup signal was amplified, phased and fed back for crystal drive excitation. The POST system oscillates at the frequency where the detection crystal produces the maximum mechanical vibration. The gain and phase circuits may be adjusted to trigger or stop the crystal oscillation. The systems were evaluated by both static and dynamic tests.

The static tests were designed to provide comparative acoustic loading sensitivities. A number of acoustic loading systems were evaluated to reduce the errors inherent in attempting to locate a crystal in exactly the same place on the specimen without substituting material other than the Saturn honeycomb. The static load system finally adapted (Figure 26) used a crystal bonded to one side of a honeycomb specimen and a plastic bag of fluid and fine shot positioned on the opposite side. The bag was allowed to rest on the specimen surface, coupled by a film of water-glycerine and wetting agent fluid. The loading force proved to be exceptionally uniform and repeatable.

The 1 inch diameter, one inch thick crystal bonded to the lower side of the specimen was excited by the four trial electrical systems to ensure equalized test conditions. The basic impedance system was also evaluated to determine a sensitivity comparison. The crystal excitation voltage was adjusted to 10 volts for each test. The crystal frequency was adjusted to the voltage null which had proven to be one of the highest sensitivity points in previous experiments. A data summary for the five systems that were tested is given in Table VI. System sensitivity was calculated from the percentage

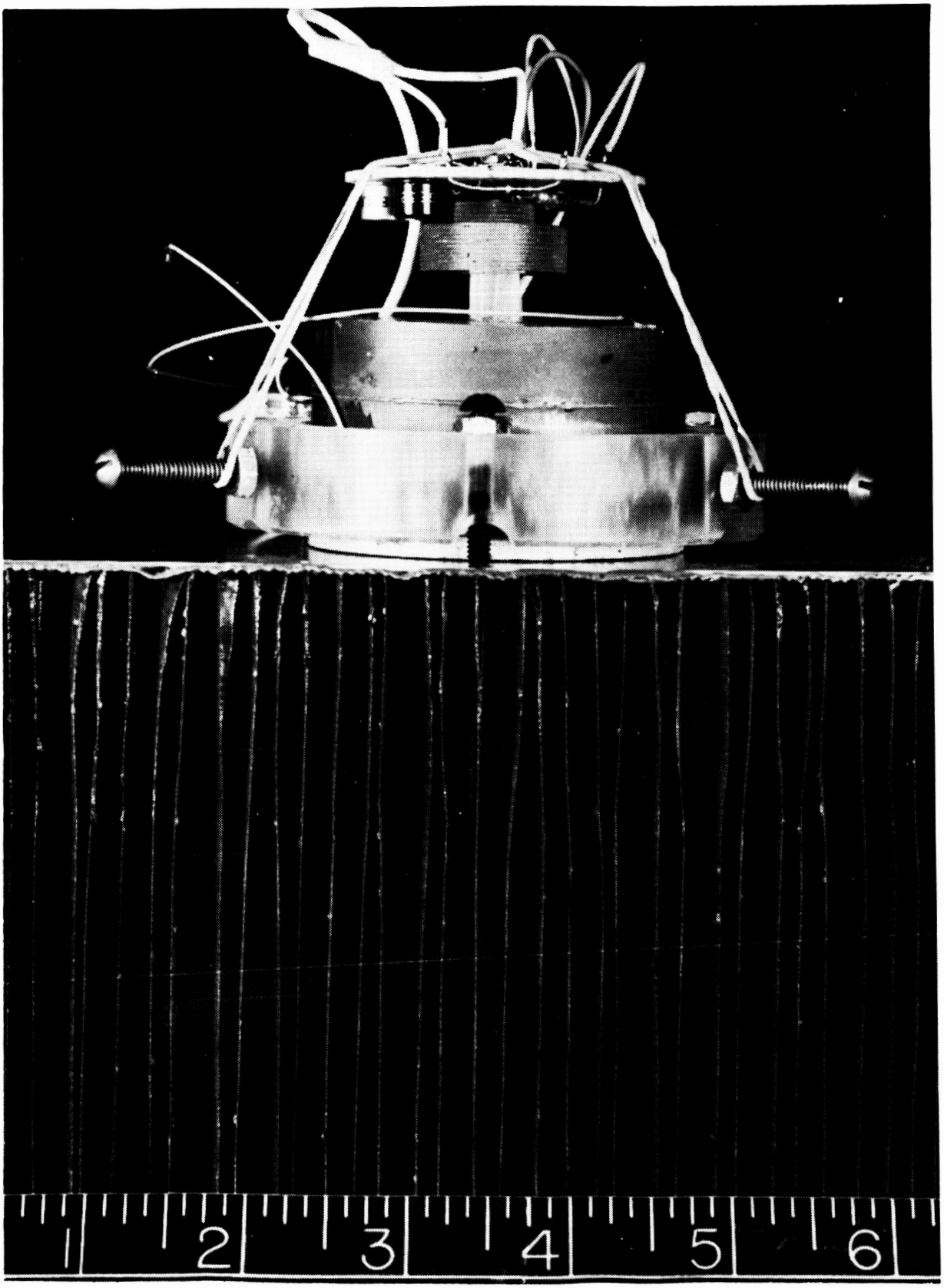

Figure 25. Post Transducer With Transistor Driver

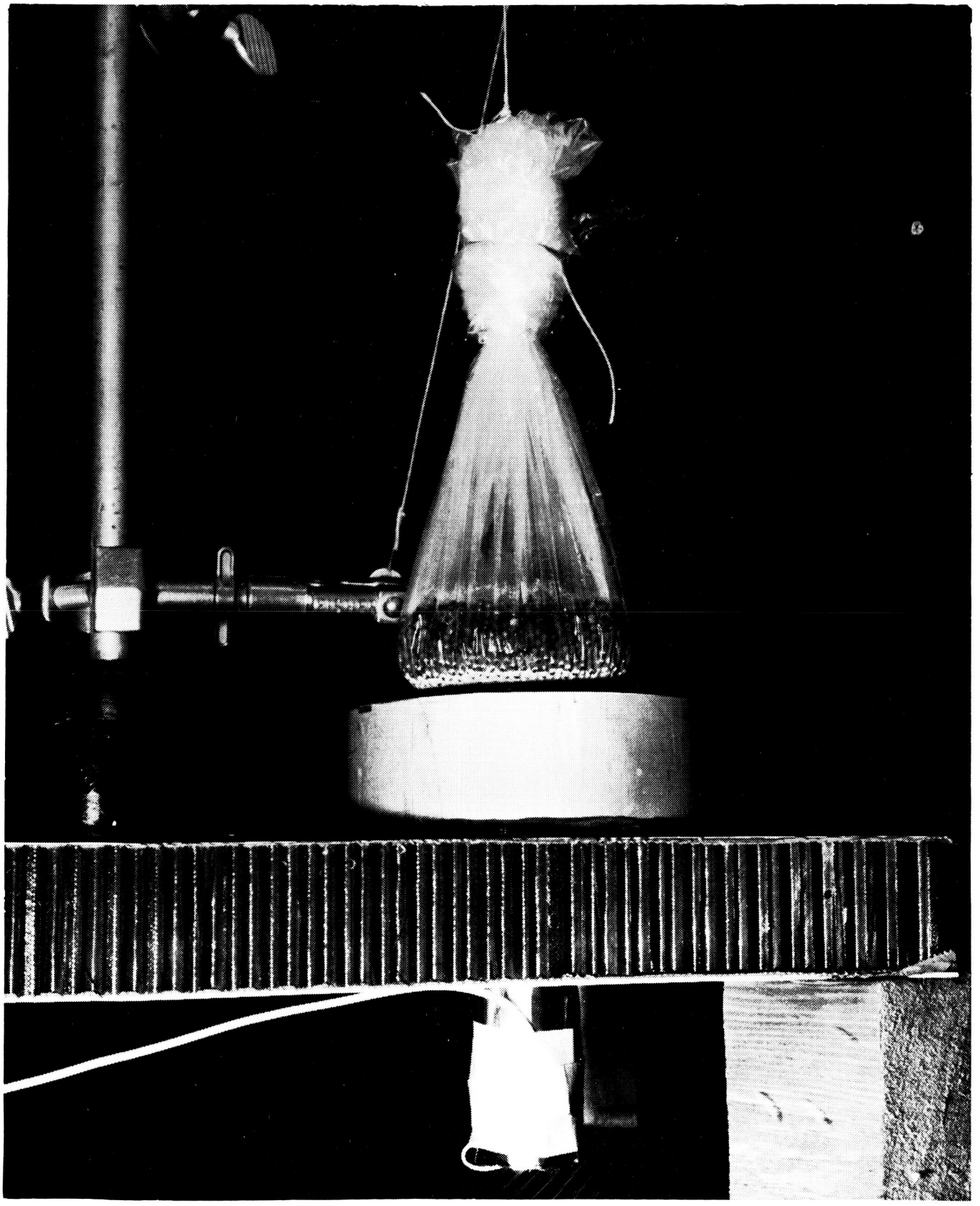

Figure 26. Static Acoustic Load for Ultrasonic System Evaluation

Table VI. COMPARATIVE EVALUATION OF ELECTRICAL SYSTEMS

	Unloaded	Static Loaded	Percent Change Crystal E or I
Impedance Bridge	5 MV AC	112 MV AC	1.12%
Constant Voltage	63 MV AC	108 MV AC	≈0.45%
Rectified Detector R = Z	0	74 MV DC	0.74 %
Rectified Detector R = 15Z	0	105 MV DC	1.05%
Constant Current	3.43 ma AC	3.37 ma AC	1.75%
POST System	10 Volts AC	0	∞

change in crystal voltage or current. The response sensitivity of bridge type circuits is indicated to be from 0.45 to 1.75 percent. Of these circuits, the Rectified Crystal Detector System showed the most significant improvement by requiring only one adjustment control. Increasing the series resistance to approximately 15 times the crystal impedance results in an approximate 25 percent increase in sensitivity. The sensitivity of the Piezoelectric Oscillator-Self Tuned System is exceptional and should be qualified by stating that the crystal oscillator was oscillating and stopped oscillation when the load was applied. The system may also be adjusted to oscillate by loading conditions such as disbonds. Dynamic tests were conducted using the 4-3/4 inch Saturn honeycomb composite with 3 inch intentional disbonds at the four adhesive interfaces. The Channelite 5500 1 inch diameter by 1 inch thick, and 2-1/2 inch diameter by 1-1/2 inch thick lead zirconate crystals were used for detection. The barefaced crystal was supported in a plexiglass ring and spaced approximately 0.006 inches above the specimen. The specimen surface was dammed and inundated with a water-glycerine couplant approximately 1/16 inch deep. The crystal frequency was adjusted, in all tests, for maximum displacement as measured by a crystal probe on the opposite side of the specimen. The crystal voltage was adjusted for 10 volts. The test results are shown in Table VII.

Table VII. COMPARATIVE EVALUATION OF ELECTRICAL SYSTEMS - DYNAMIC

	Crystal Dia. x Thickness (in.)	Disbond/Bond Ratio (on disbond layer)				Percent Change Crystal E or I on 4/5 Disbond
		1/2	2/3	3/4	4/5	
Impedance Bridge	1 x 2	10	6.3	0.9	2.3	8.5%
Impedance Bridge	2-1/2 x 1-1/2	6.6	5.0	0.4	2.3	22.9%
Rectified Detector R = 5Z	1 x 2	12	8.4	1.0	3	4.0%
Rectified Crystal Detector R = 11Z	2-1/2 x 1-1/2	14.2	3.7	-2	5.4	19.3%
Constant Current	2-1/2 x 1-1/2	8.4	4.7	-0.6	1.9	22.7%
POST System	2-1/2 x 1-1/2	670	690	520	740	7400%

The 3/4 disbond gave a negative signal change for the Rectified Crystal Detector, which is considered a usable detection signal. The POST system was connected to an amplifier which gave a 67 to 74 volt signal change over various disbond areas. The signal was zero over good bond areas.

PIEZOELECTRIC CRYSTAL CHARACTERIZATION

The ultrasonic crystal characterization was based on measurements of the crystal detection performance as defined by crystal excitation and detection in terms of voltage, frequency, current, impedance matching, coupling, and the material response. In addition, the crystal sensitivity was described in terms of the coupling, elevation, tilt angle and scanning parameters. The following paragraphs describe the experimental tests and the optimized crystal sensitivity characteristics. The tests were conducted using Channelite type 5500 crystals one inch diameter by one or two inch thickness, or

2-1/2 inch diameter by 1-1/2 inch thick, and Clevite type PZT-5A crystals 2-1/2 inch diameter by 1-1/2 inch thick.

CRYSTAL VIBRATION AND BEAM PATTERN TESTS

The use of piezoelectric crystals for ultrasonic measurement in systems requires a knowledge of the crystal vibrational characteristics. The use of improper supporting and/or positioning systems can seriously degrade the crystal sensitivity. The optimum frequency excitation mode for highest sensitivity is not necessarily at crystal resonance, but occurs at a frequency selected with the transducer coupled to the composite to be tested. Since the vibrating surfaces of the crystal and composite have displacements in the order of only 0.01 to 10 microinches, absolute measurements are difficult without precision displacement equipment and isolated background vibration conditions.

A simple piezoelectric displacement probe was developed to sense and indicate comparative crystal and composite vibrations under various supporting and loading conditions. The probe consists of a 1/10-inch thick, 1/2-inch diameter PZT-5 crystal with a 1/2-inch diameter, 3-inch long tungsten carbide backup rod silver epoxy cemented to one face, and a metallic wire cemented to the other crystal face. The wire was used to scan the vibrating surfaces of the crystal or composite. The probe was connected directly to a VTVM for voltage indication. A number of tests were conducted on a one-inch diameter, 2-inch long Channelite 5500 crystal. The crystal drive voltage was varied from 0.10 to 16.0 volts; relative displacement measurements indicated a relatively linear function up to approximately 10 volts. The face of the crystal was then scanned with the displacement sensor positioned at discrete points on the sides of the crystal. The displacement profile measurements indicated maximum crystal face displacement with three-point support system located at the center of the crystal. The displacement measurements across the face of the crystal appeared to be constant within 20 percent. Another displacement sensing probe consisted of an acoustic blast pressure sensor available from Channel Industries, Part No. PK 14-16. Vibration sensitivity measurements were conducted through a 4-3/4 inch thick Saturn honeycomb specimen. This technique used a 1/10-inch thick, 1/2-inch diameter PZT-5 crystal bonded to the bottom of the specimen. Maximum displacement signals occurred when crystal was located directly above the sensor.

An investigation was made to determine the crystal beam pattern in water. The two crystals tested included Channelite type crystals, one of which was one inch diameter by one inch thick, and two crystals each having a one inch diameter but one and two inches thick, respectively. The test system (Figure 27) included immersing the test crystal and scanning/detecting

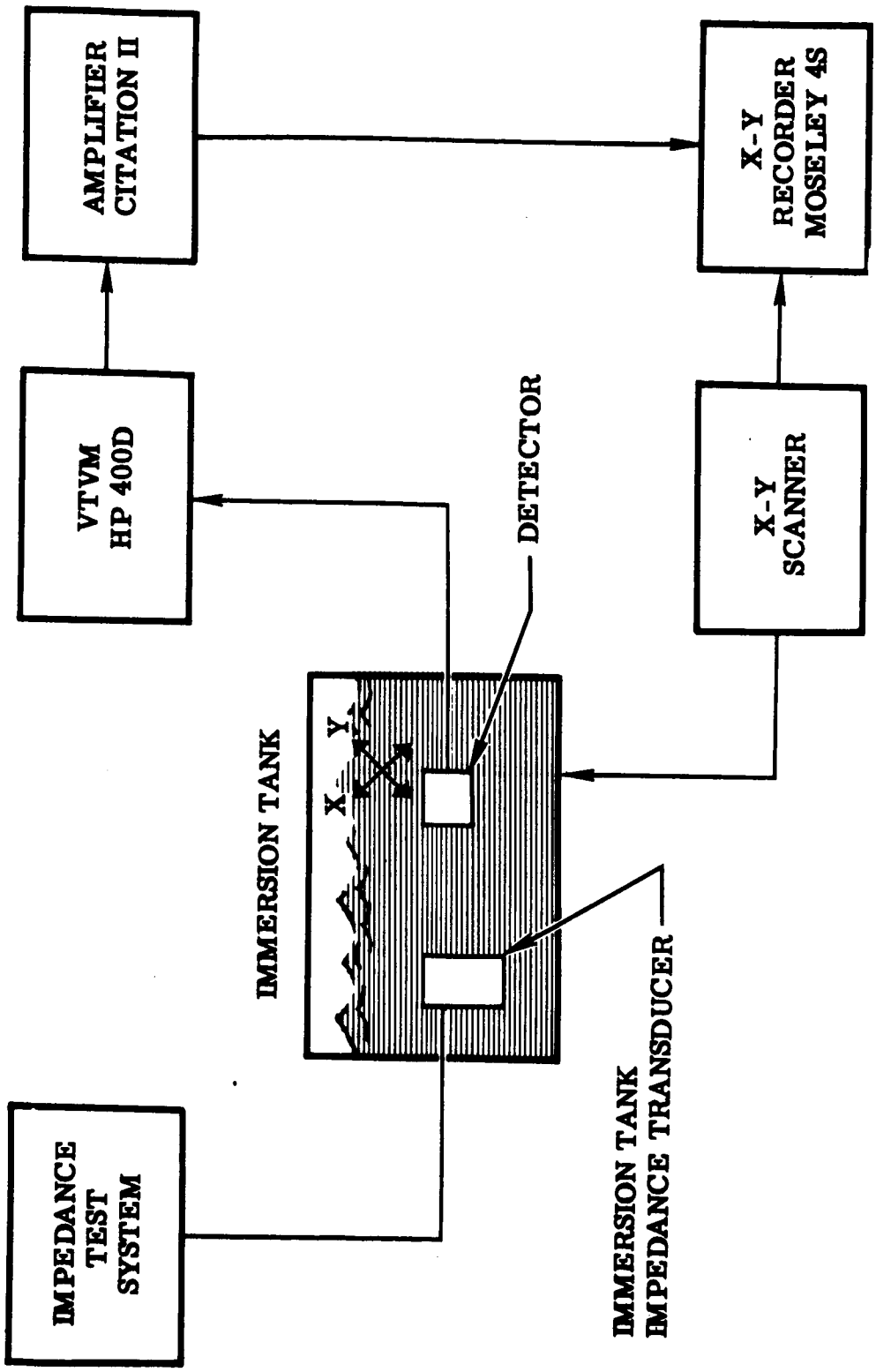

Figure 27. Crystal Beam Measuring System

the transmitted acoustic energy with the acoustic blast pressure sensor. The beam pattern for the 2-1/2 inch diameter by 1-1/2 inch thick crystal is shown in Figure 28. Scans were made at 1/2 inch increments. The maximum sensitivity scan at a 1/2 inch distance from the crystal face peaked at approximately 300 mv, and coincided with the centerline of the crystal. The background acoustic noise level was approximately 80 mv and was caused by reflections within the small immersion tank. A 4-3/4 inch honeycomb composite was immersed directly in front of the crystal and the same characteristic beam pattern was recorded. The peak sensitivity was reduced by a factor of 10. Similar beam patterns were observed for one-inch diameter crystals at reduced peak amplitudes. These tests showed two basic crystal characteristics, namely that the main acoustic beam is centered on the crystal axis, and that the energy is propagated through the honeycomb without significant beam pattern degradation.

CRYSTAL IMPEDANCE MATCHING

It has been shown by numerous authors that several methods are known to maximize the transmission efficiency of ultrasonic energy from one medium to another. Transducer arrays, focused transducers, and other techniques are commonly used to increase the acoustic energy intensity. In addition to these methods is the method wherein improvement and degradation of acoustic energy transmission is determined by acoustic impedance matching and mismatching. These transmission changes are all a function in changes in the specific acoustic impedances at the particular media interfaces in the acoustic transmission line. Specific acoustic impedance is the complex ratio of sound pressure to particle velocity at a given point in small signal linear wave field. Numerically, the specific impedance can be defined as ρc where ρ is the density, and c is the velocity of sound. This product is called the plane wave characteristic impedance of the medium. Calculations or measurement of the acoustic impedance of the Saturn honeycomb composite would have required a very complex and time consuming analysis. It was therefore decided to experimentally determine the effect of various liquid couplant transmission lengths to determine the optimum acoustic impedance match.

The experiment was conducted with a test system (Figures 29 and 30) employing a composite crystal transducer built up from Clevite PZT-5A crystals 2-1/2 inch diameter by 1/2 inch thick. The crystal disks were bonded into a 1-1/2 inch thick composite and sealed in a water tight holder. The transducer holder was acoustically isolated from reflective energies by a layer of cork. The electrical excitation and detection system employed a form of the Recitified Crystal Detector System using the single control adjustment feature but without cancellation of good bond signal.

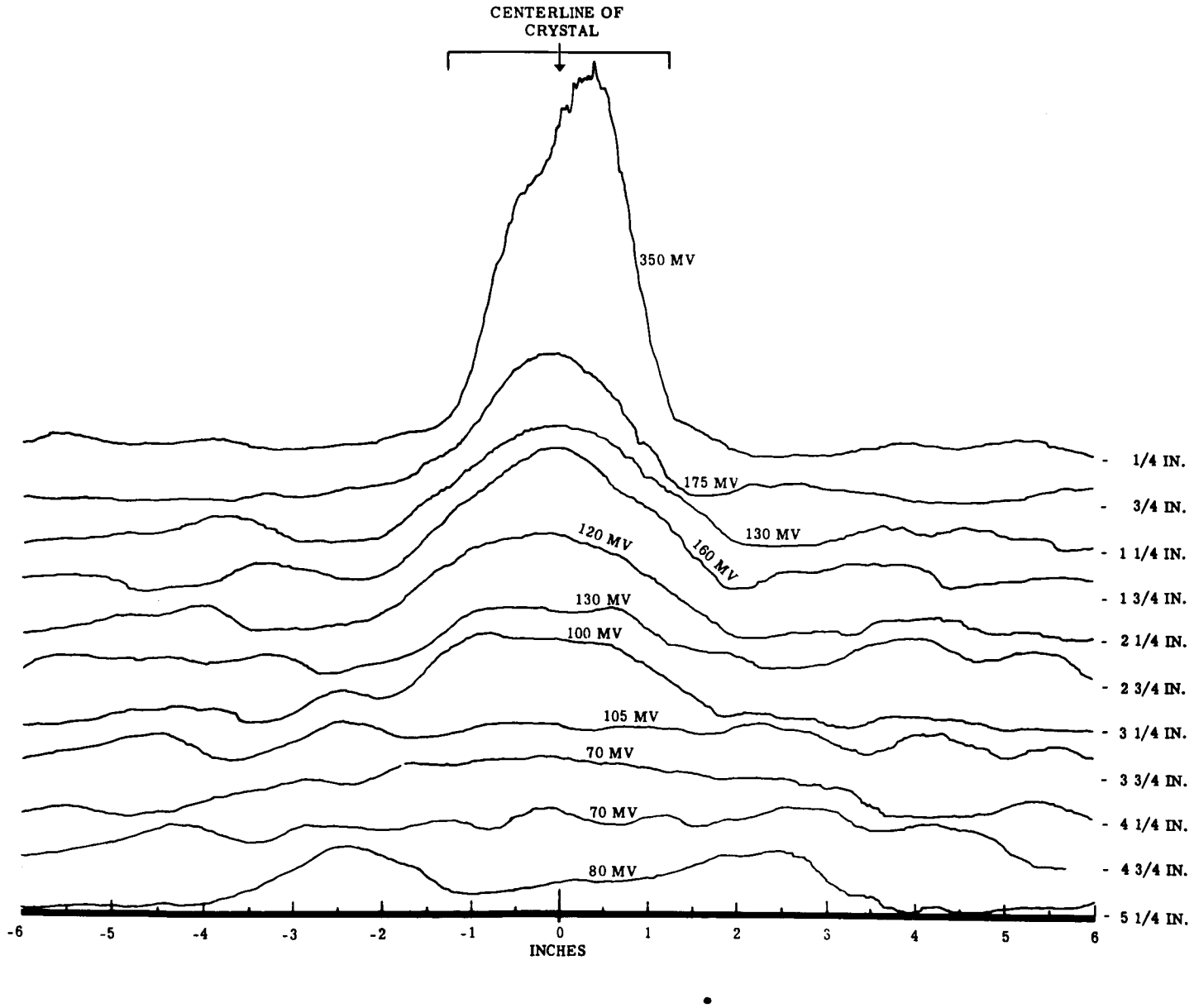

Figure 28. Crystal Beam Pattern, 2-1/2 Inch Diameter by 1-1/2 Inch Thick Channelite Type 5500

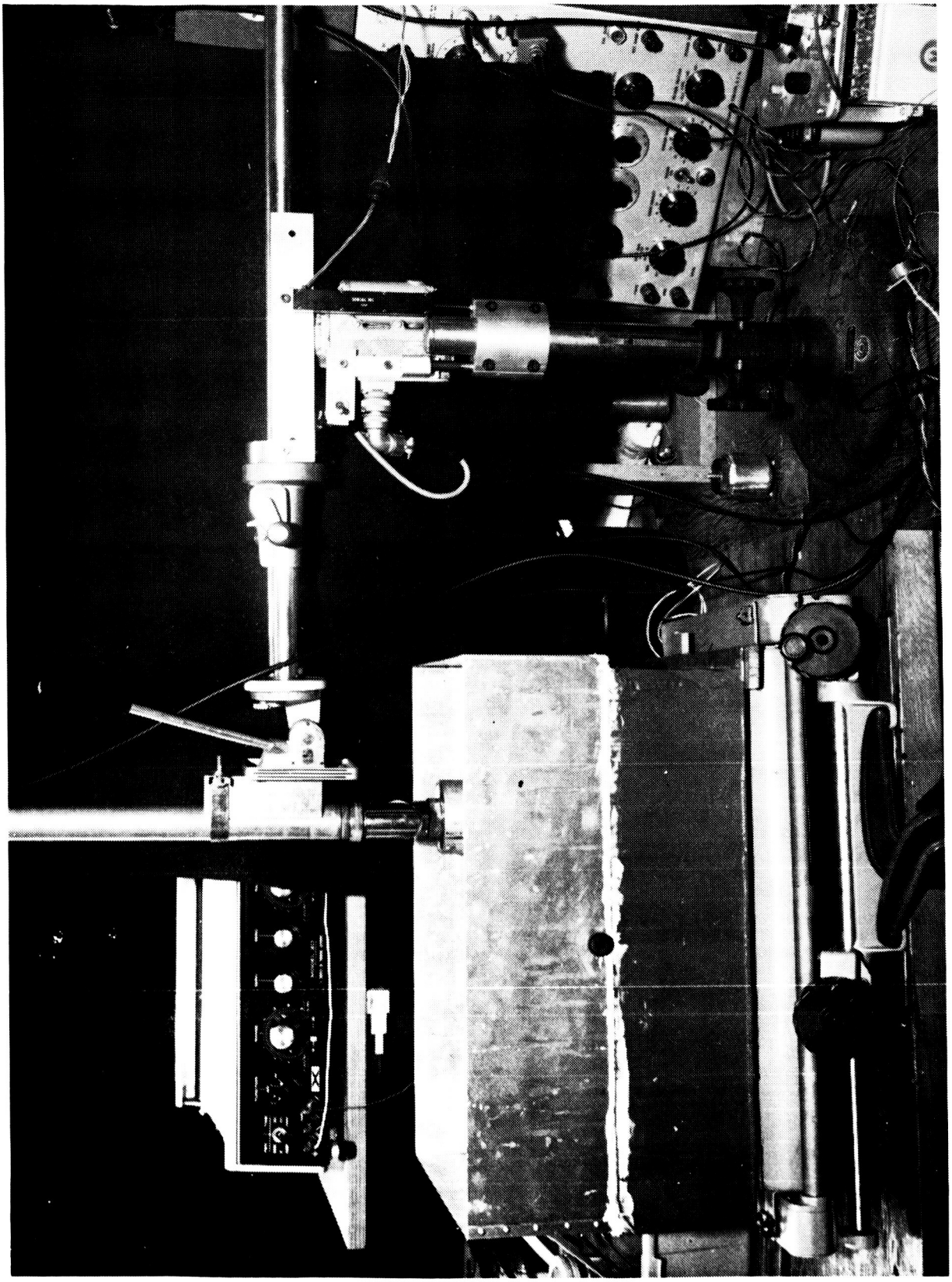

Figure 29. Crystal Evaluation Test System and Scanning Mechanism

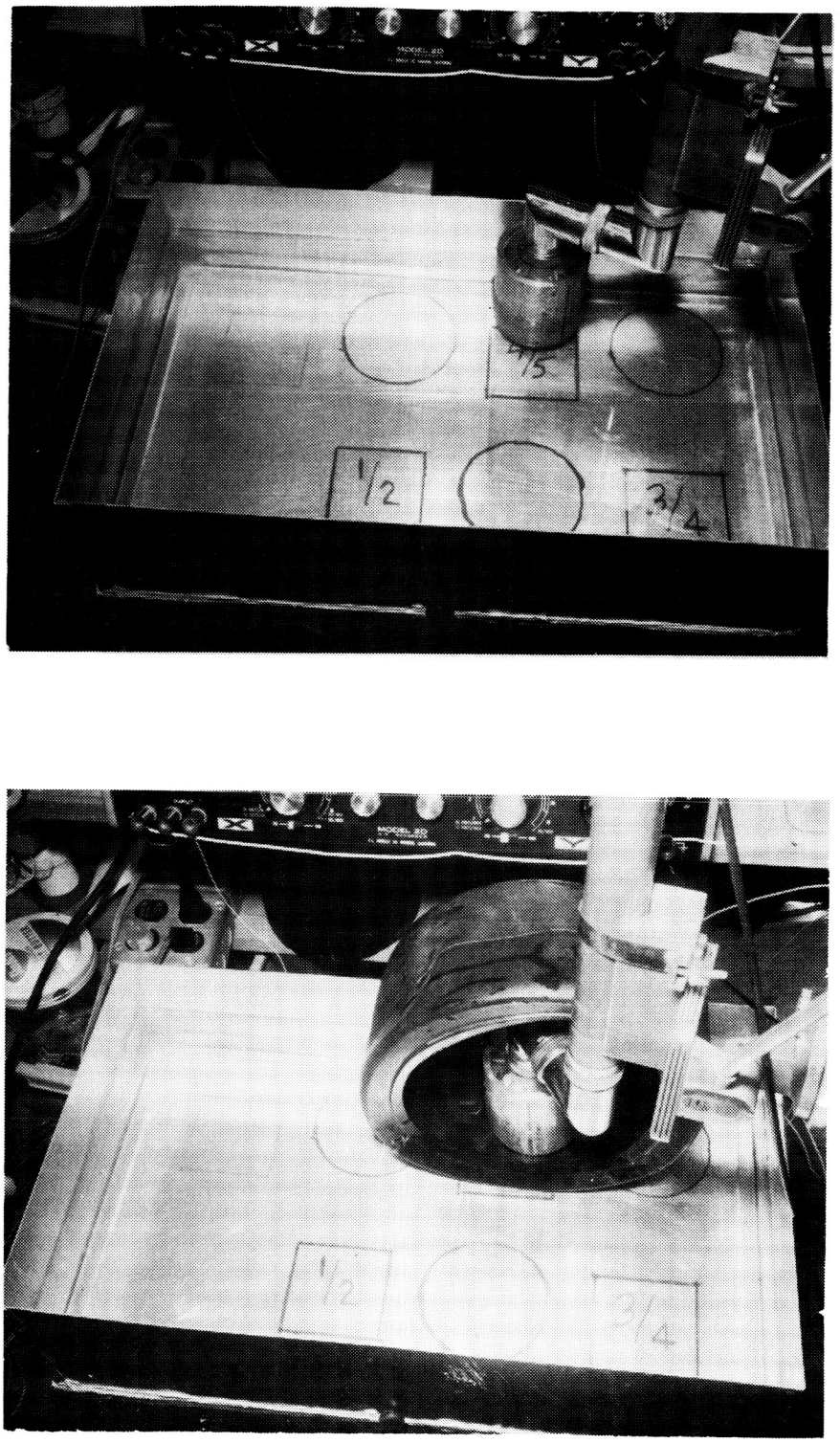

Figure 30. Crystal Support Fixture With Immersion System and Wheel Setup Used for Evaluation

Initial tests conducted with a 1K resistor in series with the crystal showed that the peak amplitude and frequency conditions were relatively constant with the crystal loaded by air, water, or the water-honeycomb specimen configuration. Preliminary scans with the crystal elevated above the specimen surface showed significant crystal current and frequency differences over well bonded and disbond honeycomb areas. Because the crystal sensitivity appeared to be directly related to elevation, a series of elevation tests were conducted with the crystal immersed and operating at 28.7 KHz. The first test measured the crystal sensitivity to various layer disbonds as related to elevation, which ranged from 0 to 2.5 inches. A dual scan recording was made for each disbond, showing the good bond signal versus the disbond signal as related to elevation (Figure 31). The dual traces were made by scanning a well bonded area with the transducer at a specific elevation, and then repeating the scan with the transducer over a far side disbond area. The vertical spacing between the traces is a measure of the ability of the system to discriminate between bond and disbond. The good bond signal appears above the zero reference line in these plots. A measure of the sensitivity can be obtained by comparing the good bond and disbond signals referencing this line. Sensitivity may be calculated by measuring the noise variation in the crystal current when scanning over a well bonded area. The voltage drop across the series impedance feeding the crystal has a typical variation of less than 0.02 volts. This unusually low noise level is likely due to both the large diameter of the crystal and to the constant coupling conditions resulting from the immersion of the crystal and specimen. The optimum elevation varies for each of the three disbonds. However, a single elevation could be judiciously selected which would provide adequate sensitivity for all disbonds. Significant sensitivity improvement may be readily achieved by using the full Rectified Crystal Detector System thereby canceling out the signal below the good bond signal and realizing sensitivities in the order of 100 to 1000.

The crystal sensitivity was also significantly affected by frequency changes. An experiment was conducted to determine the crystal frequency - sensitivity relationship at various elevation levels. The crystal was immersed at a spacing of 0.035 inch above the specimens and frequency cycled from 25 to 45 KHz. The crystal response for a good bond and disbond area was recorded in two traces, one for good bond, the other for the disbond area. The elevation was increased in 0.050 inch increments up to 2.50 inches. The records of a portion of these scans are shown in Figure 30. The major significance of these graphs is that there are as many as three different frequencies at which good disbond to bond sensitivities may be measured. Of particular note is the 0.5 inch elevation data which shows four frequency sensitive peaks. A change in frequency of 1 KHz reduced the sensitivity to unity. Tests were conducted with constant frequency and with varying inductors in series with the crystal to determine optimum tuning. The inductors caused LC resonances ranging from 15 to 30 KHz. The optimum results were obtained with 30mh inductor tuned to 20 KHz. Bond to disbond

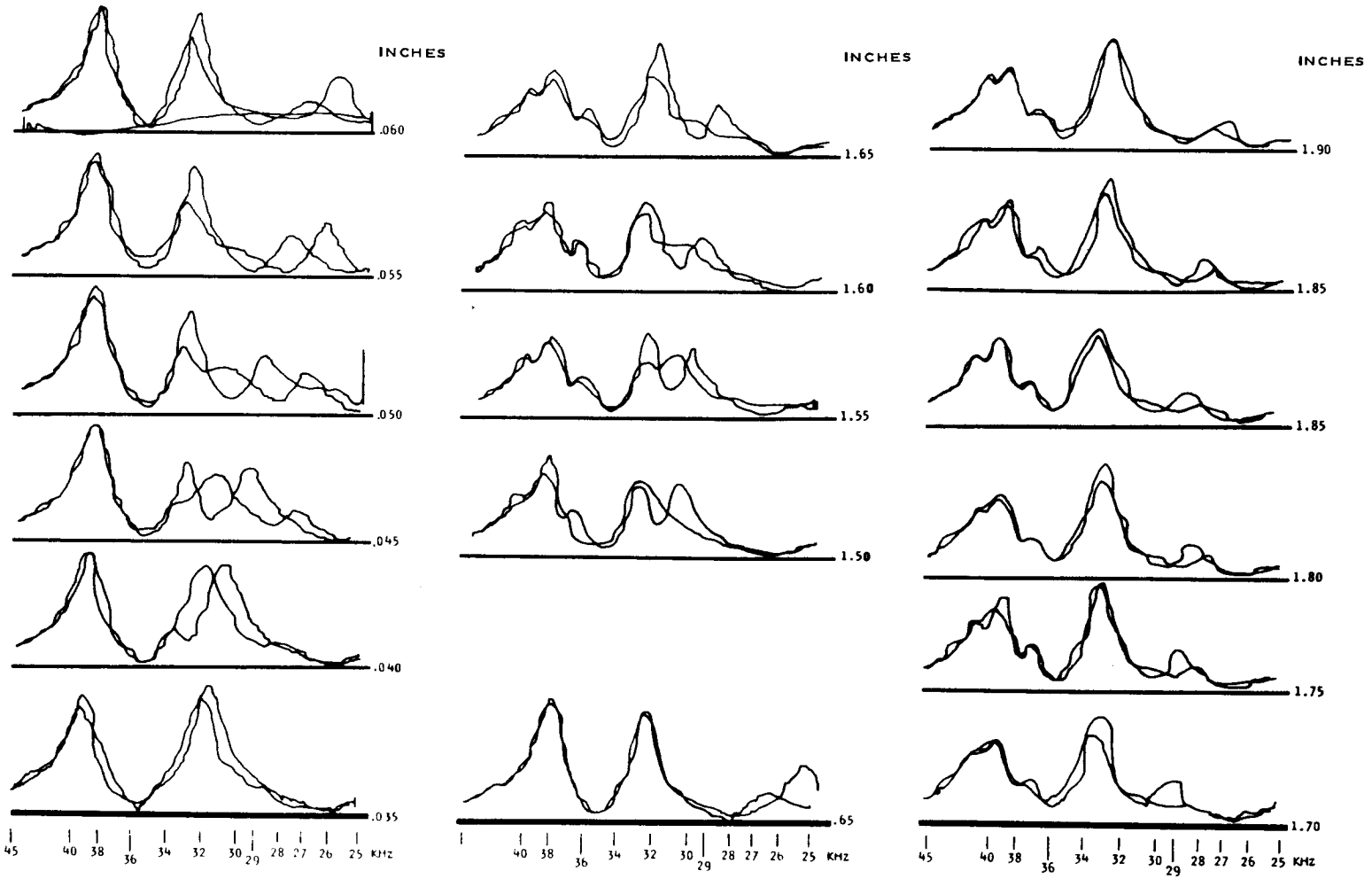

Figure 31. Crystal Sensitivity Versus Frequency Measured at Various Elevations for Good Bond and Disbond Conditions

sensitivities were moderately increased at the 0.5 and 1.8 inch elevations. Loading effects on the crystal due to detection circuits were measured and showed little effect. The crystal has a high capacitance and was not effected by vacuum tube voltmeter loading.

Tests were made with different values of series resistance ranging from 100 to 10,000 ohms. There appeared to be little advantage in one value over another. This was considered to be due to the main component of the crystal's electrical impedance being reactive rather resistive.

The results of the elevation-sensitivity tests and the elevation-frequency tests were considered significant in two respects. First, the crystal detection performance was increased from sensitivity levels of approximately ten to hundreds. Secondly, the optimization of the crystal frequency could be readily utilized for detection of single or multiple disbond conditions. And finally, the improved sensitivity of the elevated crystal makes possible the use of ultrasonic squirter and wheel couplant systems. In order to establish the criticality of the elevated crystal couplant system, the following tests were performed.

A test was made to see if there was any nonlinearity in the system by changing the driving voltage and observing the sensitivity ratio. The ratio remained constant over the input voltage range of 0.1 to 0.75 volts. The ratio fell lower at higher input voltages, due to the signal generator going into overload, causing squaring of the top of the sine waves. The 50 ohm input resistor was then removed allowing up to 8 volts input before distortion and change in ratio was observed.

When the transducer is tilted off normal, there is a reduction in sensitivity ratio. The check made with a ratio of 3.6 was reduced to 3 when the search tube was tilted at 80 degrees to the surface of the specimen (on a far side disbond). With both axes of the transducer tilted by 5 degrees, a ratio of 3 was still obtained. It appears that optimum elevation is the same as for normal operation with the distance measured to the center of the crystal. The honeycomb cells appear to channel the acoustic beam. A change in elevation of ±0.020 inches reduces the sensitivity by 84 percent.

Tests were then conducted using a prototype Sperry Ultrasonic Wheel tire to determine the effect on sensitivity. Figure 30 shows the test conditions. The tire reduced the sensitivity by approximately 20 percent which is considered negligible. Further tests are conducted with a wheel system (Figure 32) and the feasibility of manual scanning was established. Additional tests will be conducted in an automatic scanning mode.

Figure 32. Sperry Ultrasonic Wheel Assembly With Crystal and Tire

The crystal sensitivity tests were conducted with Clevite type PZT-5A and Channelite 5500 ceramic materials. Slight differences in optimum elevation (0.5 to 0.6 inch) and optimum frequency (28.7 to 29.1 KHz) were measured. These slight differences are not considered significant and the crystals are considered interchangeable with slight mechanical adjustments.

Performance of the impedance bridge circuit was also evaluated in terms of elevation optimization. With 10 volts on the crystal at bridge null, the noise level when scanning bonded honeycomb was about 0.1 volt. The calculated sensitivity was the ratio of the bridge unbalance signal to 0.1 volts. The bridge was normally balanced over a 3/4 disbond and the crystal then moved to good bond area. At 0.5 inches of water, the 3/4 disbond gave a sensitivity of 21, and a 4/5 disbond gave a sensitivity of 23.

The following table shows the relationship of crystal elevation versus crystal impedance and the sensitivity for 3/4 disbond:

Elevation	R	C	E_o	Sensitivity
0	11300	-0.0018	0.32	3.2
0.1	11300	-0.0016	0.37	3.7
0.2	11300	-0.0012	0.43	4.3
0.3	12300	-0.0008	0.60	6.0
0.4	12300	-0.0003	1.1	11.0
0.5	11100	0.0006	2.1	21.0
0.6	10000	0.0007	3.4	34.0
0.7	11000	-0.0049	2.6	26.0
0.8	4030	-0.0035	1.04	10.4
0.9	6030	-0.0027	0.6	6.0
1.0	7030	-0.0023	0.42	4.2

A negative C value means that balancing capacitance had to be added in parallel with the crystal. The crystal and associated load appears to be inductive at most elevations.

When the impedance bridge was balanced for a 3/4 disbond at a 0.5 inch elevation, the sensitivity drops rapidly as the elevation is changed because the bridge null changes. An elevation change of 0.010 inch decreases the sensitivity from 23 to 5. This is one good reason for using the much simpler technique of measuring the voltage across the crystal as in the Rectified Detector System. With this latter system, there is only one adjustment; a control that is used set the meter at zero for the weaker signal (bond or disbond area).

CRYSTAL AGING

Other studies of aging in crystal resonators have shown the following facts to be evident: First, the crystal does not return exactly to the same state of equilibrium each time it is brought into oscillation. This lack of stability is estimated to be 10 or more parts in 10^{10}. Second, temperature disturbances produce changes in the elastic properties and in the distribution of mass at the surface of the crystal. And third, these two effects are time variant and consequently cause the crystal resonant frequency at any one time to be a function of its thermal and amplitude history for months or years past. The crystals evaluated in this phase of the program included the Clevite type PZT-5A and Channel Industries type Channelite 5500 which are lead-zirconate-titanate composition. Reported aging data for these crystals show the piezoelectric properties degrading logarithmically as a function of time. Further, the aging of the dielectric constant is, for example, at a rate of one percent per time decade. The degradation rate also varies from one batch of crystals to the next and it is difficult to predict exact values for dielectric constant, or elastic modulus. However, it is also true that the longer the time period allowed after poling, the more stable the crystal becomes. The use of these types of ceramic crystals has not shown a significant sensitivity degradation in periods up to one year during this program.

CALIBRATION AND STANDARDIZATION

The Saturn honeycomb composites have been shown to fail because of defects incurred during manufacturing, handling and service. The composite failures are typified by degraded adhesive bond strength, face sheet or core failure or combinations of these materials. A calibration and standardization of an inspection system must be based on these failures. Two program approaches were designed for this purpose, first, quantitative measurements of the inspection system parameters as affected by the responses of honeycomb specimen standards representative of various composite failure modes. Second, the classification of inspection responses and the establishment of electrical inspection standards and procedures.

DESIGN OF HONEYCOMB STANDARDS

The analysis of failure modes for honeycomb structure was reviewed in terms of test standards. These standards will be used to evaluate the performance of the inspection systems in terms of defect detection, definition, and location. The defects considered included adhesive disbonds and thickness, honeycomb core thickness and joints, facing sheet thickness, and general honeycomb structure curvature. Table VIII depicts the defect description and location in the composites. Additional defects will also be considered, based on further analysis.

Table VIII. DEFECT DESIGN FOR CHARACTERISTIC STUDY

	Insulation Honeycomb							Bulkhead Honeycomb (S-4B)	
	S2					1.6			
Adhesive Layer	2	4	6	8	10	2	4	2	4
1. Precured adhesive disbond: square and triangle	√	√	√	√	√	√	√	√	√
2. Precured adhesive disbond: 1, 2, and 3 cell size	√	NA	NA	NA	√	√	√	√	√
3. Adhesive thickness variations (4)	NA	NA	NA	NA	NA	√	√	√	√
4. Core thickness variation	Constant Thickness							Tapered Section	
5. Core joint irregularities	NA	NA	NA	NA	NA	√	√	√	√
6. Crushed core						√	√	√	√
7. Facing sheet thickness variation	NA	NA	NA	NA	NA	NA	NA	√	√
8. Honeycomb panel curvature	Simulated Per Vehicle Panel								

CONCLUSIONS

The impedance system evaluation included significant sensitivity improvement by impedance matching the crystal to the composites. Optimum elevation tests proved an increase sensitivity by a factor of 100. Based on these tests the crystal transducer was mounted in a Sperry prototype wheel used to successfully inspect the 4-3/4 inch Saturn common bulkhead composite. Characterization of crystal transducer was defined in terms of dynamic coupling mechanical Q. The electrical system was evaluated and significant

improvement was achieved by two techniques. The complex bridge circuit was replaced with a series tuned circuit with a single adjustment control. The technique utilized a self driven crystal which proved successful in identifying the adhesive layer in which disbond were found. This technique also has the potential of determining the damping characteristics of the adhesive bond which was shown to be related to bond strength.

Section VI

RELATED DEVELOPMENT ACTIVITIES

EDDY-ECHO BREADBOARD SYSTEM

Previous experiments have shown that pulse-echo type inspection signals are subjected to extreme attenuation and mode conversion in honeycomb composites. Two methods were evaluated for improving pulse-echo techniques for the Saturn honeycomb composites. An electromagnetic driver was applied to the honeycomb in conjunction with a 262 KHz pulse-echo system to magnify the defect response. Then the electromagnetic driver was evaluated as the pulse source with an acoustic detector.

Preliminary tests were performed using the 2-1/2-inch diameter coil in a ferrite cup. This probe was placed on the under side of a 4-3/4-inch specimen. A 5 MHz lithium-sulfate crystal series tuned to 262 KHz was used as a receiver on the top side of the specimen. The high gain 262 KHz receiver is the same unit used in earlier echo-ranging experiments. The system was named Eddy-Echo for identification. The probe was pulsed using a 4G200 Shockley diode and a 0.1 mfd storage condenser. The resulting wave was not ideal because of current limiting by the inductance of the coil and did not tune to 262 KHz. Careful shielding was needed to reduce the air-conducted electric field interference, and grounds were required on the facing sheet of the common bulkhead specimen and the metal case around the probe. What appeared to be very weak acoustic signals were observed. An improved electromagnetic driver (Figure 33) was constructed using the same ferrite cup core wound with 37 turns of copper ribbon 1/2 inch wide, 0.005 inch thick. The wound core was installed in a heavy brass magnetic shield. The shield was extended to permit installation of the pulser and associated circuit. The shield thereby provided an electrostatic and electromagnetic enclosure.

Tests made using various ultrasonic transducers showed that there was very little eddy-current-induced acoustic energy. With a repetition rate of approximately one pulse per second, successful acoustic pulse transmission was made through an aluminum bar and honeycomb. Time measurements were made using the coil at one end, air coupled, and a 400 KHz barium titanate crystal at the opposite end. A shorter bar confirmed the generation of an acoustic pulse in aluminum. The coil was also successfully evaluated on a 1-3/4-inch thick Saturn honeycomb specimen with a 1/8 and 1 inch coil-to-specimen spacing. Evidences of the disbond detection capability is shown in figure 34. A number of crystals ranging from 30 KHz to 25 MHz through transmission were evaluated in detection tests and successful results were obtained up to about 400 KHz.

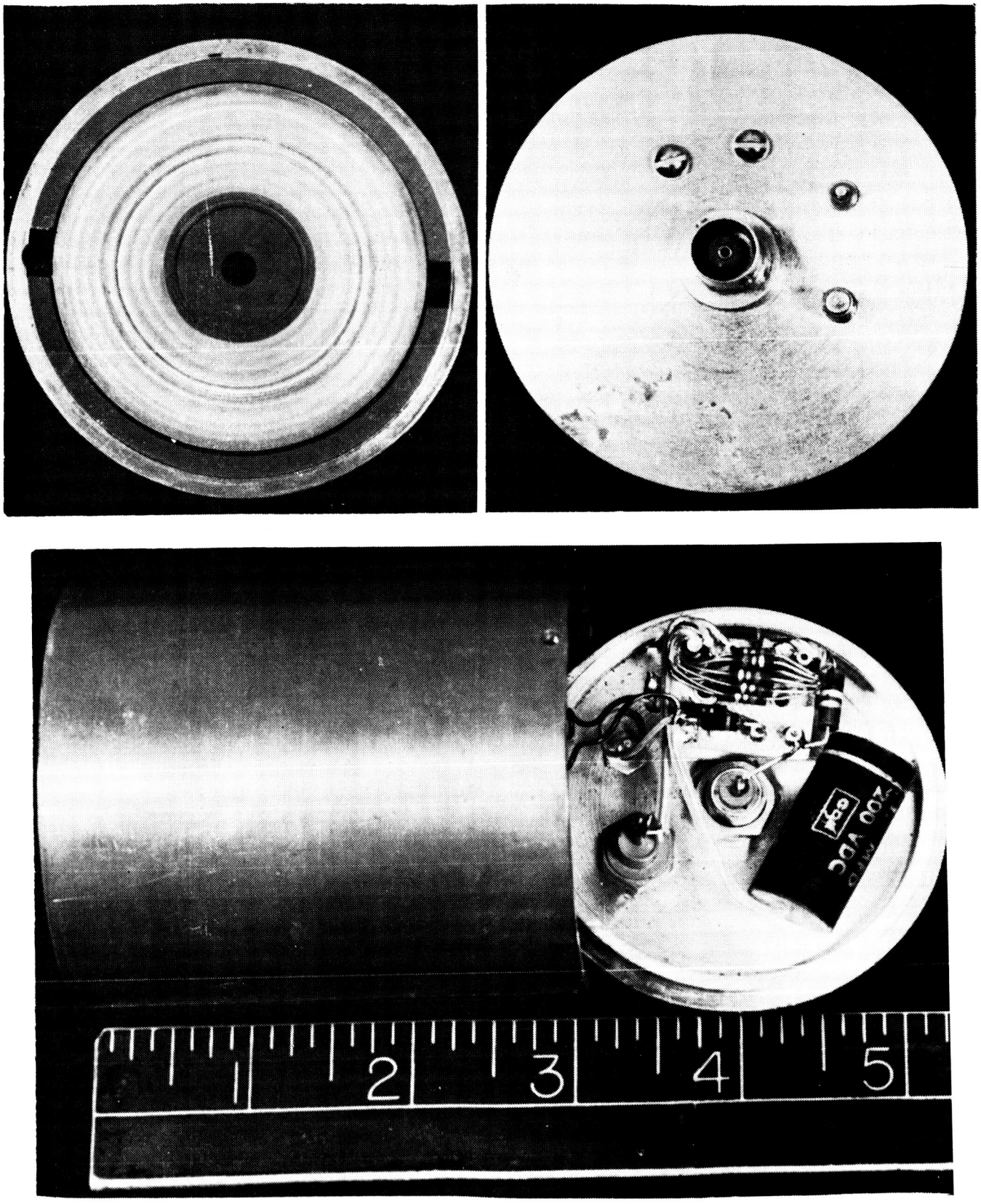

Figure 33. Eddy-Echo Transducer Showing Top, Bottom, and Internal Pulser

EDDY-ECHO SIGNAL
IN HONEYCOMB

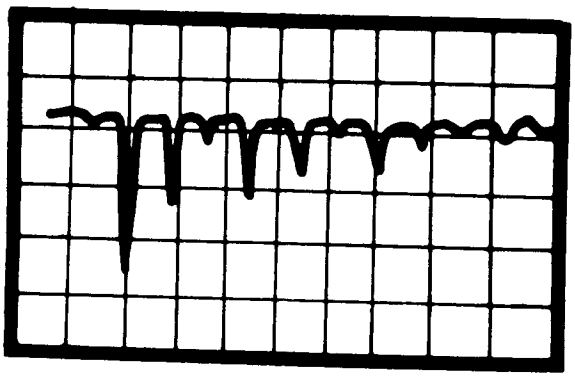

GOOD BOND HONEYCOMB
SIGNAL

DISBOND SIGNAL

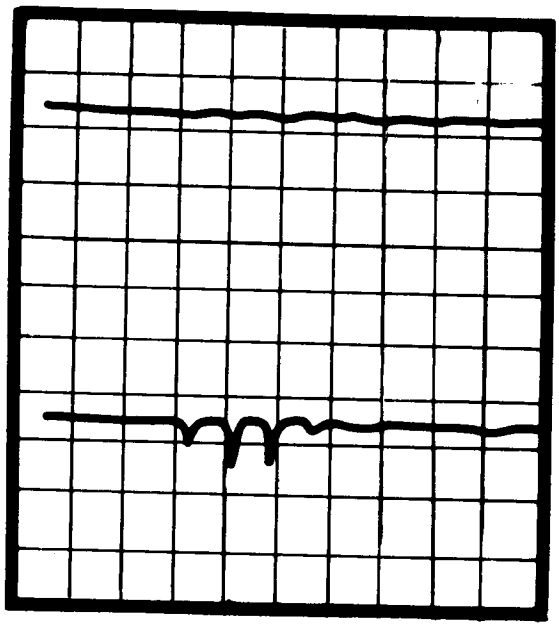

0.2 V/CM 20 μS/CM

Figure 34. Through Transmission Eddy-Echo Signals With 1-3/4 Inch Saturn Honeycomb

These experimental tests definitely establish the feasibility of electromagnetic generation of acoustic pulses with either acoustic or possibly electromagnetic detection. This technique appears to warrant further development.

PREPARATION AND SHIPMENT OF NDT SYSTEMS

Upon direction of NASA Contract Officer, the impedance and eddy-sonic breadboard systems were delivered to NASA, Huntsville, Alabama, for evaluation on the insulation-type composites. Prior to shipment, both systems were re-evaluated on insulation test specimens in both horizontal and vertical positions. The following improvements were incorporated:

1. A detection sensitivity check on all available impedance crystals showed a composite crystal (three each 2-1/2 inch diameter 1/2 inch thick, PZT-5, silver epoxy bonded together) had the highest response for far-side disbonds. A 0.006-inch teflon tape provided crystal covering without degrading the sensitivity. A new crystal holder was fabricated for the 1-1/2 inch thick, 2-1/2 inch diameter crystal.

2. Liquid coupling tests were conducted with the impedance transducer on vertically mounted specimens. Excessive leakage occurred past the O-ring supported crystal and the graphite impregnated teflon transducer support ring. Experiments with various sponge-type materials encircling the crystal were moderately successful. A General Electric Type RTV-7 silicon rubber foam was tried in a foam-in-place mold. This proved to be superior in terms of water sealing and compressibility. The silicon rubber foam was also used to seal around the crystal.

3. The eddy-sonic transducer was adapted to the scanner with a spherical bearing holder similar to the impedance transducer. Spacing tests were conducted to determine the effect of scanning curved surfaces. Variations of 0.070 inch at 0.35 inch elevation insulation honeycomb composites did not seriously degrade the sensitivity for far-side disbonds.

4. The two systems were scanned on a vertical, and detection sensitivity data was not degraded. The increased weight of the impedance transducer caused spasmodic slipping of the vertical drive belt which was replaced with a steel bicycle-type chain.

5. The systems were mounted in relay rack enclosures to facilitate shipment and on-site operation.

6. The systems were shipped to Huntsville on 14 January 1966. Mr. H. Varney, NAA/LAD, spent the period 19-21 January 1966 demonstrating the operation of the two systems. It was concluded that a noncontacting inspection system is almost mandatory, and secondly, that a reliable means of identifying far-side disbonds specifically is needed.

EDDY-SONIC BREADBOARD SYSTEM

The trip to NASA, Huntsville, Alabama, on 19 January 1966, emphasized the need for a noncontacting inspection transducer. The eddy-sonic system has a capability of noncontact inspection; however, a means of supporting/positioning the transducer necessitated a form of contact with the structure. A number of experiments were conducted to establish the feasibility of an air flotation support/positioning system. This concept utilizes an air cushion between the transducer and the test part. A reverse jet(s) forces the transducer to the required spacing. The transducer was tested on both horizontal and vertical applications and the spacing variations were less than 0.10 inch. The air flotation transducer is shown in figure 35. The vertical positioning tests used the air hose for support, however, air jets located circumferentially on the air plenum could provide support as well as positioning.

The evident need to distinguish between disbonds within the insulation composite and those at the vehicle bulkhead prompts a review of the earlier tests with the eddy-sonic system. Significant spectral differences were evident for most of the disbonds at various layers of the specimen (Annual Report, NA-65-452). Far-side disbonds exhibited minor spectral differences, however, in destructive inspection almost total bonding was evident in the disbond areas. Additional tests were conducted using a B&K Precision Condenser Microphone, Model 4135, with a 10 to 100,000 Hertz frequency range. The results of these tests proved inconclusive due to inadequate shielding between the electromagnetic driver and the microphone.

INSULATION 1.6 INCH HONEYCOMB SPECIMEN

The 1.6 honeycomb insulation composite was tested with the impedance system. The tests were conducted with manual scanning and the following detection signal data listed in Table IX was taken. The data was taken at an approximate 0.020 inch elevation. Elevation optimization should significantly improved the detection sensitivity.

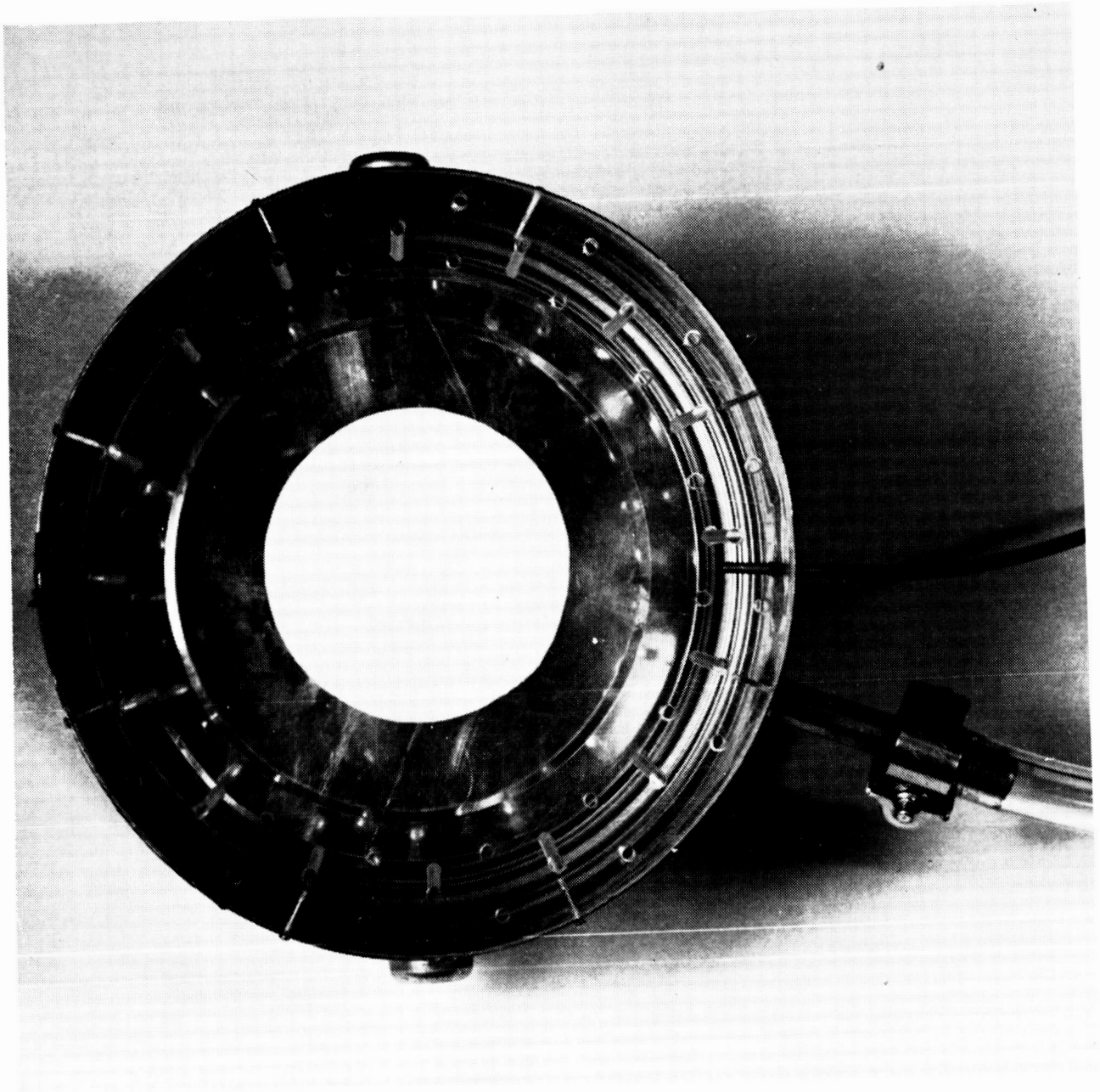

Figure 35. Air Flotation Transducer, Front View

Table IX

DATA SUMMARY, 1.6-INCH INSULATION HONEYCOMB

Disbond Type	Worst/Good Signal Ratio	Signals-Volts			
		1/2*	2/3*	3/4*	4/5*
2"	.3	2.35	2.15	1.44	0.85
2 cells	.3	1.60	1.60	1.15	0.90
1 x 2	.3	2.0	1.83	1.10	1.00
2 cells	.3	1.75	2.05	1.35	1.00
1 cell	.3	1.5	1.35	0.6	0.45

*Disbond layer.

Section VII

ANTICIPATED WORK

The following effort is planned for the next reporting period.

The literature and industrial survey will be continued for pertinent information on nondestructive testing of allied composite materials.

The impedance system characterization will include the following tasks. The crystal characteristics in terms of dynamic coupling factor and mechanical Q will be measured and related to crystal optimization. The tapered honeycomb specimens will be retested for optimum crystal frequency and elevation in terms of stub tuning action of the crystal and honeycomb. These results will be analyzed in terms of inspection of the tapered sections of the Saturn common bulkhead. The Rectified Crystal Detector and Piezoelectric Oscillator-Self Tuned techniques will be evaluated in terms of automatic scanning, deflect response, and defect location inspection capabilities.

A series of honeycomb composite standards will be fabricated with a range of defects which will permit calibration of the inspection systems.

A calibration technique will be applied for inspection purposes with both electrical and mechanical response for the composite defects.

APPENDIX A

LITERATURE AND INDUSTRIAL SURVEY

1 July 1965 through 31 December 1965

CONTRACT NAS 8-11733

Appendix A

LITERATURE AND INDUSTRIAL SURVEY

INTRODUCTION

The following literature and industrial survey was conducted under Contract NAS8-11733, during the period 1 July 1965 through 31 May 1966. The basic objective of the survey was to assure an awareness of research developments relating to nondestructive testing of honeycomb materials and structures. During the reporting period, the survey effort was directed toward information relating to ultrasonic testing of adhesive bonds, ultrasonic system characterization and standards, and honeycomb material defect characterization.

Subject material presented in this appendix was included in the quarterly program reports published during the reporting period. The individual literature survey sections appearing in these reports have been combined, to provide a single document encompassing these areas of study.

ADHESIVE BOND STRENGTH

This phase of the survey effort paralleled efforts to determine the quality of adhesive bonds by nondestructive methods. To test bonded structures effectively, measurement parameters which are indicative of bond strength are required. A literature survey, directed toward this goal, was conducted to ascertain present state-of-the-art in adhesion theory and testing.

ADHESIVES AND ADHESION THEORY

In seeking a basis for the nondestructive testing of composite materials, literature concerning adhesives and adhesion theory were surveyed. Wake (1) in reviewing work done by Dr. R.M. Vasenin concerning the diffusion theory of adhesion, states that experimental difficulties encountered with routine measurement of large numbers of test pieces has led to considerable confusion in the measurement of adhesion. He points out that for many industrial purposes, only measurement of some parameter which characterizes the mode of failure, not measurement of adhesion, of the bonded structure is required.

In a review of adhesion theory, Vasenin (2) holds that any theoretical work in the field of adhesion phenomena involves the transformation of energy into force. No one theory encompasses all types of adhesives, thus adhesion phenomena must be classified. One method of classification is by type of bond and mechanism of formation of adhesion combination. Vasenin holds that the diffusion theory of adhesion provides a criteria on the possibility of the formation of a strong bond.

Electron microscopy was used by Hock (3) to investigate the morphology of various pressure sensitive resin and rubber films. Results of his studies show that properties other than those which are morphological enter into good adhesion. Sharpe, et al (4), in a review of adhesives, tend to hold to the molecular theory of adhesion, stating that a natural adhesive force exists between any two materials. It is demonstrated that a properly made adhesive joint never fails in adhesion, but that failure is in the bulk of the adhesive or in the adherent.

A review of literature regarding adhesive strength tests indicate that results are frequently confusing and difficult to correlate. Determining the strength of an adhesive joint is also hindered by difficulties in preparation of test specimens and absence of accurate theoretical analyses from which to calculate the properties from test data. To surmount these obstacles, Sherrer (5) proposes and analyzes an adhesive test utilizing a simple test specimen comprised of two identical metal bars glued together with the adhesive to be tested. The specimen is placed in a jig and a strain gage is used to measure strain for a given load. In his theoretical investigation, the resultant curves of strain/load versus Young's modulus are used to determine Young's modulus for the adhesive tested. The proportional limit of the beam is found by taking a series of readings as the load is increased. The curves of maximum shear stress/load versus Young's modulus can then be used to determine the yield stress of the adhesive in shear.

Early tests by Moser (6), to determine effect of loading rate on the strength of adhesives, show significant differences in adhesion properties due to differences in loading rates and testing machines used. Ilkka (7) investigated several types of structural adhesives and test methods for metal bonding. From the results, he concludes that while lap-shear and tensile tests provide a means of comparing adhesion strength, the tests are of little value in determining mechanical shock resistance of an adhesive. In his opinion, a minimum of two different type of tests are required to obtain adequate information about strength properties of an adhesive.

Many investigations have been made regarding use of adhesives for structural applications. Of interest are those by Epstein (8), Pattee (9), and Pascuzzi (10). Although each case concerns a specific application, destructive methods were used to determine bond strength and quality. It was the general conclusion that, while no one nondestructive testing procedure for adhesive-bonded joints is as yet satisfactory in all respects, ultrasonic methods offer the most potential for production line testing.

NONDESTRUCTIVE TESTING OF ADHESIVE BONDED STRUCTURES

A considerable number of reports and articles concerning acoustical inspection of adhesive-bonded composite materials were surveyed. Schijve (11) reported on the application of a resonant frequency method using vibrations in the 0.5 to 1.5 MHz range, stating that voids in adhesive-bonded specimens were best detected by using the lowest natural frequency of the joint. Hughes and Burstein (12) reported on a method of analysis of waveform at resonance between the material tested and transducer. Finding this method unsuitable, they also ruled out all methods involving attenuation (pulsed and CW), concluding that a pulsed wave technique involving surface waves would be the only suitable method. While their test methods appear to be feasible for detecting disbonds on the near side of a panel, suitability for multilayer structures is unlikely.

McGonnagle and Park (13) mention the use of the resonance method and of Lamb waves in the testing of composite materials. Ramsey (14) analyzed the problem of ultrasonic inspection of plastic structures and found that because of the lower sound velocity in plastics, high noise levels were likely to mask other signals. Only through-transmission methods of inspection are reported in detail. Gray (15) described a mechanical-impedance method of checking honeycomb structures. Measuring the frequency response, the instrument was a simplification of the STUB meter in which sweep frequencies of 340 to 760 KHz were applied to a 400 KHz crystal. Only a limited number of defect types could be detected, and comparison with a good bond specimen was required.

Dealing more specifically with bond quality than with structure, an early report by Jayne (16) suggested resonance methods involving both frequency spectrum analysis and decrement measurement. Resonance measurements were also suggested by Kanamaru, et al (17) who measured the dynamic modulus and loss factor by ultrasonic means. Dietz, et al (18), suggested measurement of the dynamic modulus of glued structures. A study concerning use of Lamb waves for the inspection of near-side bonds in composite materials by damping out the waves traveling on the top surface of the core sheet, and only measuring the attenuation of the surface wave traveling on the bond side of the cover sheet, is reported by Hughes and Burnstein (19). Some correlation with peel strength was achieved.

ULTRASONIC TECHNIQUES AND EQUIPMENT

During the past 10 years, several ultrasonic inspection systems have been developed for use in nondestructive testing of adhesive bonded structures. Of recognized value, and limitation, are the systems known by the trade names of STUB meter, Fokker Bond Tester, Sperry Reflectoscope, Sonizon, Coinda-scope, Immerscope, and Vidigage, to name a few of the more common.

Anderson (20) found the Immerscope suitable for the nondestructive testing of plastic bonded aluminum honeycomb parts. Vogel (21) describes the development of laboratory type equipment for ultrasonic bond inspection, utilizing the immersion technique, in a fairly recent report. Testing was confined to test specimens and materials similar to those used in missile and solid propellant cases. Test results verified the feasibility of this method for inspection of laminates of dissimilar materials. Evaluation of the STUB meter and Sperry Reflectoscope as a nondestructive inspection system for bonded sandwich panels is reported in NAA/LAD reports prepared by Cizek (22) and Kammerer (23). Of the three systems evaluated at NAA/LAD, the Reflectoscope appeared to offer the most potential as good correlation of nondestructive and destructive test results was obtained.

STUB Meter

Development of the STUB meter resulted from an extensive research study carried out by Arnold (24), in researching nondestructive means for testing adhesive bonds. The instrument was based on the observation that the performance of a transducer, mechanically coupled to a test specimen, was affected by the properties of the test specimen. No aspect of low frequency behavior (less than 15, 000 cps) was found to be indicative of joint strength. It was also determined that mechanical interference techniques offered only limited applicability. The validity of STUB meter performance was evaluated using aluminum test specimens bonded with organic adhesive. Specimens were subjected to both destructive and nondestructive tests, the results of which showed good correlation. Determination of bond quality for brazed, welded and cemented-plastics joints is deemed more difficult to evaluate. Application of the STUB meter is further discussed in articles by Vincent (25), Hughes and Burnstein (19), and Grindrod (26).

Use of the STUB meter and Coindascope for nondestructive testing is described in detail in an FAA Digest (27). However, it is recommended that caution be exercised in interpretation of results as good contact conditions without a bond may give the same signal as a good bond. The use of standardizing panels for regular standardization checks is recommended. Similar conclusions were reached by Clotfelter (28) who recommended combinations of damping and impedance techniques for the inspection of materials having high attenuation and large variations in acoustic impedance.

Fokker Bond Tester

An extensive research study concerning evaluation of ultrasonic test devices for the nondestructive testing of adhesive bonds was carried out by Boruff (29) and various associates. This program was a cooperative endeavor by various NATO members, to evaluate NDT methods for adhesive bond inspection (AGARD Program).

The four nondestructive test devices investigated were the Fokker Bond Tester, STUB meter Model VI, Coinda-scope and Sonizon. Four different adhesive systems and five processing variables were incorporated in preparation of test specimens. Specimens were first surveyed by the ultrasonic devices and then subjected to destructive tests, to obtain data for correlation of results. Data provided by program participants show variance according to the type of adhesive specimen tested. Results of tests conducted by the Netherlands group indicate that the Fokker Bond Tester is capable of detecting voids in sandwich panels, however they reason that it is improbable that an ultrasonic device can be used to evaluate adhesive properties of a bond. However, a complete analysis of this work must be deferred until the related final report is available for review.

A considerable amount and variety of material has been written concerning evaluation and application of the Fokker Bond Tester, including evaluations and descriptions by Clemens (30), Schliekelman (31), and Ramsey (14). Recent papers by Smith (32) and Gonzales (33) generally conclude that this test method is limited to determination of the cohesive strength of the adhesive material itself; it has not been used successfully in determining strength of adhesion between the adhesive and adherends. This conclusion coincides with that presented in an article by Boruff and Miller (34).

Procedures for use of the Fokker Bond Tester are available in specifications prepared by Hughes Aircraft (35), ASTM Standard (36), and Fokker (37). The Hughes and ASTM specifications call attention to limitations of the tester. Both state that it is not sensitive to bonding anomalies caused by (1) improper surface preparation, (2) contaminated adherend surfaces or adhesive materials, (3) undercured, overage, or improperly compounded adhesive materials, or (4) improper processing. Because of these limitations, inspection of bonds must be carried out in conjunction with other applicable quality assurance procedures.

INDUSTRIAL SURVEY

Representatives of the 3M Company (38) and Bloomingdale Rubber Co. (39), manufacturers of the adhesives utilized in the Saturn honeycomb composite, were contacted to determine the factors affecting adhesive bond quality and the presently applied destructive and nondestructive test techniques. The manufacturers reported that the quality of adhesive bonding is dependent upon the mechanical properties of the adhesive and adherend materials, and the bond process. Variations in bond strength may occur between different batches of adhesive, between specimens bonded at the same time, and even between various locations within a single adhesive joint. They also reported that destructive testing of the completed joint was the only reliable method of ascertaining the actual bond strength. However, during their adhesive development programs, thousands of lap-shear tests are conducted per

MIL-A-5090D, "Adhesives, Heat Resistant, Airframe Structure, Metal to Metal," and a high degree of bond reliability is reported under laboratory conditions. Bond failures in the field, they reported, were caused primarily because of improper cleaning procedures, and secondly, due to incorrect part alignment and cure cycles.

It was requested that the manufacturers recommend a means of deliberately degrading adhesive joint quality over a one foot area, that would result in a cohesive failure of the joint. Recommendations were reluctantly given, suggesting that time-temperature variations in the cure cycle should reduce the bond strength, although specific values were not available. They stated that variations in cure pressure would not significantly affect the bond quality.

A number of commercial companies engaged in adhesive bonding were also contacted. Their experience with the subject and allied adhesives were reviewed. Almost complete agreement was expressed in the difficulty of nondestructively testing adhesives and the problem of producing reliably reduced quality of adhesive joints. The exception to this was a company using the Fokker Bond Tester. However, they did not have any suggestions for producing reliable substandard bonds.

The MRD division of American Transport Corp. (40, 41) has developed a method of degrading the adhesive bond quality by contaminating a controlled percentage of the adherend surface area. This method appears to simulate the failure due to an improperly cleaned/prepared bonding surface.

Failure of adhesive bond joints was generally attributed to one or more of the following conditions:

1. Variations of glue line thickness caused by improper bond pressure or misalignment of adherends.

2. Porosity in glue line caused by improper bond time-temperature-pressure conditions.

3. Voids at adhesive surface caused by improper cleaning of adherend surface, or aged adhesive.

A division of North American Aviation developed a bond degradation method which was evaluated for the HT-424 adhesive. This method exposes the adhesive to room temperature conditions for extended time periods prior to use. The peel strength of HT-424 adhesive film after 180 hours of film exposure at room temperature was comparable to that of properly stored adhesive. However, after 144, 168, and 192 hours at room temperature, a 15 percent decrease in peel strength was measured.

Another bond cycle variation evaluated was the effect of increased time-to-temperature cure cycle. The standard 30- to 60-minute heat-up was increased to 5 hours. Honeycomb tensile and shear test results were similar to those of the standard one-hour cycle.

ULTRASONIC SYSTEM CHARACTERIZATION

This phase of the literature and industrial survey effort was conducted during the period 1 October 1965 through 31 December 1965. During this period, a search was conducted to establish background information, factors, and parameters relating to characterization of ultrasonic inspection systems. Soon after initiating the search, it became apparent that there were no universal characterization parameters nor standard criteria which could be applied to all ultrasonic inspection systems. Characterization of ultrasonic systems appears to be a matter of individual preference and application.

The pertinent literature surveyed to date revealed many approaches to the study, analysis and evaluation of ultrasonic systems, methods, and components. Attempts to establish detailed characterization of a system as a whole, utilizing universally applicable parameters, are conspicuous by their absence. No doubt this is due to the many variables encountered when attempting to establish characterization on a common basis. The delay in establishing universal standards for this purpose also may be a contributing factor.

General characteristics of several systems utilizing the more common ultrasonic modes are presented by Baldanza (42). Evaluation for the application of commercially available equipment for specific applications have been reported in previous reports (43). Evaluation of the system characteristics was, in most cases, dealt with in only general terms.

In a discussion of pertinent factors in ultrasonic testing, Morgan (44) points out the significance of transducer sensitivity versus flow indication display. Indications from two apparently identical transducers differed in response as distance from the search units to the test specimen was varied. It was also shown by Erickson (45) that the size and frequency of the transducer affect the extent of the close-field or Fresnel Zone. Upon plotting amplitude versus distance curves for test blocks of various sizes, it was observed that the height of indication for a given crystal probe varied as the size and shape of the original test block was altered. Results were similar for both reflection and immersion type tests. It was also noted that instrument performance, i.e. test results, were affected by such things as changing tubes in the amplifier, or operating the system at near its peak capacity, rather than at low or midrange.

Morgan (44) recommends the use of an amplitude versus distance curve, prepared by plotting data obtained from a series of tests using "standard" specimens and test conditions, as a means of correcting for these variables. The related "standard" curve would be using search units of particular size and frequency.

In discussing construction of a pulsed transmitter and receiver for use in measuring ultrasonic attenuation in solids, Roderick (46) lists the primary characterization parameters as receiver signal-to-noise ratio and maximum transducer excitation and receiver recovery time. McMaster, et al (47) calls attention to the need for reliable instrumentation for sonic and ultrasonic frequency ranges, as no feasible means existed for measurement of power levels during operation. Parameters in electronic power supplies are easily measured. But a practical and simplified means of measuring sonic power input are needed for tests of transducer performance, and tuning transducers during use, to attain maximum power levels under various mechanical loading conditions.

Descriptions of ultrasonic methods and testing generally include details relating to the transducer characteristics and excitation frequency, but little concerning a signal bandwidth. Investigation of the effect of bandwidth in an ultrasonic application was conducted by Merhib (48), to determine if bandwidth influences the amplitude of indications obtained from test blocks used to calibrate equipment sensitivity. Test results indicated a relationship between bandwidth and test block hole size. Effects of bandwidth on back echo/defect echo ratios are negligible except at low frequencies with small defects, where defect diameter is of the same order of magnitude as the ultrasonic wave length. Merhib concludes that any calibration procedure for general usage by testing agencies in which test blocks are used should include reference to bandwidth, otherwise a variation in calibration between agencies could result.

The use of multifrequencies in pulse-echo flaw detection was investigated by Gericke (49) to determine applicability in terms of flaw definition. Flaws of the same order of magnitude or smaller than the beam width are not readily detected when a single frequency is used. Results of the investigation indicate that effectiveness of pulse-echo testing can be enhanced by introduction of multifrequency signals.

From these, and results of similar investigations, it appears that definition of system frequency characteristics should be more definitive than a simple statement of frequency range. Factors as variable as multifrequency parameters, bandwidth, method or ease of control, maintainability, and adjustment are important in evaluating system characteristics.

The ultimate efficiency of an ultrasonic system depends on the transducer. This factor introduces numerous variables due to the variety of transducers that may be applicable to the system.

Transducers have been the subject of many studies conducted since the inception of ultrasonic applications. In a recent paper, May (50) states that transducers may be characterized by the electromechanical coupling factor. This may be defind for certain geometrics in terms of piezoelectric, dielectric, and elastic parameters of the material. In a review of transducer materials, Dr. Sittig (51) presents a list of desired transducer material properties, all of which could be used in establishing characterization parameters. That these factors are applicable is illustrated by a table presented by Walker and Lumb (52) in which they list piezoelectric properties of some commonly used transducer materials. Thurston (53) presents a comprehensive analysis of transducer loss and bandwidth as a function of the mechanical and electrical terminations. A method of identifying, measuring, and recording transducer characteristics is presented by McElroy (54). Both procedures (which represent but two of many other analyses) provide a means of selecting, and categorizing transducers to match the characteristics of a particular ultrasonic system.

Transmission efficiency of an ultrasonic system is ultimately dependent upon the coupling between probe and surface being tested. Crecraft (55) points out that oil and water films do not propagate shear waves whereas phenyl solicilate or polyisobutylene do. Harris (56) showed that coupling fluids required for optimum system performance vary with the material to be tested, the transducer, and the frequency range. Water with a wetting agent is a good couplant for measurement of plastics. Glycerine provided high sensitivity for measurement of steel having rough surfaces, but caused overcoupling when used on smooth surfaces at frequencies below 4 mc. Grease or heavy oil proved more satisfactory for the latter case, yet proved unsatisfactory at frequencies above 10 MHz. The transmission efficiency of liquid couplants for rough surfaces was investigated by Lavender (57). Water, Polycell, light or medium machine oil, thick grease and Electrolube 1 or 2 all proved to be effective couplants. Glycerine proved to be the most efficient couplant. Measurements were made with an Ultrasonoscope MK2 at frequencies of 1.25, 2.5, and 5 MHZ, respectively. All couplants demonstrated a loss in transmission energy with increased surface roughness. Measurement errors caused by variations in the couplant film thickness are also discussed by Lavender. For example, the thickness of a glycerine film was shown to be dependent on the amount used, the area over which it was spread, and the manner and force with which the transducer was floated on top of the film. For his experiments, a bonding clamp was required to provide a uniformily

repeatible coupling pressure. Tests performed using glycerine and phenyl solicylate reduced the deviation of ultrasonic attenuation measurements by an order of magnitude.

These and other similar studies evidence the effect the couplant, or lack of it, can have on attempts to establish system characteristics through system performance testing.

Finally, the couplant must be chemically compatible with the test article, and be efficiently removed where problems of contaminations are present.

The effect of curved entry surfaces is discussed by Patsey (58) in which it is shown that the ultrasonic response from discontinuities of both shear and longitudinal waves is significantly reduced. Patsey has further suggested the feasibility of establishing a numerical correction.

A tentative list of items for consideration in establishing ultrasonic system characterization are presented in table A-I. Further definitive study is required to determine the measurement and applicability of some items.

INDUSTRIAL SURVEY

The following technical meetings were attended and/or reviewed for information relevant to honeycomb structure inspection.

1. 1965 National Metal Exposition, ASM Metals/Materials Congress, 25th National Convention, Soc. for NDT, 18-22 October, 1965, Detroit, Michigan.

   "Influence of Curved Entry Surfaces Upon Ultrasonic Response From Discontinuities," J. A. Patsey: This paper described preliminary tests that demonstrated a reduction of longitudinal or shear wave test responses on curved surfaces. Suggested numerical corrections were hypothesized.

   "An Evaluation of Probe Coils With Ferrite Cores for Use in Electromagnetic Testing," R. C. Grubinskas: The design of ferrite cores was defined in terms of electrical and mechanical characteristics.

   "Viscoelastic Properties Testing," C. W. Hargens: The measurement of various soft and hard materials' fundamental viscous and elastic coefficients was described. Correlations were given for measurements and material properties.

   "A Schlieren Photograph Guide to Ultrasonic Transducers," K. Erickson: A presentation illustrating Schlieren techniques for defining transducer beam configurations for far and near field studies.

Table A-I

GENERAL PARAMETERS FOR SYSTEM CHARACTERIZATION

General Parameter	Characterization
System	
Operating mode	Identification
Couplant	Type, efficiency,
Calibration	Method, frequency, standard
Operational parameters	Beam definition, velocity; target area, range,
Power supply	
Type	Identification
Power rqmts	Volts, amps
Power output	Volts, amps, phase or cycles
Operating parameters	Temperature, stability, noise ratio
Excitation source	
Type	Identification
Power rqmts	Volts, amps, phase
Power output	Watts
Operational parameters	Frequency range, bandwidth, output impedance
Transducer	
Type	Identification (material, etc)
Physical parameters	Size, configuration
Operational parameters	Impedance, % efficiency, noise level (db) damping factor, energy distribution, acoustical properties, acoustical coupling (critical angle and distance)
Detector	
Type	Identification
Power rqmts	Volts, amps
Operational parameters	Input impedance, frequency range, sensitivity, delay factor, defect definition, accuracy, type
Display	
Method	Identification
Power Rqmts	Identification
Coupling	Method
Operational range	Identity

2. American Society for Testing and Materials, Fifth Area National Meeting, 31 October - 5 November 1965, Seattle, Washington.

"An Ultrasonic Evaluation of an Ablative Type Lunar Engine Module," W. W. Hitt: The acoustic properties of the ablative materials are determined by through-transmission tests conducted between 2-10 MHz. From these data, test parameters were selected and an automated C-scan test system was developed.

"Nondestructive Test Development for Advanced Airplanes," H. A. Johnson: This presentation described a unique transducer assembly consisting of an array of shear transducers with an integral water couplant reservoir. Tests were reported on transducer wave patterns, effects of surface finish, effect of holder design, effects of shear wave angles, and scanning system requirements.

ULTRASONIC INSPECTION STANDARDS

Acceptance-rejection criteria for nondestructive testing are based generally upon the detection of defects and subsequent comparison to an established standard and/or specification. Acceptance limits can be established by means of destructive tests and/or service history; the problem lies in reliable identification and interpretation of defects revealed by the method used for nondestructive inspection. The latter is particularly true of ultrasonic means of inspection as the defect response is affected by equipment and material variables, test method, and operator skill.

A literature search was conducted to establish a basis for developing an optimized inspection standard for application in the nondestructive testing of the Saturn heat shield composites. The purpose of the search was to assure an awareness of research and development efforts relating to the establishment and utilization of ultrasonic inspection standards and specifications. The search revealed that a wide variety of ultrasonic reference standards are being used, but usually are specifically designed for a particular application. Problems relating to the inspection variables and resultant excessive rejection rates are frequently mentioned. Results of the survey and a discussion of factors relating to development of ultrasonic inspection standards are presented herein.

FACTORS EFFECTING ULTRASONIC INSPECTION

Consistency in equipment and test procedures is required to achieve reproducible, nondestructive test results. Specifications and standards are a means of providing a basis for uniformity. In reviewing the relationship of these items, Kleint and Hagemaier (Reference 59) are of the opinion that development of standards encompass three major elements, namely, (1) specifications, (2) the test method, and (3) the reference standard itself. The specification provides the basis for establishing and developing the reference standard. According to Kleint, the initial problem in establishing a nondestructive testing specification is attributed to the difficulty in clearly defining what constitutes a "detrimental defect." Vague and loosely defined parameters make it difficult to establish definitive standards. As three major sources of information for establishing quality levels, Kleint lists the following: (1) theoretical considerations and/or stress analysis, (2) correlation of NDT results with mechanical properties, destructive tests or service life results, and (3) quality level of similar parts used successfully in the past.

The importance of test jig and fixture location, to produce reliable and repetitive test results is emphasized by Canady (Reference 60), in a discussion of NDT test equipment and methods. Stating that test results should correlate when the same tests are performed in different labs, he suggests (1) that maintenance instrumentation should be set to standards traceable to the National Bureau of Standards, and (2) that a scheduled (test equipment) maintenance program is necessary to ensure that equipment remains within the calibration limits.

Establishing a basis for customer-producer agreement on acceptance-reject criteria is also a factor in establishing standards. Smiley (Reference 61) stresses the importance of correlation studies in achieving this objective. He presents a six-step program used in choosing a particular regime of NDT for the Polaris missile; the program is summarized as follows:

1. Select attributes to be examined.

2. Try the various NDT techniques, to select the optimum method.

3. Verify validity of the technique selected, by comparison with other methods and with destructive test results, if possible.

4. Establish the effect of defects, to determine basis for acceptance limits.

5. Prepare an NDT plan, charting the optimum technique, acceptance-reject criteria, and method of implementing the plan.

6. Eliminate redundancy in tests after production has started.

In discussing the pitfalls that sometimes beset NDT programs, he lists the following items:

1. Lack of identification of failure modes
2. Arbitrary selection of the NDT technique
3. Failure to evaluate the effect of defects
4. Neglecting to re-evaluate the NDT program after it is established
5. Absence of a system of checks and balances, to assure consistency of results
6. Inadequate financial support for NDT programs in the budgeting phase
7. Failure to require NDT and reliability personnel to predict the performance of hardware they inspect

He states that experience has shown that when personnel are required to predict hardware performance, based on NDT, the effectiveness of the program showed marked improvement.

MATERIAL RESPONSE

Ultrasonic inspection has been used extensively by the metal industries as a means of quality control inspection. Consequently, a considerable amount of research has been done to determine the effect of material factors of metals on ultrasonic inspection. Morgan (References 62, 63) has conducted extensive investigations to determine the effects of various alloys, thermal treatment, discontinuity size, surface conditions, and similar conditions, on ultrasonic inspection results. For example, he has demonstrated that ultrasonic transmissibility decreases as material particle size increases; that the effect of distance, varying with crystal (transducer) size and test frequency is considerable; that discontinuity size affects the height of the indication received, but the height of indication does not bear a linear relationship to the area of the discontinuity. Surface conditions such as roughness, scale and cleanliness also affected the ultrasonic response. These factors have resulted in the use of reference blocks of different materials as a standard for inspection of a particular product. In cases where the use of reference blocks is not feasible, the percent back

reflection technique is used for testing. This technique involves placing the search unit over an indication-free area of the article to be inspected and adjusting the instrument controls to obtain a predetermined height of the first back reflection indication; the material is then evaluated on the basis of the presence or absence of indications from discontinuities equal to or greater than a certain percentage of the back reflection. However, he concludes that experience best dictates the proper technique for performing an ultrasonic inspection, a factor which also must be considered in preparation of specifications.

The effects of forming method and heat treatment upon ultrasonic signal response of several alloys were investigated by Rowand, et al. (Reference 64). In investigating material variables, the effects were found to be similar to those discussed in the previous paragraph. Specific acoustic impedance and other acoustical properties were subsequently determined. It was found that the impedance mismatch at the water/metal interfaces was the most important factor when comparing one material to another due to the large energy loss at the interface. Correction factors were developed to compensate for different acoustical properties of materials. By correcting the difference in impedance, attenuation, and defect size in terms of decibels between a set of reference blocks of one material and the material being tested, a good approximation of defect size could be obtained. The use of beam collimators was investigated with particular emphasis on the use of C-scan recording. The minimum useful collimator size was found to be about 2-1/2 wavelengths measured in the material being tested. The propagation of shear and surface waves was also investigated. Shear waves generated over a wide range of incident angles had nearly the same reflected amplitude. Signal losses due to attenuation became significant at higher frequencies, however. The use of surface waves in the higher frequency range was apparently limited due to the low signal strength obtainable.

A similar investigation was conducted by Cross, et al. (Reference 65) with comparable results. In the shear and surface wave studies, significant variables with regard to signal response were determined to be as follows:

1. Sheet thickness

2. Distance between crystal and test block groove.

3. Changes in groove depth as compared to total sheet thickness.

4. Sample width, where less than crystal width.

5. Groove length, where less than crystal width.

In some applications of immersed testing, it was found advantageous to use collimation techniques to resolve defects which lie at small distances beneath the test surface. By reducing the size of the wavefront by collimation, the energy reflected from small flaws near the surface produces a greater amplitude of indication, relative to the surface echo, despite the overall loss of energy caused by the reduced wavefront.

In conducting a series of detail tests to establish parameters for reference blocks, Cline and Morgan (Reference 66) investigated the affect of grain structure on test results. A forged aluminum alloy stock was used for the test. Considered typical of a forged or rolled bar, the grains are flattened in a plane perpendicular to the compression axis and elongated in a direction parallel to the longitudinal axis. A high-gain ultrasonic beam directed perpendicular to the flattened grain structure produced considerable hash on the CRT screen. When the beam was directed parallel to the elongated grain, the hash disappeared.

A survey on the subject of ultrasonic testing as applied to plastics is presented by Baldanza (Reference 67). He notes that standards are usually set by contractors after appropriate service testing. Correlation of test data is accomplished by comparison of plotted or computer-programmed test data from destructive and nondestructive tests. He indicates that emphasis is often placed on detection of material property variables and material property design measurements rather than on flaw detection. He also emphasizes the importance of correlating inspection data and determining realistic defect parameters for establishing accept-reject standards. Baldanza presents a comprehensive cataloging of plastic defect definitions and classifications.

The foregoing literature evidences factors which further complicate establishment of standards for ultrasonic inspection. While these investigations were pertinent to metals, the problems are indicative of those encountered in testing other materials.

EFFECT OF EQUIPMENT CHARACTERISTICS

Ultrasonic equipment characteristics have a direct effect on ultrasonic inspection results. For example, with equipment incorporating CRT display, the height or amplitude of the display generally determines the magnitude of the defect and subsequent acceptance or rejection of the item being inspected. To determine factors which effect ultrasonic inspection results, Morgan (Reference 68) investigated the effects of equipment characteristics and usage. Several tests were conducted under varying conditions using a standard Sperry Reflectoscope with

quartz and barium tintanate transducers. Results of the investigation are summarized as follows:

1. Distance of defect from testing surface: display height was found to be proportional to distance, up to a maximum at which point it begins to decrease exponentially.

2. Transducers: size and frequency of the transducer were found to effect the extent of the Fresnel zone. In addition, it was found that two transducers of the same size and frequency did not necessarily provide identical test results.

3. Geometry of article under test: changes in shape and cross-sectional area of the original test blocks resulted in changes in amplitude of indication.

4. Equipment performance: changes in tube characteristics, as may be introduced by replacing tubes, aging, etc, affected the defect display. (It is conceivable that similar changes in other components would also affect the display.)

Similar results were obtained when the tests were repeated using the immersion method. Morgan concluded that the factors affecting display amplitude are interrelated and difficult to isolate from each other. Attempts to correct one factor frequently influenced the others. As a method of correction, he proposes preparation of an amplitude versus distance curve which is subsequently transposed to the CRT screen. Search units and instruments are then standardized using the same reference blocks used in preparation of the curve. The resulting curve and instrument settings would then be valid for search units of a particular size and frequency.

EQUIPMENT APPLICATION

The effects of inspection scanning speed on ultrasonic flaw detection were investigated by Bacon (Reference 69). Tests were conducted to (1) determine how fast the transducer could be scanned and still detect flaws, and (2) determine width of the transducer detection path. Employing immersion type tests and both quartz and lithium sulphate transducers, a series of tests were performed at different scanning speeds and results were plotted for comparison. It was shown that optimum test speed was determined by inspection equipment characteristics and application. Larger diameter transducers permitted greater scanning speeds as compared to smaller units. However, scanning speed was considered to be less a problem than that of achieving a wider scan path. In regard to transducer sensing width, it was found that (1) the relationship between transducer size and sensing width was insignificant, (2) sensing width varied directly with flaw size, and

(3) there was evidence of relationship between sensing width and pulse height. In the author's opinion, the need for quality assurance measurements of the test equipment is paramount to achievement of testing reliability.

Determination of actual flaw size is also a problem in ultrasonic inspection as the response is affected by the equipment application and material being inspected. In investigating methods to determine actual flaw size in materials, Posakony and Loetz (Reference 70) developed a breadboard system capable of three-dimensional display of defects. By using a multiple transducer system and additional electronic networks to sequence, time and display transducer outputs, a three-dimensional display of defects in a series of test blocks was obtained. Changes in test frequency had no adverse effect on test results.

In the literature reviewed, frequent reference is made to operator skill requirements. In a discussion of factors affecting ultrasonic testing reliability, Kay (Reference 71) states that ultrasonic inspection is more of an art than a science, depending upon operator experience and skill. The high incidence of unnecessary part rejection is also frequently mentioned. Erdman (Reference 72) and Thielsch (Reference 73) both indicate that one difficulty found in using higher frequencies in inspection is the operator inclination to reject a high percentage of items due to the increased sensitivity to defects or slight discontinuities.

Both operator training and equipment use are dependent upon clear, concise equipment specifications. It is the general concensus of the foregoing authors, and others, that present specification are either too vague or too restrictive to be conducive to an optimized inspection process. Equipment sensitivity, frequency, angle of sonic beam, mask size, and other related factors must be defined in clear, concise terms. To do so necessitates not only skill in preparation of the specification, but a reliable means of instrument calibration and test.

INSTRUMENT STANDARDS AND CALIBRATION

The need for frequent checking of the ultrasonic apparatus during inspection is emphasized by Morgan (Reference 62). By so doing, changes in instrument performance (due to failure, temperature effects, aging or physical damage to components) are revealed and test results are consistent. Some ASTM recommended practices specify procedures for calibrating test instruments before initiating a test. The reason given is that differences usually exist in the amplification characteristics of receivers and amplifiers used in various test instruments. Premarked dial settings, mentioned in some documents, are neither accurate or dependable enough to provide consistent results.

While the need for instrument checks and calibration is frequently mentioned in the literature surveyed, general calibration parameters or standards are not offered. The calibration technique most frequently mentioned utilizes a steel ball. This method is discussed in detail by Boghosian and Orner (Reference 74). The response obtained from a steel ball in water can be utilized for accurately defining any desired level of instrument sensitivity. Acceptance levels can be specified in terms of parameters which can be defined for specification purposes.

Articles relating to instrumentation dependability and accuracy are commonplace in publications dealing with instrumentation standards. Julie (Reference 75) states that many relatively new complex devices are being "warranted" to perform at levels of accuracy that cannot be supported by service experience. Borsei (Reference 76) relates that the simple algebraic error sum in any complex system using many different signal channels and making many measurements in a short time is usually so pessimistic as to be unrealistic. He presents a typical acceptance test to illustrate how accuracy determination is performed, using computer programmed testing. Computed test results provide a permanent record of instrument acceptance test performance in addition to clues to long-term operating characteristics of the system.

While these items are not directly related to ultrasonic systems, they illustrate basic factors to be considered in establishing ultrasonic system instrument standards.

ULTRASONIC INSPECTION AND EQUIPMENT STANDARDS

Several approaches have been taken in the development of ultrasonic standards, predominant of which are reference blocks containing natural flaws, blocks containing artificial flaws, and the percent back reflection technique. The use of other methods appears to be in the minority.

Morgan (Reference 77) conducted an evaluation of the percent back reflection technique using reference blocks of various stainless steels. The test disclosed that indication height was affected by the material grain size and other factors. Efforts to correct for ultrasonic transmissibility were not particularly encouraging.

Grebennick, et al. (Reference 78) developed a method of determining the dimension of flaws without using standard specimens. The method is based on a measurement of the ratio between the signal amplitude from a flaw for various positions of a transducer, to the distance from the surface of an object as the transducer is shifted from the position corresponding to the greatest amplitude of reflected signal. Nomograms are plotted for use in

determining flaw dimension by either the contact or immersion technique of echo flaw detection. It is claimed that flaw measurement is independent of instrument adjustment and of material properties.

A method of ultrasonic inspection standardization is described by Hayes (Reference 79) which, in his opinion, is suitable for general adoption. The principle is essentially that of the radiographic penetrameter in that at any point in the material under inspection, the sensitivity in terms of an artificial flaw should not be less than a given level. This system requires a suitable artificial flaw or reference block. A cylindrical hole 1/16 inch in diameter, approximately 1/2 inch long, and 1/8 inch from the surface of the test block was used as an artificial flaw. A matched calibrated attenuator was used to provide a means of scaling down signals from the artificial flaw. Specifications for application of the method are brief; the material is to be inspected ultrasonically at a sensitivity of not less than 12 db with respect to the signal from the 1/16-inch diameter hole using transducers not more than 1/2 inch in diameter. Resolution of the signal from this hole situated 1/8 inch from the surface of the material is to be not less than 3 db. Advantages claimed for this technique are that it is applicable to any of the ultrasonic inspection methods, or any make of ultrasonic equipment. Any doubt as to the position of minimum sensitivity in any technique can be reconciled by making a series of test blocks and checking the variations in sensitivity across the material section. Preparation of the test blocks does not require critical machining operations.

Reference Blocks

Boghosian's report (Reference 74) states that if a reference test block is to meet all the requirements for an equipment calibration standard it must be completely reproducible. The reproducibility factor is evidenced in the majority of related articles reviewed. Factors concerning fabrication of aluminum test blocks, as cited in ASTM standard E127-61T(80), are summarized in table A-II. These typify the complexity of fabricating reference blocks. However, Graboski (Reference 81) points out that meeting the physical requirements in fabrication of aluminum reference blocks is not as difficult as that in fabricating steel blocks. The major problem is in attaining proper ultrasonic response from the flat bottom hole used as a reference.

Panian and Van Valkenberg (Reference 82), in presenting a comprehensive review of the development of ASTM standard reference blocks, indicate that to be widely applicable, the optimum test standardization should calibrate the entire ultrasonic system. Techniques discussed are summarized in table A-III.

Table A-II

PARAMETERS FOR REFERENCE BLOCK FABRICATION/TEST

1. Definition of terms

2. Description of recommended sets

   Basic standard set
   Area - amplitude set
   Distance - amplitude set
   Coatings
   Controllable physical variables
   Material and size

3. Quality of material

   Evaluation procedure - general
   Test instrumentation
   Test frequency
   Search unit
   Immersion equipment
   Adjustment of sensitivity
   Evaluation procedure - detail
   Material standards

4. Physical characteristics check

   Entry surface
   Surface roughness

5. Ultrasonic characteristics check

   Objective
   Test frequency
   Apparatus
   Instrument calibration
   Calibration of search unit
   Adjustment of test apparatus
   Block preparation
   Checking for angular error)
   Checking response) procedures
   Plugging

6. Data record

Table A-III

POTENTIAL TECHNIQUES FOR TEST STANDARDIZATION

1.	Method:	Premark instrument controls to permit duplication of settings.
	Remarks:	Limited application as no correction for changes in instrument performance is provided.
2.	Method:	Electronic calibration checks to establish pulser output and receiver gain.
	Remarks:	Possibly feasible in immersion testing, no practical application to date.
3.	Method:	Produce artificial flaw by introducing a target into the beam, either between search unit and specimen or at rear surface of specimen.
	Remarks:	Same as Method 2.
4.	Method:	Use reflection from geometric discontinuity in specimen, as hole, keyway, etc.
	Remarks:	Specimens do not always contain natural reflective surfaces.
5.	Method:	Fabricate a standard discontinuity in noncritical portion of specimen.
	Remarks:	a. Impractical; generally not permissible due to nature of specimen. b. Specimen may exhibit significant differences in ultrasonic penetration. c. Accurate only at flaw depth unless elaborate compensation measures employed.
6.	Method:	Use one or more reference blocks, to establish test sensitivity.
	Remarks:	a. Most generally accepted method. b. Must exhibit same ultrasonic response for a given set of test parameters.

The majority of articles concerning test blocks relate to either their fabrication or their use in the metal industries. Rhoades (Reference 83) discusses an improved block of semicircular design used by the metal industry and claimed to provide increased accuracy. Standardization in the aluminum industry is discussed by Lavender and Pilgrim (Reference 84). The authors suggest the use of two test blocks for standardization purposes, a point which is also brought out by several of the other authors referenced herein. One block is used for instrument and probe control, the other (having identical characteristics of the material under test) serves as a testing standard.

Fabrication of test blocks for inspection of filament-wound structures is presented by Adams (Reference 85). Filament-wound reference blocks containing simulated defects were fabricated. Cellophane, teflon shims, and drops of oil were introduced at interfaces, and shallow, flat bottom holes were drilled in the bottom of the blocks. The cellophane and teflon shims failed to produce reliable disbond simulation because of partial adhesion occurring at the shims. The flat bottom holes of minimal depth, to avoid effects from hole sides, more closely simulated disbond conditions when the test block was adhesively bonded to a rubber liner.

Morris (Reference 86) states that reference blocks should be based on ultrasonic properties rather than chemical composition or other properties of the material. It was established that, within limits, the ultrasonic responses produced by a given material can be translated into equivalent responses which would be produced by some other material if a suitable attenuation factor is applied.

The British Aeronautical Inspection Directorate laboratories (Reference 87) have conducted extensive tests regarding drilling flat bottom holes in reference blocks and checking parallelism of the end of the hole with respect to the scanning surface. Test blocks are checked by including an attenuator in the flaw detector "receiving path," and inserting about 40 db of attenuation. Amplitude of top surface reflection is then adjusted to an arbitrary height indication and the probe adjusted in two vertical planes until maximum height is obtained. Attenuation is then reduced until the reflection from the hole can be detected, maximum amplitude of reflection being obtained by movement of the probe holder on the cross slides. The probe is then adjusted in the vertical planes and if the hole is parallel with the scanning surface there will be no increase in amplitude of the reflection. The hole is considered satisfactory provided it does not increase reflection amplitude more than 1 db. This type of reference standard is used for setting flaw detector sensitivity and for correlating the size of a natural defect. However, the optimum value is in being able to set instrument sensitivity to precise and repeatable values. The author cautions that estimation of defect

size is subject to considerable error if an indication can only be obtained in one position with a longitudinal wave probe. Two probe techniques provide more conclusive evidence of defect size.

Krautkramer (Reference 88) states that much to the detriment of standardization attempts, efforts to compare results from different types of equipment used to detect the echo of a back wall or a small defect were unsuccessful. He developed a method by which an equivalent circular disc which simulates the defect can be compared to an actual defect. This was accomplished by use of a calibrated gain control as an equipment accessory item and a mathematical representation of the equivalent defect characteristics and response. Meadows (Reference 87) points out that material characteristics can affect results obtained by this method.

Merib (Reference 89) investigated the effect of bandwidth on the reliability of equipment calibration using reference blocks with flat bottom holes, and the effect on defects of various sizes. Reliability was found to be satisfactory only for those blocks with large diameter holes. Blocks with small diameter holes, such as 3/4-inch, yielded less reliable results. He concludes that any calibration procedure for general usage, which uses test blocks, should include reference to bandwidth.

SUMMATION

The most generally accepted standard for ultrasonic testing are the reference blocks. However, the situation in the field of ultrasonic testing is best summed up by Graboski's (Reference 81) statement that ". . . the standards are more unstandard than in almost any other field."

This condition is no doubt due to the relative infancy of ultrasonic testing, variety of equipment used, and yet unexplored potential applications. The fairly widespread use of ultrasonic inspection by the metals industries exemplifies the fact that a specific need precipitates a specific solution. Typical of related problems are those of defining acceptance standards (Reference 90) and the use of different types of ultrasonic inspection such as surface wave inspection (Reference 91). In a recently published listing of specifications and standards (Reference 92), only 19 items were listed for ultrasonic inspection. The majority of these related to testing of metals; none pertained to honeycomb sandwich materials.

In a paper presented by Van Valkenburg in 1960 (Reference 93), he outlines standardization activities in the United States as falling in the following categories:

1. Investigation and establishment of calibration techniques.

2. Formulation of test specifications.

3. Fabrication of improved standard references.

4. Application of automated scanning, data processing and read-out.

5. Basic investigation of test phenomena and relationship to material properties.

6. Correlation of test results with destructive tests and service life.

Although much has been accomplished in these areas over the subsequent period, the primary elements of standardization are yet to be refined, clarified and condensed.

Based on the literature surveyed, the following basic needs concerning standardization become evident:

Definitive specifications

Operator training manuals and courses

Equipment performance standards

Definitive, easily interpreted methods of display or readout.

Instrument performance quality assurance measures (in-process inspection)

Universal reference standards

Standardized method of data recording

While much has been written concerning reference blocks, their use as a universal reference standard is limited to specific applications. Conventional reference blocks containing flat-bottomed holes are of little value as a standard for ultrasonic inspection of honeycomb sandwich composites because of differences in material characteristics, defect types, and response. For honeycomb sandwich inspection, reference standards consisting of actual composite specimens containing known defects would provide a more realistic reference. Reference standards of this type remain to be developed. However, the NAA/S&ID Saturn and Apollo development programs have demonstrated the successful use of honeycomb standards for disbond defects.

HONEYCOMB FAILURE CHARACTERIZATION

Defect characterization requires identification of the typical failure mechanisms of honeycomb structure and attendant cause/effect. Honeycomb structural defects may be grouped into two general classes: (1) Those introduced during, or the result of, manufacturing and/or fabrication processes, and (2) those caused by physical damage incurred during assembly or service. Identification of such defects is a prerequisite to establishing ultrasonic response for typical inherent defects encountered in honeycomb structures. A preliminary tabulation of failure mechanism characterization is presented in table A-IV. While not all-inclusive, it provides a basis for investigation of defect and failure mechanisms.

Literature surveyed to date indicates that adhesive bonds are a primary concern in the manufacturing/fabrication processes. Defects incurred as a result of physical damage are generally related to assembly and service experience. Physical damage of this nature is usually apparent by visual inspection techniques.

Stresses which cause core damage, such as fracture or crushing, would normally be evidenced by distortion of the facing sheets. The other possibility is internal damage or defects incurred during fabrication or repair processes involving splicing or joining of panels. Resulting anomalies could encompass either or both the adhesive bond and/or internal structure. Determination of bond and structural integrity would, in such case, entail ultrasonic inspection. Typical primary loading stresses are illustrated in figure A-1. Under beam loading stresses, figure 1-A, the loads are resisted by the tensile and compression strengths of the facings and by the shear resistance of the core. Loads on the core material are minimal under column loading stress (figure 1-B), with the facings carrying the majority of the load. Under these conditions, deflection must occur from edge-wise compression of the facing materials; facing load stability is dependent on stiffness or shear modulue of the core. Shear web loading stresses (figure 1-C) cause potential deflection in the facing sheets while the core forces the facing material to remain in the same plane. Maximum load capability under these conditions is dependent on the shear modulus of the core and the core-to-face bond. Poor bonding or low core shear modulus may cause deflection of the structure.

Impact loads may result in the item bouncing from or crushing the honeycomb structure, depending on the severity of the load and/or structure design. Poor structural design (References 94, 95) or precrushed core introduces factors which alter impact resistance. For

Table A-IV

CHARACTERIZATION OF FAILURE MECHANISMS - HONEYCOMB STRUCTURES

CHARACTERIZATION OF FAILURE MECHANISMS - HONEYCOMB STRUCTURES

Considerations	Defect Types	Possible Cause(s)	Applicable Test Methods
Design factors	Buckling	Design application	Visual
	Core failure	Design load application	NDT
	Fitting/joint failure	Design application	Destructive & NDT
Materials:			
a. Face sheets	Cracks, flaws, contamination	Manufacturing anomaly	NDT
b. Core	Over-under expansion	Manufacturing anomaly	Visual and NDT
c. Adhesive	Substandard bond	Storage, application or cure	Destructive and NDT
Fabrication	Substandard bonds	Environmental conditions, manufacturing controls	NDT and Destructive
	Disbonds	Worksmanship, contaminates	NDT
	Core voids	Worksmanship	NDT
	Crushed core	Worksmanship, methods, tooling	NDT
	Fractured core	Worksmanship, methods, tooling	NDT
	Surface damage	Tooling, handling methods	Visual
	Thick glue lines (porosity)	Materials, methods	NDT
	Thin glue lines	Materials, methods	NDT
Service experience	Visible physical damage	Shipment, handling, service	Visual
	Core/face sheet separation	Loading, environment	NDT
	Joint or fitting failure	Static and/or dynamic loads	Visual and NDT
Storage	Adhesive bond deterioration	Environmental conditions, loads	NDT
	Physical damage	Handling	Visual

*Assuming optimum design, manufacturing and fabrication conditions.

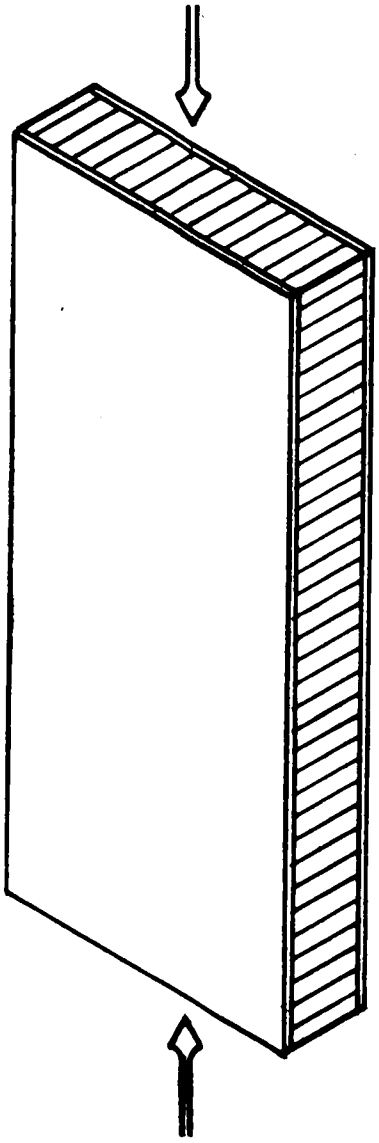

B. COLUMN LOADING STRESS

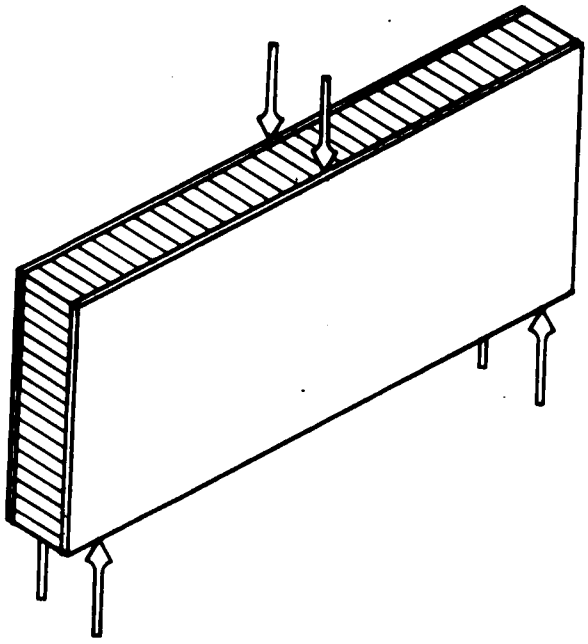

C. SHEAR WEB LOADING STRESS

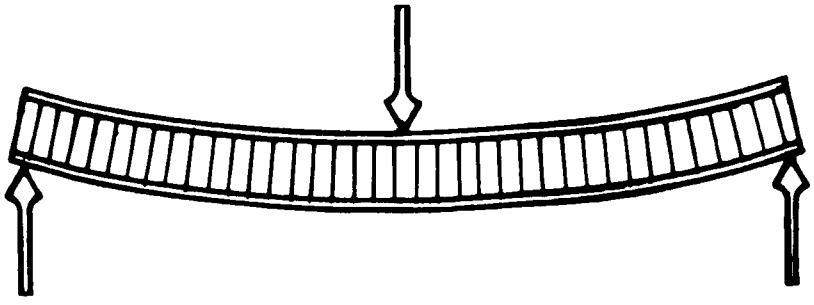

A. BEAM LOADING STRESS

Figure A-1. Basic Loading Stresses on Honeycomb Sandwich Panels (Hexel Products)

example, a very thick piece of narrow width honeycomb may buckle sideways rather than compress under impact. The effect of precrushed core on crushing resistance produces a typical load deflection curve as illustrated in figure A-2.

Static tests conducted by Hexel Products (Reference 96) have shown that core permeations (such as pin holes through cell walls of permeated aluminum honeycomb) have no apparent effect on crushing stress. They conclude that such permeations may help to relieve rapid increases in air pressure within the cells under dynamic impact conditions. This may tend toward preventing bursting of the cells by maintaining cell integrity which in turn would result in higher structural impact resistance. The effect of core permeations would vary with core thickness, conceivably being of greater benefit in thicker cores.

Maintenance of the strength characteristics of honeycomb materials is dependent upon the bond integrity between core and facing sheets. The core alone carries less load than do the facing sheets. While conducting node bond strength tests, Hexel Products (Reference 97) found that a decline in node bond strength in a bonded sandwich resulted in a decline in the mechanical properties of the sandwich. However, this decline was found to have a definite lower limit. Tests performed on a sandwich structure in which all node bond adhesive was leached out indicated that the structure retained a large portion of its integrity so long as the core-to-face bond had not deteriorated.

The NAA/LAD Structures Laboratory is conducting biaxial load tests of common bulkhead type specimens. The objective is to determine acceptance criteria for adhesive disbonds. The disbonds are simulated by placing various size teflon shims at both adhesive-core interfaces. The simulated disbonds include 1-, 2-, 3-, and 4-inch-diameter teflon discs in a specimen having 0.040-inch-thick facing sheets. Teflon discs 1/2-inch larger in diameter were used in a specimen having 0.070-inch-thick facing sheets. During preliminary tests, a specimen containing a 2-inch simulated disbond failed at 35 percent of limit load, and the facing sheet buckled on a line bisecting the disbond. The tests are continuing, being scheduled for completion during July 1966.

Investigation of field repair methods for a honeycomb sandwich insulation composite is being conducted by the NAA Space and Information Division (S&ID). As the honeycomb composite is used as an insulation barrier, gas barrier leads are an additional potential defect.

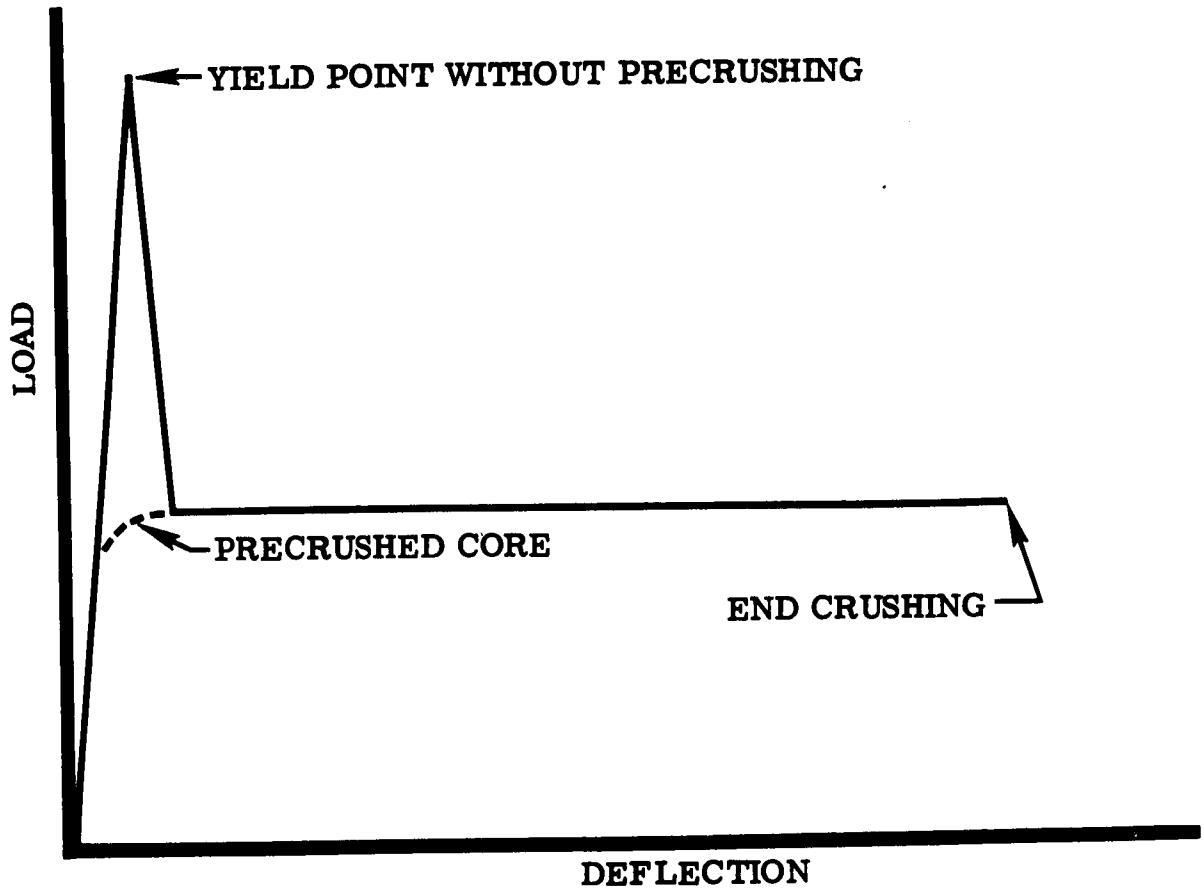

Figure A-2 **Typical Load Deflection Curve (Hexel Products)**

Structure tests include a leak detection and purge system checkout which will normally detect insulation leaks. These tests involve internal pressurization of the sandwich; a disbond can usually be detected by visual inspection as the unbonded skin bulges outward. Pinholes and similar skin penetrations are evidenced by a loss of test pressure. Defects of prime significance include gas barrier leaks, unbonded core or laminate areas, and impact or abrasion damage.

Temperature, humidity, dust control and handling procedures are a major consideration in effecting repairs. For example, to avoid possible contamination of cleaned and/or prepared details, personnel are required to wear white fabric gloves while making the repair. Preparation of the defect area, patch details, and the adhesive are rigidly controlled to ensure optimum repair conditions. Specimen samples are prepared using identical materials, during the repair procedure. These samples are subsequently subjected to proof tests to provide a basis for evaluating the adhesive bond.

Limits for reparable defects are dependent upon the defect type, location and size. For example, the defect proximity in relation to panel edge, fitting or attachment points, and other defects are prime considerations in establishing repair parameters. Other considerations are the accessibility of the defect, and physical applicability of the particular repair method to be used.

While the foregoing discussion deals with a specialized type of honeycomb composite structure, it typifies factors to be considered in establishing defect characterization and repair parameters.

The literature reviewed serves to illustrate but several of the factors bearing investigation in attempting defect characterization. It does emphasize the importance of the following factors:

- Good design practices
- Optimum adhesive bond integrity in the honeycomb panel
- Maintaining structural integrity of core materials
- Need for service experience, history, and failure data to establish optimum accept-reject criteria

It is evident that these factors reflect the effect of fabrication variables, especially in the case of adhesively bonded joints. To achieve maximum bond quality (98), four variables were investigated by Aerojet-General as follows; (1) surface condition of adherends, (2) air entrapment in liquid epoxy adhesives, (3) the use of primer coats and their degree of cure, and

(4) the amount of pressure used in the cure cycle. Tensile-shear strength was significantly increased by treating the surface of titanium, beryllium, nickel, and steel alloys with Bloomingdale Pre-Bond 700. Other factors found to contribute to increased strength include the use of vinyl-phenolic primer, complete evacuation of air entrapped in the bond, and curing the powdered epoxy-base adhesives used for the test under a pressure of 15 psi.

THEORETICAL STUDIES

The problem of predicting impending failure in sandwich structures has been the subject of many studies. New material combinations and nondestructive testing techniques used in advanced aerospace vehicles have increased both the scope and magnitude of such studies. These studies are of value to nondestructive techniques in that they assist in the characterization of structural failure mechanisms, and the possible effect that test methods may have on the structure.

A bibliography has been prepared by Foss (99) listing over 800 papers on theoretical and experimental stress analysis as related to sandwich materials and construction. Factors common to both nondestructive testing and direct characterization of failure mechanisms were considered as a basis for the literature selection.

An extensive study of structural vibrations in space vehicles was performed by Eldred, et al (100). Structural integrity was of fundamental concern in the study; the effect of vibration and fatigue due to acoustic excitation was investigated from the standpoint of sources, response and simplified composite response for testing. It is pointed out that, in general, the maximum vibration in space vehicles occurs at either launch or during the maximum dynamic pressure flight phase, as a result of boundary layer pressure fluctuations. The effect of sonic and ultrasonic radiation on rocket and missile safety factors is reported by Langenecker (101). He states that that sound energy is absorbed by lattice imperfections, whereas thermal energy is absorbed homogeneously in the material. Test results indicate that catastrophic effects may occur in vehicle parts where the sonic and ultrasonic energy is concentrated by reflections, to produce very high intensities. Conditions used to produce fatigue cracks in metals and resins by ultrasonic vibration are discussed by Weiss, (102) in the evaluation of fracture characteristics in these materials. Several studies have been conducted at NAA/LAD involving investigation of sonic effects on honeycomb panels and adhesive bonds (Moskal, 103, Botsco and Whittington, 104).

There is a recognized correlation between surface waviness of honeycomb core panels and attendant face wrinkling when panels are subjected to compressive forces. Investigations conducted by Rogers (105) indicate that

predictions of this type can be applied, by interpolation, to panels having a large degree of waviness. In his opinion, the theory has potential application to practical design situations. Failure criteria as related to reliability measurements is presented by Earles and Eddins (106). Considerations for structural failure criteria are presented, primarily with respect to structural strength and design limits. Theoretical analysis of strength and loading properties of structural panels are presented by Hirsch (107), and of foam-filled honeycomb radome structures by Fretz (108). Structural optimization of foam-core and honeycomb core sandwich cylinders was investigated by Burns (109). Instability considerations are reviewed, and structural optimization analysis are given, including the related computer programs. An evaluation of structural damage in glass-fiber reinforced structures, and representative failure mechanisms, is presented in a paper by Smith (110).

The effects of heating and freezing of water in honeycomb panels was investigated by the McDonnell Company (111). Test results indicated that neither skin-to-core bond or node bond failure occurs due to these conditions. Skingle (112) describes a system used to follow changes in the resonant frequency of a structure, due to damage in structural characteristics. Sapowith (113) proposes a method of detecting impending failure of large-scale structures under bending loads; a simple method for computation of shear wave velocity from torsional resonant frequency is presented by McCoy (114).

Krondratenko (115) made an analytical determination of the temperature at which the stresses in a honeycomb sandwich structure attain their critical values. The method used is based on the postulation that rapid localized heating of the structure induces thermal stresses which result in local stability loss. The stability of the joint between an outer plate and the honeycomb can then be estimated from the magnitude of deformation of the plate.

CONCLUSIONS

Information obtained from the surveys did not resolve the basic question of how to reliably measure adhesive bond strength by nondestructive means is still undeterminant. However, the measure of basic adhesive-bonded joint properties appears to be the logical and preliminary step. These measurements should include velocity, attenuation, etc, singly and in combinations. The survey has also raised a second problem. In order to determine a correlation between measurement parameters and bond quality, specimens are required with degraded adhesive bond strengths. No reliable and repeatable method of accomplishing this has been found than to fabricate trial specimens containing degraded bonds and subject these to destructive tests. The survey was subsequently extended to include vibrational properties of simple adhesive bonds and the bibliography was reviewed for vibrational analysis.

The references cited in the review of honeycomb failure characterization are representative of the literature available on theoretical studies of composite, sandwich, and honeycomb materials and structures. Many other references of this type were reviewed in the search for information on characterization of failure mechanisms, but few evidence a direct correlation with this subject. As pointed out earlier in the literature review, service correlation of defects and failures is the optimum criteria in a NDT program. Unfortunately, information of this nature seldom appears in a published report.

BIBLIOGRAPHY

Lessen, M.

Thermoelastic Damping at the Boundary Between Dissimilar Solids Jour. Appl. Phys., Vol. 28, No. 3, pp. 364-366, 1957

The problem of thermoelastic damping at the boundary between dissimilar solids is investigated for the case of small sinusoidal, longitudinal disturbances of long-wave length propagating normally through the interface. The relevant equations are derived from thermodynamic considerations, and it is found that the mechanical energy absorption per unit time is proportional to the square root of the disturbance frequency.

Stephens, R. W. B.

The Applications of Damping Capacity for Investigating the Structure of Solids Paper from Progress in Non-Destructive Testing, Vol. 1, Macmillan Co., N.Y., pp. 167-198, 1959

This paper reviews various ways of defining the damping capacity of a system, measuring it, and the effect on measured damping of several environmental variables. The author discusses the various micromechanisms which give rise to damping and the phenomena which can be investigated by damping capacity measurements. He emphasizes the need for linking-up internal friction measurements with measurements of other physical characteristics.

Entwistle, K. M.

The Damping Capacity of Metals
In book: The Physical Examination of Metals, edited by B. Chalmers and A. G. Quarrell, Edward Arnold (Publishers) Limited, London, pp. 487-558, 1960

This chapter concerns itself more with the use of damping capacity measurements as a metallurgical tool than with the engineering use of these measurements. He discusses units used and methods of measurement. The major part of the chapter is devoted to the experimental investigation and theoretical explanation of the origins of damping capacity. The author then considers damping capacity and fatigue, the assessment of the condition of a metal and flaw detection using damping capacity measurements, and damping capacity and vibration limitation. The damping properties of more than 25 materials are given.

Van Bueren, H. G.

Imperfections in Crystals. Chapter XVII. Internal Friction in Metals North-Holland Publ. Co., Amsterdam, 1960. Intersci. Publ. Inc., N. Y., 1960

Mechanisms of internal friction are discussed first. Subjects discussed under this heading are relaxation spectrum, relaxation and anelasticity, mechanical hysteresis, damped resonance, and viscous damping. The second part of the chapter is concerned with observations of internal friction. Subjects discussed here are experimental techniques, dislocation damping, internal friction not exclusively associated with dislocation motion, internal friction related to the presence of foreign solute atoms in the metal, thermal, magnetic, and electronic damping. Finally a table which is a survey of internal friction in metals is given. A fairly extensive bibliography concludes the chapter.

Kharitonov, A. V.

An Apparatus for Measuring Internal Friction in Solids Over the Range 20-400 kcps
Akust. Zh. USSR, Vol. 7, No. 1, pp. 104-106, 1961

The apparatus described is designed to investigate materials with low internal friction ($Q^{-1} = Q^{-2}$ to 10^{-6}). Longitudinal oscillations of the sample are produced by means of a plate condenser formed by the face of the sample and an electrode. The sample is mounted in the nodal plane by means of wires. The arrangement is placed in a vacuum. The attenuation decrement is measured by determining the width of the resonance curve or the rate of decay of free oscillations. Measurements are made by either an eddy current method (for non-ferromagnetic substances) or by using a barium titanate pick-up ring holding the mounting wires. Measurements in aluminum, magnesium and copper showed very small values of the internal friction.

Lazan, B. J. and Goodman, L. E.

Material and Interface Damping
Chapter 36, Shock and Vibration Handbook, Harris, C. M. and Crede, C. E., editors, McGraw-Hill Book Co., Inc., N. Y., 1961

In this article the term damping is defined, and its significance as an engineering property is discussed. Various methods for measuring damping in metals and for interpreting damping data are reviewed. The mechanisms thought to be responsible for energy dissipation in metals are presented. The damping of viscoelastic materials and their use as interface adhesives is studied. The bibliography has 40 entries.

..
Koster, W.

Damping Measurements as a Research Tool in Physical Metallurgy.
(In German)
Zeit, für Metallk., Vol. 53, pp. 17-27, 1962

The author presents the theory and application of damping measurements in metallurgical research. A detailed discussion is made of the following items: diffusion; Snoek-damping in body-centered cubic solid solutions; Zener-damping in face-centered cubic substitutional solid solutions; matrix atoms and foreign atoms interstitially dissolved in face-centered cubic alloys; phase-transformations; grain-boundary viscosity; interfaces.

Lazan, B. J.

Damping Properties of Materials and Material Composites Appl. Mech. Rev., Vol. 15, No. 2, pp. 81-88, February 1962

The author discusses energy dissipation within a material under cyclic stress or at an interface or joint between mating members where relative mechanical motions may occur. He summarizes the motivations for damping research, categories of mechanical damping, and gives a historical review. Damping nomenclature and units for materials, and classification of damping mechanisms are discussed.

Lazan, B. J.

Damping of Materials and Members in Structural Mechanics Pergamon Press, Inc., New York. Manuscript submitted August 10, 1964, to be published in 1965.

Damping studies have become increasingly significant in two general areas of engineering science: (a) materials science and (b) structural mechanics. The solution of several types of problems in structural mechanics requires information on the damping in the system before an analysis can be undertaken. This monograph is concerned primarily with damping as an important material property in the performance of machines and structures.

A fundamental and general viewpoint is emphasized in this monograph with the aim of reviewing phenomena and analytical approaches that are applicable not only to current problems but hopefully the unforeseen problems of the future. To provide a base for a consistent development Chapter II includes a review of the various damping phenomena encountered in structural mechanics and their distinguishing characteristics. Based on the categories of damping identified several viewpoints on nomenclature and units in common use are discussed, and a standard nomenclature is presented.

The next two chapters deal with the relations between mechanisms and phenomenology and the idealization of damping phenomena. Various types of linear and nonlinear models are reviewed in order to clarify the relations between macromechanisms and phenomenology, to indicate interrelations among various rheological properties, to reveal general patterns of behavior, and to facilitate the development of expressions for the hysteretic loop and damping relations. Chapter V is concerned with idealized damping-stress relations when several mechanisms are operative in order to provide relations that are valid for many types of engineering problems.

Chapter VI develops relations between the unit properties of materials and the total or average damping of an entire member, where a member is defined as a specimen or part made of a single uniform material. The criteria for relating damping properties under uniaxial and multiaxial stress and experimental data for appraising the validity of such criteria are presented in Chapter VII.

Chapter VIII is a compilation of much of the published data on damping properties of materials both in tabular and graphical form. Near resonant and other types of dynamic response are reviewed in Chapter IX for mechanical systems that include various categories of damping. Finally a listing of over 2000 publications on damping is given.

Truell, R., Chick, B., Anderson, G., Elbaum, C., and Findley, W.

Ultrasonic Methods for the Study of Stress Cycling Effects in Metals
WADD TR 60-920, April 1961

Authors discuss the use of ultrasonic methods to study defects of formation and their consequences in connection with stress cycling and fatigue of

aluminum. Measurements, especially in the very early stages of stress cycling support the idea that the cycling is accompanied by a dying out of dislocation damping effects, including recovery, as the result of the immobilization of dislocation oscillation by slip processes.

Aeronautical Systems Division, Wright-Patterson AF Base, Ohio. Rpt. No. ASD-TDR-62-1096. The Damping of Aluminum Honeycomb Sandwich Beams. Summary report, Jan 63

Considers the various sources of damping in a transversely vibrating plate of honeycomb sandwich. Expression derived for total damping ratio of unjointed honeycomb beam. Shown experimentally that energy dissipation through bending strain in adhesive layer is principal source. Nonlinearity of adhesive damping is allowed, and a parameter defined to predict beam damping for a given adhesive film. The parameter (and nonlinear coefficients) have been found experimentally from tests on beams. Low values of damping measured (0.01 to 0.04 percent of critical) suggest that "internal" damping deriving from joints in the structures.

University of Minnesota, Minneapolis, Minnesota. Damping and Fatigue Properties of Sandwich Configurations in Flexure, by Leon Keer and B. J. Lazan, November 1961.

A combined theoretical and experimental study is undertaken to develop an analytical approach for predicting the damping of sandwich configurations in flexure. The theory developed analyzes the various contributions to total damping, considering stress distribution and unit damping properties of skin and core, and employs a simple summation process to determine the damping of the composite. To confirm the theory a special test set-up was developed in which sandwich configurations were vibrated as free-free beams utilizing electromagnetic excitation. A series of tests were performed on several types of conventional sandwich beams. Damping predicted by the theory is in good agreement with that measured experimentally.

Fatigue tests were also performed in the specially designed damping machine and S-N curves are presented. Methods of failures and influence of discontinuities are discussed.

A. V. Kharitonov, "An Apparatus for Measuring Internal Friction in Solids over the Range 20-400 Kc," Akust. Zh. USSR, Vol. 7, n 1, 1961

E. G. Stanford and J. H. Fearon, "Progress in Non-Destructive Testing," Vol. 1, the Macmillan Company, N. Y., 1959

L. S. Jacobsen and R. S. Ayre, "Engineering Vibrations," McGraw-Hill Book Company, N. Y., 1958

C. R. Freberg and E. N. Kemler, "Elements of Mechanical Vibration," John Wiley & Sons, N. Y., 1957

American Society of Testing and Materials, "Internal Friction, Damping, and Cyclic Plasticity," ASTM Spec. Technical Publication No. 378, 1965

W. J. Trapp and D. M. Forney, Jr., "Acoustical Fatigue in Aerospace Structures," Syracuse University Press, Syracuse, N. Y., 1965

REFERENCES

1. Wake, W. C., "Adhesion of High Polymers," Adhesive Age, pp 18-20, May 1965.

2. Vasenin, R. M., "The Phenomenon of Adhesion," Adhesive Age, pp 21-25, May 1965; "Predicting Adhesion," Adhesive Age, pp 30-35, June 1965.

3. Hock, C. W., "Pressure Sensitive Adhesives: What Makes Them Stick?" Adhesive Age, pp 21-25, March 1964.

4. Sharpe, L. H., et al, "Adhesives," Inter. Science and Technology, pp 26-37, April 1964.

5. Sherrer, R. E., "Analysis of a Proposed Adhesive Test," Matls Research and Standards, pp 125-131, March 1965.

6. Moser, F., and Knoell, Sandra S., "The Effect of Loading Rate on Adhesive Strength," ASTM Bulletin, pp 60-63, January 1958.

7. Ilkka, G. A., "The Properties and Testing of High-Strength Adhesives," Metals Engrg Quarterly, pp 30-34, May 1962.

8. Epstein, Geo., "Adhesive Bonds for Sandwich Construction," Adhesive Age, pp 30-34, August 1963.

9. Pattee, H. E., et al, "Adhesive Bonding of Titanium," Matls in Design Engrg, pp 96-99, February 1959.

10. Pascuzzi, Bruno, and Hill, J. R., "Structural Adhesives for Cryogenic Applications," Adhesive Age, pp 19-26, March 1965.

11. Schijve, J., "Ultrasonic Resonance Testing of Glued Metal Joints," Aircraft Engrg; p 269, Sept 1958.

12. Hughes, E. T., and Burnstein, E. B., "Evaluation of Bond Quality in Honeycomb Panels Using Surface Wave Technique," Nondestructive Testing, p 373, November 1959.

13. McGonnagle, W. I., and Park, F., "Nondestructive Testing," Inter. Science and Technology, p 14, July 1964.

14. Ramsey, J. B., "Ultrasonic Techniques for Plastics Inspection," British Plastics, p 63, February 1964.

15. Gray, E. L., "Adhesive-Bonded Joints," American Machinist, p 122, 17 December 1956.

16. Jayne, B. A., "A Nondestructive Test of Glue Bond Quality," Forest Products Journal, p 294, October 1955.

17. Kanamaru, U., et al, "Nondestructive Quality Test of Adhesive Joints by Means of Resonance Measurements," Volloid Zeitschrift, 0.170 No. 2, p 123, 1960.

18. Dietz, A. G. H., "Measurement of Dynamic Modulus in Adhesive Joints at Ultrasonic Frequencies," ASTM 53rd Annual Meeting, 1950.

19. Hughes, E. T., and Burstein, E. B., "The Evaluation of Bond Quality in Honeycomb Panels," Nondestructive Testing, p 373, November-December 1959.

20. Anderson, R., "Evaluation of the Immerscope for the Nondestructive Evaluation of Metal Honeycomb Sandwich Parts," NAA/LAD Report CD-3526, August 1956.

21. Vogel, P. E. J., and Gericke, O. R., "Development of Improved Ultrasonic Bond Inspection Equipment," AMRA TR-63-16, Materials Testing Laboratory, October 1963.

22. Cizek, G., "Study of the Stub-Meter for Nondestructive Testing of Metal Sandwich Adhesive Bonds," NAA/LAD Report CD-3343, October 1955.

23. Kammerer, C., "Evaluation of the Sperry Reflectoscope Lamb Wave Ultrasonic Technique for Nondestructive Inspection of Aluminum Sandwich Adhesive Bonds," NAA/LAD Report CD-3704, May 1959.

24. Arnold, J. S., et al, "Development of a Nondestructive Test for Structural Adhesive Bonds," WADD TR 54-231, Parts 1 through 7, May 1954 - April 1959.

25. Vincent, C. T., "Nondestructive Tests for Structural Adhesives," WESCON Proceedings, Vol. 01, Part 09, 1957.

26. Grindrod, J., "Testing Adhesive-Bonded Metal-Sandwich Structures," Sheet Metal Industries, p 444, June 1955.

27. FAA, "Bonding Inspection," Quality Control Digest No. 5, July 1960.

28. Clotfelter, W. N., "Acoustic Techniques for the Nondestructive Evaluation of Adhesive Bonded Composite Materials," NASA TM-X 53219, March 1965.

29. Boruff, V. H., et al, "Evaluation of Ultrasonic Test Devices for Inspection of Adhesive Bonds," ER 10911-1 through ER 10911-11, Quarterly Progress Reports, July 1959 to March 1962.

30. Clemens, R. E., "Evaluation of Fokker Bond Tester System for Nondestructive Testing of FM 47 Adhesive Bonded Honeycomb," SNT Tech. Meeting at Los Angeles, California, 13 February 1962.

31. Schliekelman, R. J., "Nondestructive Testing of Adhesive-Bonded Metal Structures," Adhesives Technology, p 30, May 1964.

32. Smith, D. F., and Cagle, C. V., "Ultrasonic Testing of Adhesive Bonds Using the Fokker Bond Tester," Presented at Spring Nat Mtg Soc of NDT, 16-20 March 1964.

33. Gonzalez, H. M. and Cagle, C. V., "Nondestructive Testing of Adhesive Bonded Joints," Presented at 4th Pac. Area Nat Mtg of ASTM, Los Angeles, California, 4 October 1962.

34. Boruff, V. H., and Miller, N. B., "Adhesive Bonds Tested Ultrasonically," Adhesive Age, p 32, June 1962.

35. Hughes Aircraft Co, "Ultrasonic Testing of Adhesive Bonds, Procedure For," HP 6-24, 5 November 1964.

36. ASTM Standard, "Inspection of Adhesive Bonded Structures Using the Fokker Bond Tester."

37. Fokker-Royal Netherlands Aircraft, "Applications and Adjustment of the 1510 Probe of Fokker Bond Tester," Report No. R-296, August 1961.

38. Minnesota Mining and Manufacturing Co. (3M), Adhesives, Coatings and Sealers Division, 6411 Randolph St., Los Angeles, California, Messrs. S. Purdin and A. Bowman, representatives.

39. Bloomingdale Rubber Company (subsidiary of American Cyanamide Company, Aberdeen, Md.), Regional Office: Hawthorne, California, Mr. G. Martin, representative.

40. Mr. G. L. Schmitz, MRD Div General American Transportation Corp, Niles, Illinois - Personal communication, 8 August 1965.

41. Schmitz, G. L., "Nondestructive Testing for Evaluation of Strength of Bonded Material," Monthly Report No. 11 (May 1965), MRD Division, General American Transportation Corp, Niles, Illinois.

42. Baldanza, N. T., "A Review of Nondestructive Testing for Plastics: Methods and Applications," Plastec Report 22 (Aug 1965).

43. NAA/LAD, "Development of Nondestructive Testing Techniques for Honeycomb Heat Shields," Annual Program Report NA-65-452 (June 1965) and Quarterly Progress Report NA-65-814 (Oct 1965).

44. Morgan, J. B., "Some Factors of Importance in Ultrasonic Testing," J. NDT, May-June 1954.

45. Erickson, K., "A Schlierin Photograph Guide to Ultrasonic Transducers," Technical Paper presented at 25th National Convention, SNT, Detroit, Michigan, 21 October 1965.

46. Roderick, R. L., "On the Measurement of Ultrasonic Attenuation in Solids and Some Results in Steels," AT1 112-532 (May 1951).

47. McMaster, R. C., et al, "Ultrasonic Engineering - After One Year," News in Engineering (Nov 1963).

48. Merhib, C. P., "Frequency Bandwidth Considerations in Ultrasonic Testing," WAL-TR-143.7/1 (Jan 1963).

49. Gericke, O. R., "Geometry of Hidden Defects Determined by Ultrasonic Pulse Analysis and Spectroscopy," WAL-TR-830.5/5 (Dec 1962).

50. May, Jr., J. E., "Ultrasonic Traveling - Wave Devices for Communications," IEEE Spectrum (Oct 1965).

51. Sittig, E., "Where Transducers are Today," Electronic Industries (June 1963).

52. Walker, D. C. B., and Lumb, R. F., "Piezoelectric Probes for Immersion Ultrasonic Testing," App. Materials Res. (July 1964).

53. Thurston, R. N., "Effects of Electrical and Mechanical Terminating Resistances on Loss and Bandwidth According to the Conventional Equivalent Circuit of a Piezoelectric Transducer," IRE Nat. Conv. Record Part 6 (1959).

54. McElroy, J. T., "A Method of Identification, Measurement, and Recording Ultrasonic Transducer Characteristics," TR-64-22 (June 1964).

55. Crecraft, D. I., "Launching Ultrasonic Shear Waves Into Solids at Normal Incidence by Pressure Coupling," J. Sound Vib. (1964).

56. Harris, R. V., and Bobbin, J. E., "Frequency Dependent Effects in Ultrasonic Resonance Testing," J. NDT (Sept-Oct 1960).

57. Lavender, J. V., "The Transmission Efficiency of Liquid Couplants on Rough Surfaces When Using Longitudinal Waves," Journal B. S. C. R. A, No. 37 (June 1963).

58. Patsey, J. A., "Influence of Curved Entry Surfaces Upon Ultrasonic Response from Discontinuities," Technical Paper presented at 25th National Convention, SNT, Detroit, Michigan. 21 Oct 1965.

59. Klient, R. E., and Hagemeir, D. J., "Relationship of Standards and Specification to Nondestructive Testing," Materials Evaluation, Vol. 23 N 8, August 1965.

60. Canady, C. P., "Standardization of Test Equipment and Methods," Test Engineering, December 1965.

61. Smiley, R. W., "Service Correlation - The Key to Successful Nondestructive Testing," Material Research and Standards, March 1966.

62. Morgan, J. B., "Ultrasonic Testing Procedures," NDT, January-February 1959.

63. Morgan, J. B., "Differences in Ultrasonic Testing of Various Materials," NDT, March-April 1963.

64. Rowand, R. R., et al, "Development of Ultrasonic Techniques for Defect Evaluation," ASD-TDR 62-8, February 1963.

65. Cross, G. L., et al, "Research and Development Leading to the Establishment of Ultrasonic Test Standards for Aircraft Materials," WADC Technical Report 59-466, February 1960.

66. Cline, C. W., and Morgan, J. B., "Standardization in Ultrasonic Testing," NDT, July-August 1955.

67. Baldanza, N. T., "A Review of Nondestructive Testing for Plastics: Methods and Application," Plastec Report 22 August 1965.

68. Morgan, J. B., "Some Factors of Importance in Ultrasonic Testing," NDT, May-June 1954.

69. Bacon, J. P., "Effect of Test Speed on Ultrasonic Flaw Detection Reliability," NDT, November-December 1962.

70. Posakony, G. J., and Loetz, M. R., "Investigation of Methods for Determining Actual Flaw Size in Materials by Non-destructive Ultrasonic Techniques," WADC Technical Report 59-302, December 1959.

71. Kay, L., et al, "The Physical Factors Affecting the Reliability of Ultrasonic Non-destructive Testing," Journal British I. R. E., May 1962.

72. Erdman, D., "Ultrasonic Testing," NDT, Fall 1949.

73. Thielsch, H., "Do People Really Understand Non-destructive Testing?" Welding Design & Fabrication, July 1962.

74. Boghosian, S. D., and Orner, J. W., "A Primary Ultrasonic Standard," WAL TR 143. 8/1, December 1961.

75. Julie, L., "NBS Traceability," Electronic Instrument Digest, November-December 1965.

76. Borsei, A. A., "Testing and Predicting the Long-term Accuracy of Digital Instrument Systems," Electronic Instrument Digest, November-December 1965.

77. Morgan, J. B., "Ultrasonic Testing Standards for Steel Products," NDT, May-June 1962.

78. Grebennik, U. S., et al, "Determining the Dimensions of Flaws Ultrasonically Without Standard Specimens," Zavodskaya Laboratoriya Vol. 29 N 10 October 1963.

79. Hayes, D. J., et al, "Method of Standardization in Ultrasonic Flaw Detection," Metallurgia, December 1961.

80. ASTM E 127-61T, "Fabricating and Checking Aluminum Alloy Ultrasonic Standard Reference Blocks."

81. Graboski, E. T., "Review of Currently Available Specifications and Procedures for the Ultrasonic Inspection of Steel," NDT, July-August 1962.

82. Panian, F. C., and Van Valkenburg, H. E., "Development of ASTM Standard Reference Blocks for Ultrasonic Inspection," NDT, January-February 1961.

83. Rhoades, R. C., "New Moly Reference Blocks Improve Sonic Testing," Iron Age, 27 October 1960.

84. Lavender, J. D., and Pilgrim, R. M., "Standardization in Ultrasonic Testing," J. British Steel Casting Research Asso. No. 75, October 1963.

85. Adams, C. J., et al, "Ultrasonic Techniques and Standards for Testing Filament-Wound Structures, ML TDR 64-117, May 1966.

86. Morris, J. W., "Ultrasonic Standards for the Evaluation of Missile Materials and Components," paper presented at 3rd Pac. Area Nat. meeting of ASTM, San Francisco, October 1959.

87. Meadows, C. A., "Survey of Present Day Ultrasonic Equipment," Brit. J. of NDT, Vol. 3 N 1, March 1961.

88. Krautkramer, J., "Determination of the Size of Defects by the Ultrasonic Impulse Method," Brit. J. of NDT, June 1959.

89. Merhib, C. P., "Frequency Bandwidth Considerations in Ultrasonic Testing," WAL TR 143.7/1, January 1963.

90. Sinclair, N., "Some Considerations for Establishing Test Acceptance Standards," paper presented at SNT Conference, March 1966.

91. Binczewski, G. L., "Standardization and Application of Ultrasonic Surfacewave Inspection," Sperry Products reprint 50-857, 1957.

92. "Commonly Used Specifications and Standards for Nondestructive Testing," Materials Evaluation, Vol. XXIV, N 3, March 1966.

93. Van Valkenburg, H. E., "Ultrasonic Testing Calibration and Standardization Programs in the United States," Sperry reprint No. 50-806.

94. Hexel Products Brochure "E", "Honeycomb Sandwich Design," 1959.

95. Hexel Products TSB 120, "Mechanical Properties of Hexel Honeycomb," January 1964.

96. Hexel Products TSB 110, "Energy Absorption Properties of Aluminum Honeycomb," 10 January 1960.

97. Hexel Products TSB 106, "Node Bond Delamination Strength of Expanded Aluminum Honeycomb Under Various Environmental Conditions," 30 September 1959.

98. "Adhesives, Still Lots of Potential for Aerospace Structures," Aircraft and Missiles, pp 34-37, February 1960.

99. Foss, J. I., "A Bibliography of Sandwich Plates and Shells for the Space Age," Douglas Report SM-42883, December 1962.

100. Eldred, K., et al, "Structural Vibrations in Space Vehicles," WADD TR 61-62, December 1961.

101. Langenecker, B., "Effect of Sonic and Ultrasonic Radiation on Safety Factors of Rockets and Missiles," AIAA Journal.

102. Weiss, V., and Oelschlagel, D., "Ultrasonic Vibration Causes Fatigue Cracking in Metals and Resins," Matls and Res Stds, April 1966.

103. Moskal, B. J., "Sonic Fatigue Tests of Aluminum Honeycomb Panels for Goodyear Aerospace Corporation," NAA/LAD Report No. NA65H-251, April 1965.

104. Botsco, R., and Whittington, J., "Sonic Velocity and Attenuation in the Adhesive of Bonded Laminars," NAA/LAD Progress Report No. CD-3022.

105. Rogers, C. W., "Face Wrinkling as a Function of Surface Waviness," EER-FW-196, January 1964.

106. Earles, D. R., and Eddins, M. F., "Reliability Engineering Data Series - Failure Criteria," Avco Corporation, May 1962.

107. Hirsch, W. Z., "Transformation of New Knowledge for Economic Growth," NASA SP-5018, June 1964.

108. Fretz, Jr., G. C., "Feasibility of Monolithic Foam Radomes," NASA Accession, N6511840, June 1964.

109. Burns, A. B., "Structural Optimization of Foam-core and Honeycomb-core Sandwich Cylinders Under Axial Compression," Lockheed Missiles and Space Company Report 6-62-64-17, December 1964.

110. Smith, R. H., "Glass-fiber Reinforced Plastic Structures," NASA SP-5018, June 1964.

111. McDonnell Company Report A077, "Investigation of Heating and Freezing Effects on Honeycomb Panels," September 1963.

112. Skingle, C. W., "A Vibration Frequency Control System for Resonance Following Which Maintains a Preselected Phase Angle Between the Excitation Force and the Displacement of a Structure," Royal Aircraft Establishment Technical Note No. Structures 310, March 1962.

113. Sapowith, A. D., "Nondestructive Testing of Complex Structures Under Bending," Experimental Mechanics, January 1964.

114. McCoy, Jr., E. E., "A Resonant Vibration Technique for Laboratory Determination of Shear Wave Velocity," Matls and Res Stds, May 1966.

115. Kondratenko, R. M., "Stability of the Joint Between Coating and Filler in Three-Layer Structures," Aviatsionnaia Tekhnika, Vol. 7, N 3, 1965.

APPENDIX B

VIBRATION ANALYSIS OF

ADHESIVE BONDED LAP SHEAR SPECIMENS

CONTRACT NAS 8-11733

CASE I

Consider the load P only and assume weightless beam, but two portions of the thin beam have different lengths (figure 1).

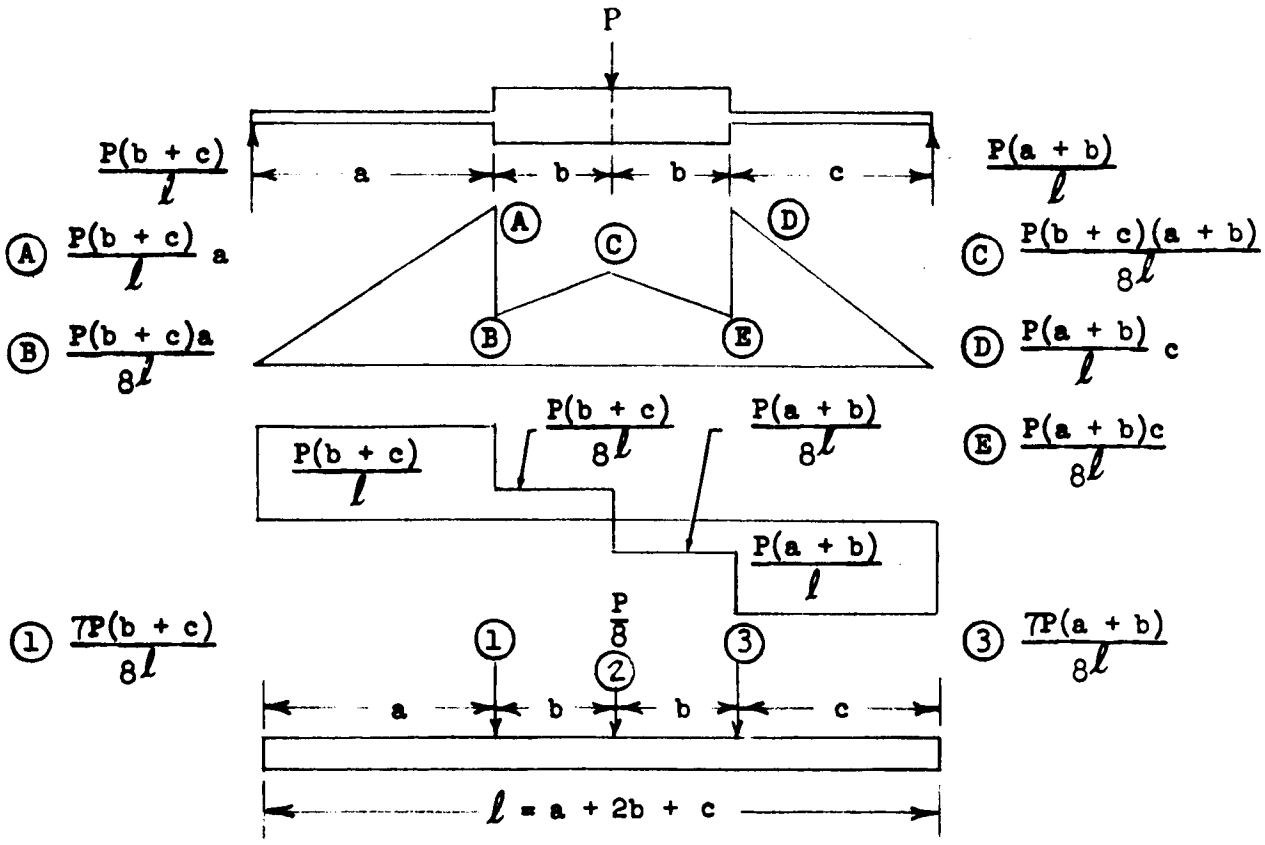

Figure B-1.

y_1 due to $W_1 = \frac{7P(b + c)}{8\ell} \cdot \frac{a^2(2b + c)^2}{3EI\ell} = \frac{7Pa^2(b + c)(2b + c)^2}{24EI\ell^2}$

due to $W_2 = \frac{(b + c)a}{6EI\ell}\left[\ell^2 - a^2 - (b + c)^2\right] \frac{P}{8} = \frac{Pa(b + c)}{48EI\ell}$
$\left[\ell^2 - a^2 - (b + c)^2\right]$

due to $W_3 = \frac{ac}{6EI\ell}\left[\ell^2 - a^2 - c^2\right] \frac{7P(a + b)}{8\ell} = \frac{7Pac(a + b)}{48EI\ell^2}$
$\left(\ell^2 - a^2 - c^2\right)$

y_2 due to $W_1 = \frac{7P(b + c)a(b + c)}{48EI\ell^2}\left[\ell^2 - (b + c)^2 - a^2\right]$

due to $W_2 = \frac{P(b + c)^2(a + b)^2}{24EI\ell}$

due to $W_3 = \frac{7P(a + b)c(a + b)}{48EI\ell^2}\left[\ell^2 - (a + b)^2 - c^2\right]$

y_3 due to $W_1 = \frac{7P(b + c)ac}{48EI\ell^2}\left(\ell^2 - c^2 - a^2\right)$

due to $W_2 = \frac{P(a + b)c}{48EI\ell}\left[\ell^2 - c^2 - (a + b)^2\right]$

due to $W_3 = \frac{7P(a + b)c^2(2b + a)^2}{24EI\ell^2}$

$P = 0.1103$ lb

$a = 2.33$ in.

$b = 0.26$ in.

$c = 2.27$ in.

$\ell = 5.12$ in.

$$y_1 = \frac{7 \times 0.1103 \times 2.33^2 \times 2.53 \times 2.79^2}{24 \times 187.5 \times 5.12^2} + \frac{0.1103 \times 2.33 \times 2.53 \times 14.385}{48 \times 187.5 \times 5.12}$$

$$+ \frac{7 \times 0.1103 \times 2.33 \times 2.27 \times 2.59 \times 15.633}{48 \times 187.5 \times 5.12^2} = .000700 + .0002031$$

$$+ .0007009 = .001604 \text{ in.}$$

$$y_2 = \frac{7 \times 0.1103 \times 2.53^2 \times 2.33 \times 14.385}{48 \times 187.5 \times 5.12^2} + \frac{0.1103 \times 2.53^2 \times 2.59^2}{24 \times 187.5 \times 5.12}$$

$$+ \frac{7 \times 0.1103 \times 2.59^2 \times 2.27 \times 14.353}{48 \times 187.5 \times 5.12^2} = 007023 + 002056 + 007153$$

$$= .0016232 \text{ in.}$$

$$y_3 = \frac{7 \times 0.1103 \times 2.53 \times 2.33 \times 2.27 \times 15.633}{48 \times 187.5 \times 5.12^2} + \frac{0.1103 \times 2.59 \times 2.27 \times 14.353}{48 \times 187.5 \times 5.12}$$

$$+ \frac{7 \times 0.1103 \times 2.59 \times 2.27^2 \times 2.85^2}{24 \times 187.5 \times 5.12^2} = .0006847 + .0002020 + .0007094$$

$$= .0015961 \text{ in.}$$

W	y	Wy	Wy^2
0.04768	0.001604	7.632×10^{-5}	1.221×10^{-7}
0.01379	0.0016232	2.239×10^{-5}	0.3550×10^{-7}
0.04882	0.0015961	7.793×10^{-5}	1.244×10^{-7}

$\Sigma Wy = 17.664 \times 10^{-5}$

$\Sigma Wy^2 = 2.820 \times 10^{-7}$

$$W = \sqrt{\frac{386 \times 176.64 \times 10^{-6}}{2.82 \times 10^{-7}}} = 486.1 \text{ radians/sec}$$

$$f = \frac{486.1}{2\pi} = 77.38 \text{ cps}$$

CASE II

Assume no central load (P = 0) and consider free vibration of the beam having overhang at either end support, as follows:

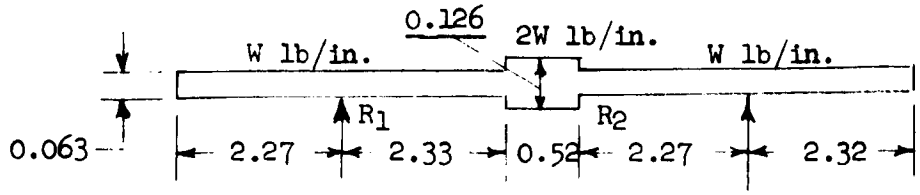

Numerical value of each dimension must be known because the solution involves graphical approximation. The dimensions shown above are taken from a lap joint specimen of solid aluminum which weighs 27.1 grams.

Let W = weight of beam per inch = $\frac{27.1/453.6}{(0.063 \times 9.19 + 0.126 \times 0.52) \times 1 \times 1 \times 0.063}$ = 0.00663 lb/in. Actual bending moment diagram must be constructed.

$$-W(2.27 + 2.33)(2.3 + 0.52 + 2.27) - 2W \times 0.52(0.26 + 2.27) - W\frac{2.27^2}{2} + R_1(2.33 + 0.52 + 2.27) + W\frac{2.32^2}{2} = 0$$

$$-23.414W - 2.6312W - 2.5765W + 5.12R_1 + 2.6912W = 0$$

$$R_1 = \frac{25.93}{5.12}W = 5.063W = 5.063 \times 0.0663 = 0.03356 \text{ lb}$$

The equivalent bending moment diagram is next constructed from the actual bending moment diagram. Since the ratio of I between the thin section and the thick section is 1 to 8, the bending moment in the thick section is divided by 8 to obtain its equivalent bending moment referring to I of the thin section. The complete equivalent bending diagram is shown in figure 2 in which the diagram is also approximated by a number of straight lines.

The equivalent shear force diagram (figure 3) can then be constructed from the approximate equivalent bending moment diagram. The equivalent shear forces are:

$$\frac{-0.4W - 0}{1.05 - 0} = \frac{-0.4 \times 0.00663}{1.05} = -0.00252 \text{ lb}$$

$$\frac{-2.58W - (-0.4W)}{2.27 - 1.05} = \frac{2.18 \times 0.00663}{1.22} = -0.01183 \text{ lb}$$

$$\frac{0.175W - (-2.58W)}{3.45 - 2.27} = \frac{2.755 \times 0.00663}{1.18} = +0.01544 \text{ lb}$$

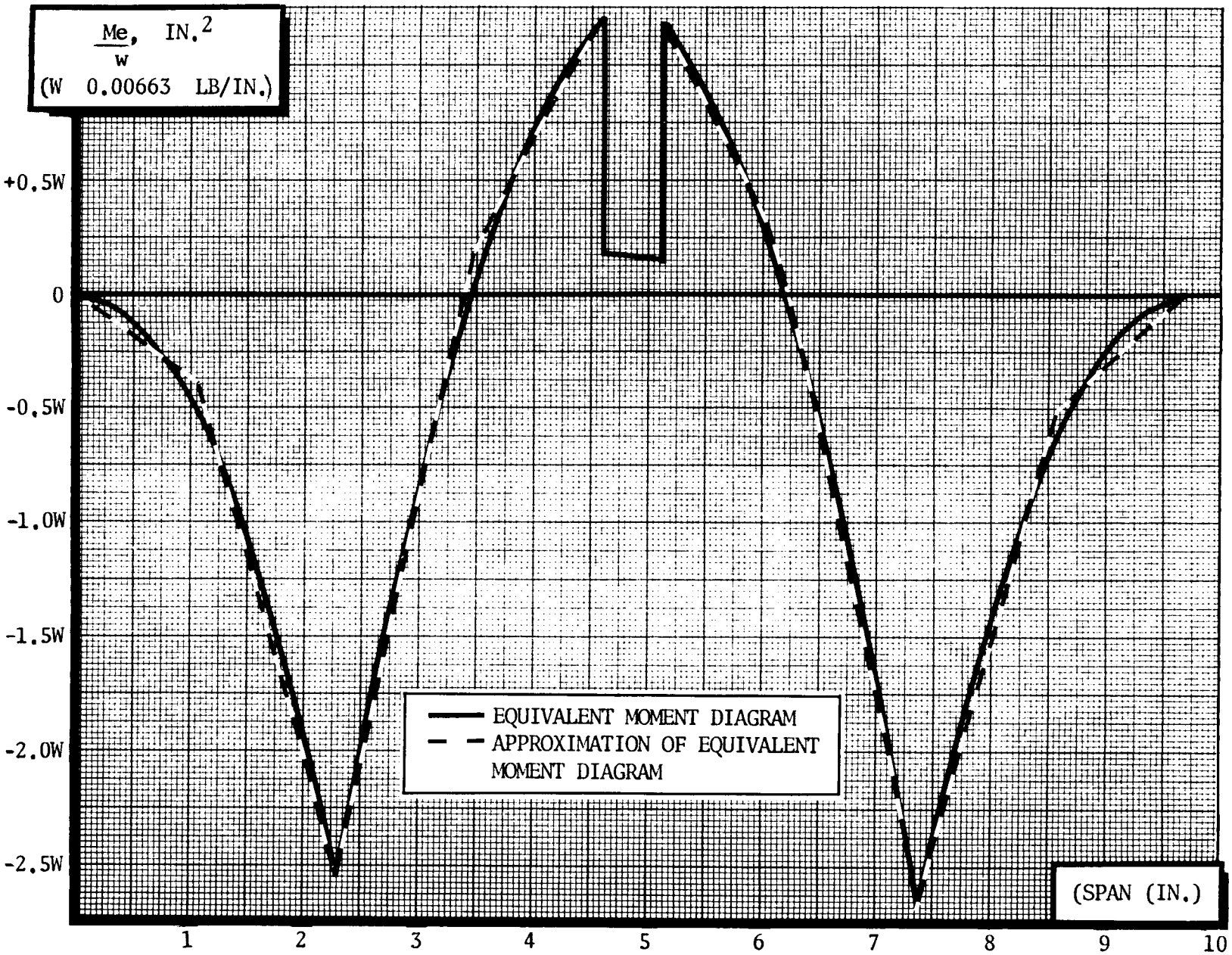
Me/w, IN.2
(W 0.00663 LB/IN.)
+0.5W
0
-0.5W
-1.0W
-1.5W
-2.0W
-2.5W
EQUIVALENT MOMENT DIAGRAM
APPROXIMATION OF EQUIVALENT MOMENT DIAGRAM
(SPAN (IN.)
1
2
3
4
5
6
7
8
9
10

Figure B-2

Equivalent Shear Force Diagram

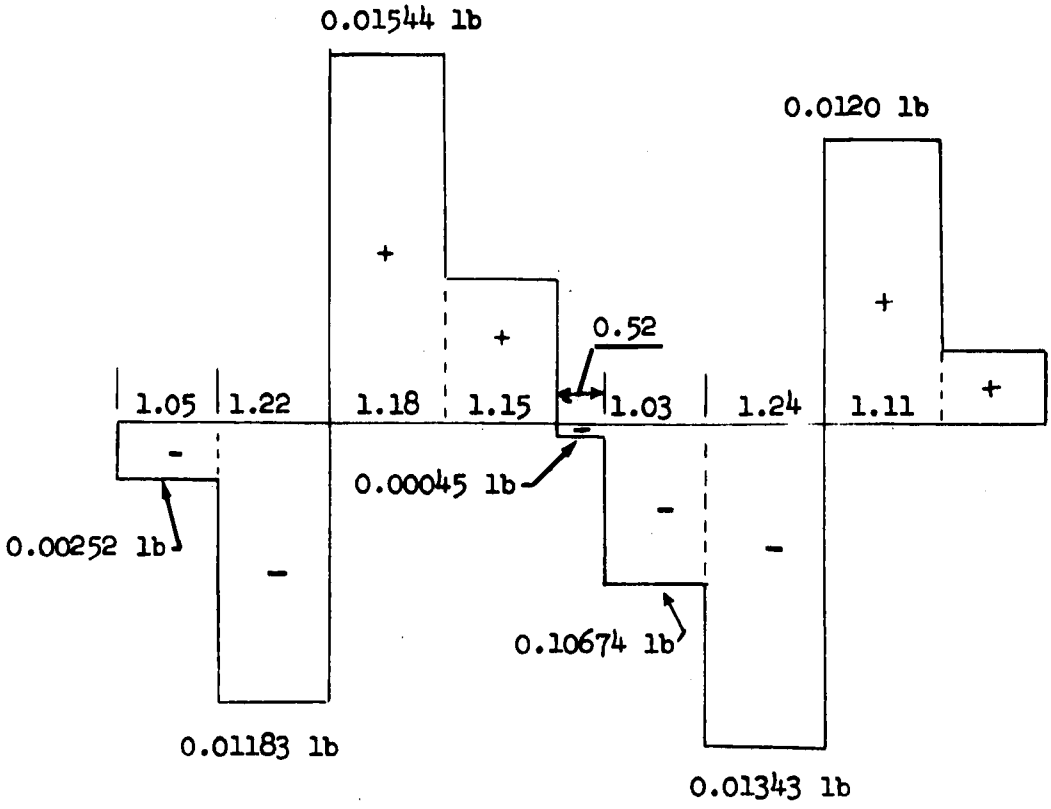

Equivalent System

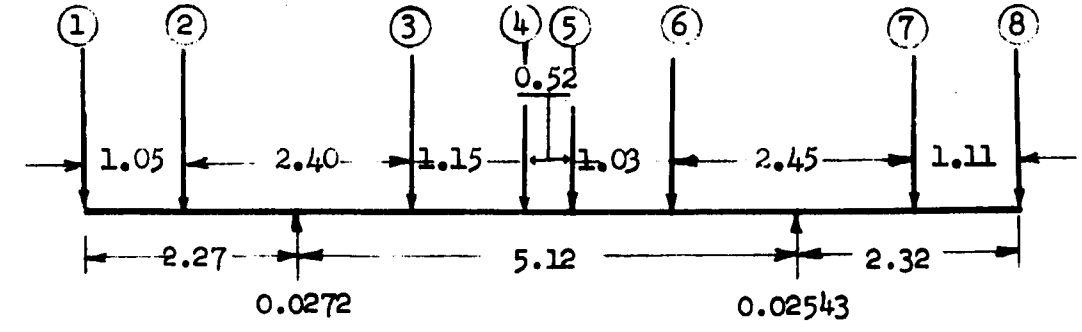

(1) 0.00252	(3) 0.00944	(5) 0.00629	(7) 0.00902
(2) 0.00931	(4) 0.00645	(6) 0.00669	(8) 0.00298

Figure B-3. Equivalent Shear Force Diagram and Equivalent System

$$\frac{1.216W - 0.175W}{4.60 - 3.45} = \frac{1.41 \times 0.00663}{1.15} = +0.0060 \text{ lb}$$

$$\frac{0.14W = 0.175W}{5.12 - 4.60} = \frac{-0.035 \times 0.00663}{0.52} = -0.000446 \text{ lb} = -0.00045 \text{ lb}$$

$$\frac{0.175W - 1.187W}{6.15 - 5.12} = \frac{-1.012 \times 0.00663}{1.03} = -0.00674 \text{ lb}$$

$$\frac{-2.69W - 0.175W}{7.39 - 6.15} = \frac{-2.515 \times 0.00663}{1.24} = -0.01343 \text{ lb}$$

$$\frac{-0.5W - (-2.69W)}{8.6 - 7.39} = \frac{2.19 \times 0.00663}{1.21} = 0.0120 \text{ lb}$$

$$\frac{0 - (-0.5W)}{9.71 - 8.6} = \frac{0.5 \times 0.00663}{1.11} = +0.00298 \text{ lb}$$

The fundamental frequency of the original beam having variable stiffness is equal to the fundamental frequency of the equivalent beam having uniform stiffness based on I of the thinner section of the original beam.

$$y_1 \text{ due to } W_1 = \frac{0.00252 \times 2.27^2(5.12 + 5.12)}{3EI} = \frac{0.03199}{EI}$$

$$\text{due to } W_2 = \frac{0.00931 \times 1.22^2(1.22 + 5.12)}{3EI} + \frac{1.05 \times 0.00931 \times 1.22(3.66 + 10.24)}{6EI} = \frac{0.02929}{EI} + \frac{0.02763}{EI} = - \frac{0.05692}{EI}$$

$$\text{due to } W_3 = \frac{0.00944 \times 3.94(5.12^2 - 3.94^2)}{6 \times 5.12EI} \times 2.27 = + \frac{0.02939}{EI}$$

$$\text{due to } W_4 = \frac{0.00645 \times 2.79(5.12^2 - 2.79^2)}{6 \times 5.12EI} \times 2.27 = + \frac{0.02451}{EI}$$

$$\text{due to } W_5 = \frac{0.00629 \times 2.27(5.12^2 - 2.27^2)}{6 \times 5.12EI} \times 2.27 = + \frac{0.02222}{EI}$$

$$\text{due to } W_6 = \frac{0.00669 \times 1.24(5.12^2 - 1.24^2)}{6 \times 5.12EI} \times 2.27 = + \frac{0.01512}{EI}$$

y_1 due to $W_7 = \frac{0.00902 \times 1.21 \times 5.12 \times 2.27}{6EI} = -\frac{0.02113}{EI}$

due to $W_8 = \frac{0.00298 \times 2.32 \times 5.12 \times 2.27}{6EI} = -\frac{0.01339}{EI}$

Total deflection at $W_1 = \Sigma y_1 = 1/EI(-0.03199 - 0.05692 + 0.02939 + 0.02451 + 0.02222 + 0.01512 - 0.02113 - 0.01339)$

$= -0.03140/EI$

$E = 9 \times 10^6 \qquad I = (1/12) \times 1 \times 0.063^3 = 20.83 \times 10^{-6} \qquad EI = 187.5$

$\Sigma y_1 = -0.03219/187.5 = -.0001715$ in.

y_2 due to $W_1 = \frac{0.00252 \times 1.25(3 \times 1.22 \times 2.27 - 1.22^2 + 2 \times 2.27 \times 5.21)}{6EI}$

$= \frac{-0.009543}{EI}$

due to $W_2 = \frac{0.00931 \times 1.22^2(1.22 + 5.12)}{3EI} = -\frac{0.02929}{EI}$

due to $W_3 = \frac{0.00944 \times 3.94(5.12^2 - 3.94^2) \times 1.22}{6 \times 5.21EI} = +\frac{0.0158}{EI}$

due to $W_4 = \frac{0.00645 \times 2.79(5.12^2 - 2.79^2) \times 1.22}{6 \times 5.21EI} = +\frac{0.01317}{EI}$

due to $W_5 = \frac{0.00629 \times 2.27(5.12^2 - 2.27^2) \times 1.22}{6 \times 5.21EI} = +\frac{0.01195}{EI}$

due to $W_6 = \frac{0.00669 \times 1.24(5.12^2 - 1.24^2) \times 1.22}{6 \times 5.12\ EI} = +\frac{0.008128}{EI}$

due to $W_7 = \frac{0.00902 \times 1.21 \times 5.12 \times 1.22}{6EI} = -\frac{0.01136}{EI}$

due to $W_8 = \frac{0.00298 \times 2.32 \times 5.12 \times 1.22}{6EI} = -\frac{0.007201}{EI}$

Total deflection at $W_2 = \Sigma y_2 = 1/EI(-0.009543 - 0.02929 + 0.0158 + 0.01317$

$+ 0.01195 + 0.008128 - 0.01136 - 0.007201)$

$= -0.008346/187.5 = -.0000445$ in.

y_3 due to $W_1 = \frac{0.00252 \times 2.27 \times 1.18}{6 \times 5.12EI}(2 \times 5.12 - 1.18)(5.12 - 1.18)$

$= + \frac{0.007843}{EI}$

due to $W_2 = \frac{0.00931 \times 1.22 \times 1.18}{6 \times 5.12EI}(2 \times 5.12 - 1.18)(5.12 - 1.18)$

$= + \frac{0.01557}{EI}$

due to $W_3 = \frac{0.00944 \times 1.18^2 \times 3.94^2}{3 \times 5.12EI} = - \frac{0.01328}{EI}$

due to $W_4 = \frac{0.00645 \times 1.18 \times 2.79(5.12^2 - 1.18^2 - 2.79^2)}{6 \times 5.12EI} = - \frac{0.01178}{EI}$

due to $W_5 = \frac{0.00629 \times 1.18 \times 2.27(5.12^2 - 1.18^2 - 2.27^2)}{6 \times 5.12EI} = - \frac{0.01079}{EI}$

due to $W_6 = \frac{0.00669 \times 1.18 \times 1.24(5.12^2 - 1.18^2 - 1.24^2)}{6 \times 5.12EI} = - \frac{0.007418}{EI}$

due to $W_7 = \frac{0.00902 \times 1.21 \times 3.94}{6 \times 5.12EI}(2 \times 5.12 - 3.94)(5.12 - 3.94)$

$= + \frac{0.01041}{EI}$

due to $W_8 = \frac{0.00298 \times 2.32 \times 3.94}{6 \times 5.12EI}(2 \times 5.12 - 3.94)(5.12 - 3.94)$

$= + \frac{0.006592}{EI}$

Total deflection at $W_3 = \Sigma y_3 = 1/EI(0.007843 + 0.01557 - 0.01328 - 0.01178$

$- 0.01079 - 0.007418 + 0.01041 + 0.006592)$

$= \frac{-0.002853}{187.5} = -.00001522$ in.

y_4 due to $W_1 = \frac{0.00252 \times 2.27 \times 2.33}{6 \times 5.12EI}(2 \times 5.12 - 2.33)(5.12 - 2.33)$

$= + \frac{0.009576}{EI}$

due to $W_2 = \frac{0.00931 \times 1.22 \times 2.33}{6 \times 5.12EI}(2 \times 5.12 - 2.33)(5.12 - 2.33)$

$= + \frac{0.01901}{EI}$

due to $W_3 = \frac{0.00944 \times 1.18 \times 2.79}{6 \times 5.12EI}(5.12^2 - 1.18^2 - 2.79^2) = - \frac{0.01724}{EI}$

due to $W_4 = \frac{0.00645 \times 2.33^2 \times 2.79^2}{3 \times 5.12EI} = - \frac{0.01775}{EI}$

due to $W_5 = \frac{0.00629 \times 2.33 \times 2.27}{6 \times 5.12EI}(5.12^2 - 2.27^2 - 2.33^2) = - \frac{0.01692}{EI}$

due to $W_6 = \frac{0.00669 \times 2.33 \times 1.24}{6 \times 5.12EI}(5.12^2 - 2.33^2 - 1.24^2) = - \frac{0.01212}{EI}$

due to $W_7 = \frac{0.00902 \times 1.21 \times 2.79}{6 \times 5.12EI}(2 \times 5.12 - 2.79)(5.12 - 2.79)$

$= + \frac{0.01721}{EI}$

due to $W_8 = \frac{0.00298 \times 2.32 \times 2.79}{6 \times 5.12EI}(2 \times 5.12 - 2.79)(5.12 - 2.79)$

$= + \frac{0.01090}{EI}$

Total deflection at $W_4 = \Sigma y_4 = 1/EI(0.009576 + 0.01901 - 0.01724 - 0.1775$

$- 0.01692 - 0.01212 + 0.01721 + 0.01090)$

$= \frac{-0.007334}{187.5} = -.0000391$ in.

y_5 due to $W_1 = \frac{0.00252 \times 2.27 \times 2.85}{6 \times 5.12EI}(2 \times 5.12 - 2.85)(5.12 - 2.85)$

$= + \frac{0.00890}{EI}$

due to $W_2 = \frac{0.00931 \times 1.22 \times 2.85}{6 \times 5.12EI}(2 \times 5.12 - 2.85)(5.12 - 2.85)$

$= + \frac{0.01767}{EI}$

due to $W_3 = \frac{0.00944 \times 1.18 \times 2.27}{6 \times 5.12EI}(5.12^2 - 1.18^2 - 2.27^2) = - \frac{0.01619}{EI}$

due to $W_4 = \frac{0.00645 \times 2.33 \times 2.27}{6 \times 5.12EI}(5.12^2 - 2.33^2 - 2.27^2) = - \frac{0.01736}{EI}$

due to $W_5 = \frac{0.00629 \times 2.85^2 \times 2.27^2}{3 \times 5.12EI} = - \frac{0.01714}{EI}$

due to $W_6 = \frac{0.00669 \times 2.85 \times 1.24}{6 \times 5.12EI}(5.12^2 - 2.85^2 - 1.24^2) = - \frac{0.01273}{EI}$

due to $W_7 = \frac{0.00902 \times 1.21 \times 2.27}{6 \times 5.12EI}(2 \times 5.12 - 2.27)(5.12 - 2.27)$

$= + \frac{0.01832}{EI}$

due to $W_8 = \frac{0.00298 \times 2.32 \times 2.27}{6 \times 5.12EI}(2 \times 5.12 - 2.27)(5.12 - 2.27)$

$= + \frac{0.01161}{EI}$

Total deflection at $W_5 = \Sigma y_5 = 1/EI(0.00890 + 0.01767 - 0.01619 - 0.01736$

$- 0.01714 - 0.01273 + 0.01832 + 0.01161)$

$= - \frac{0.00692}{187.5} = -.0000369$ in.

y_6 due to $W_1 = \frac{0.00252 \times 2.27 \times 3.88}{6 \times 5.12EI}(2 \times 5.12 - 3.88)(5.12 - 3.88)$

$= + \frac{0.005698}{EI}$

due to $W_2 = \frac{0.00931 \times 1.22 \times 3.88}{6 \times 5.12EI}(2 \times 5.12 - 3.88)(5.12 - 3.88)$

$= + \frac{0.01132}{EI}$

due to $W_3 = \frac{0.00944 \times 1.18 \times 1.24}{6 \times 5.12EI}(5.12^2 - 1.18^2 - 1.24^2) = - \frac{0.01047}{EI}$

due to $W_4 = \frac{0.00645 \times 1.24 \times 2.33}{6 \times 5.12EI}(5.12^2 - 1.24^2 - 2.33^2) = - \frac{0.01168}{EI}$

due to $W_5 = \frac{0.00629 \times 1.24 \times 2.85}{6 \times 5.12EI}(5.12^2 - 1.24^2 - 2.85^2) = - \frac{0.01198}{EI}$

due to $W_6 = \frac{0.00669 \times 1.24^2 \times 3.88^2}{3 \times 5.12EI} = - \frac{0.01008}{EI}$

due to $W_7 = \frac{0.00902 \times 1.21 \times 1.24}{3 \times 5.12EI}(2 \times 5.12 - 1.24)(5.12 - 1.24)$

$= + \frac{0.01538}{EI}$

due to $W_8 = \frac{0.00298 \times 2.32 \times 1.24}{6 \times 5.12EI}(2 \times 5.12 - 1.24)(5.12 - 1.24)$

Total deflection at $W_6 = \Sigma y_6 = 1/EI(0.005698 + 0.01132 - 0.01047 - 0.01168$

$- 0.01198 - 0.01008 + 0.01538 + 0.009743)$

$= - \frac{0.00207}{187.5} = -.00001103$ in.

y_7 due to $W_1 = \frac{0.00252 \times 2.27 \times 5.12 \times 1.21}{6EI} = -\frac{0.005906}{EI}$

due to $W_2 = \frac{0.00931 \times 1.22 \times 5.12 \times 1.21}{6EI} = -\frac{0.01173}{EI}$

due to $W_3 = \frac{0.00944 \times 1.18 \times 1.21}{6 \times 5.12EI}(5.12^2 - 1.18^2) = +\frac{0.01089}{EI}$

due to $W_4 = \frac{0.00645 \times 2.33 \times 1.21}{6 \times 5.12EI}(5.12^2 - 2.33^2) = +\frac{0.01231}{EI}$

due to $W_5 = \frac{0.00629 \times 2.85 \times 1.21}{6 \times 5.12EI}(5.12^2 - 2.85^2) = +\frac{0.01277}{EI}$

due to $W_6 = \frac{0.00669 \times 3.88 \times 1.21}{6 \times 5.12EI}(5.12^2 - 3.88^2) = +\frac{0.01141}{EI}$

due to $W_7 = \frac{0.00902 \times 1.21^2}{3EI}(1.21 + 5.12) = -\frac{0.02787}{EI}$

due to $W_8 = \frac{0.00298 \times 1.21(3 \times 1.21 \times 2.32 - 1.21^2 + 2 \times 5.12 \times 2.32)}{6EI}$

$= -\frac{0.01847}{EI}$

Total deflection at $W_7 = \Sigma y_7 = 1/EI(-0.005906 - 0.01173 + 0.01089 + 0.01231$

$+ 0.01277 + 0.01141 - 0.02787 - 0.01847) = -\frac{0.016596}{187.5}$

$= -.0000884$ in.

y_8 due to $W_1 = \frac{0.00252 \times 2.27 \times 5.12 \times 2.32}{6EI} = -\frac{0.01131}{EI}$

due to $W_2 = \frac{0.00931 \times 1.22 \times 5.12 \times 2.32}{6EI} = -\frac{0.0225}{EI}$

due to $W_3 = \frac{0.00944 \times 1.18 \times 2.32}{6 \times 5.12EI}(5.12^2 - 1.18^2) = +\frac{0.02088}{EI}$

due to $W_4 = \frac{0.00645 \times 2.33 \times 2.32}{6 \times 5.12EI}(5.12^2 - 2.33^2) = +\frac{0.02360}{EI}$

y_8 due to $W_5 = \frac{0.00629 \times 2.85 \times 2.32}{6 \times 5.12EI}(5.12^2 - 2.85^2) = + \frac{0.02449}{EI}$

due to $W_6 = \frac{0.00669 \times 3.88 \times 2.32}{6 \times 5.12EI}(5.12^2 - 3.88^2) = + \frac{0.02187}{EI}$

due to $W_7 = \frac{0.00902 \times 1.21^2(1.21 + 5.12)}{3EI}$

$+ \frac{1.11 \times 0.00902 \times 1.21(3 \times 1.21 + 2 \times 5.12)}{6EI} = \frac{0.02787}{EI}$

$+ \frac{0.02800}{EI} = - \frac{0.05587}{EI}$

due to $W = \frac{0.00298 \times 2.32^2(2.32 + 5.12)}{3EI} = - \frac{0.03978}{EI}$

Total deflection at $W_8 = \Sigma y_8 = 1/EI(-0.01131 - 0.02250 + 0.02088 + 0.02360$

$+ 0.02449 + 0.02187 - 0.05587 - 0.03978) = \frac{-0.03862}{187.5}$

$= -.000206$ in.

$$W^2 = \sqrt{g \frac{\sum_{i=1}^{i=8} W_i y_i}{\sum_{i=1}^{i=8} W_i y_i^2}} \qquad \text{and} \quad f = W/2\pi \text{ cps}$$

CASE III

Consider both the central load P and weight of the beam

① 0.00252 ③ 0.00944 ⑤ 0.00629 ⑦ 0.00902

② 0.00931 ④ 0.00645 ⑥ 0.00669 ⑧ 0.00298

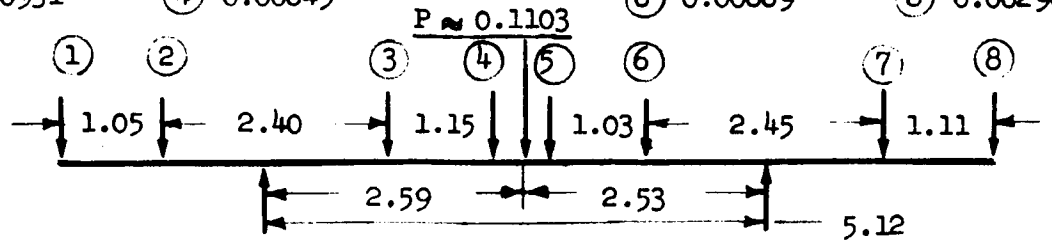

Figure 4.

y_1 due to P = $\frac{0.1103 \times 2.53 \times 2.27}{6 \times 5.12\ EI}(5.12^2 - 2.53^2) = +\frac{0.4083}{187.5} = +.002178$ inch

y_2 due to P = $\frac{0.1103 \times 2.53 \times 1.22}{6 \times 5.12\ EI}(5.12^2 - 2.53^2) = +\frac{0.2195}{187.5} = +.001170$ inch

y_3 due to P = $\frac{0.1103 \times 2.53 \times 1.18}{6 \times 5.12\ EI}(5.12^2 - 1.18^2 - 2.53^2)$

$= -\frac{0.1973}{187.5} = -.001052$ inch

y_4 due to P = $\frac{0.1103 \times 2.53 \times 2.33}{6 \times 5.12\ EI}(5.12^2 - 2.33^2 - 2.53^2)$

$= -\frac{0.3043}{187.5} = -.001624$ inch

y_5 due to P = $\frac{0.1103 \times 2.59 \times 2.27}{6 \times 5.12\ EI}(5.12^2 - 2.59^2 - 2.27^2)$

$= -\frac{0.3028}{187.5} = -.001615$ inch

y_6 due to P = $\frac{0.1103 \times 2.59 \times 1.24}{6 \times 5.12\ EI}(5.12^2 - 2.59^2 - 1.24^2)$

$= -\frac{0.2072}{187.5} = -.001106$ inch

y_7 due to P = $\frac{0.1103 \times 2.59 \times 1.21}{6 \times 5.12\ EI}(5.12^2 - 2.59^2) = +\frac{0.2194}{187.5} = +.001170$ inch

y_8 due to P = $\frac{0.1103 \times 2.59 \times 2.32}{6 \times 5.12\ EI}(5.12^2 - 2.59^2) = +\frac{0.4206}{187.5} = +.002244$ inch

Total deflection at W_1 = -.0001715 + .002178 = +0.0020065 inch
at W_2 = -.0000445 + .00117 = +0.0011255 inch
at W_3 = -.00001522 - .01052 = -0.00103678 inch
at W_4 = -.0000391 - .001624 = -0.0016631 inch
at W_5 = -.0000369 - .001615 = -0.0016519 inch
at W_6 = -.00001103 - .001106 = -0.00111703 inch

at W_7 = -.0000884 + .00117 = +0.0010816 inch
at W_8 = -.000206 + .002244 = +0.002038 inch

$$y_p \text{ due to } W_1 = \frac{0.00252 \times 2.27 \times 2.59}{6 \times 5.12\ EI}(2 \times 5.12 - 2.59)$$

$$(5.12 - 2.59) = + \frac{0.009335}{EI}$$

$$y_p \text{ due to } W_2 = \frac{0.00931 \times 1.22 \times 2.59}{6 \times 5.12\ EI}(2 \times 5.12 - 2.59)$$

$$(5.12 - 2.59) = + \frac{0.01854}{EI}$$

$$y_p \text{ due to } W_3 = \frac{0.00944 \times 1.18 \times 2.53}{6 \times 5.12\ EI}(5.12^2 - 1.18^2 - 2.53^2)$$

$$= - \frac{0.0169}{EI}$$

$$y_p \text{ due to } W_4 = \frac{0.00645 \times 2.33 \times 2.53}{6 \times 5.12\ EI}(5.12^2 - 2.33^2 - 2.53^2)$$

$$= - \frac{0.0178}{EI}$$

$$y_p \text{ due to } W_5 = \frac{0.00629 \times 2.27 \times 2.59}{6 \times 5.12\ EI}(5.12^2 - 2.59^2 - 2.27^2)$$

$$= - \frac{0.01728}{EI}$$

$$y_p \text{ due to } W_6 = \frac{0.00669 \times 2.59 \times 1.24}{6 \times 5.12\ EI}(5.12^2 - 2.59^2 - 1.24^2)$$

$$= - \frac{0.01257}{EI}$$

$$y_p \text{ due to } W_7 = \frac{0.00902 \times 1.21 \times 2.53}{6 \times 5.12\ EI}(2 \times 5.12 - 2.53)$$

$$(5.12 - 2.53) = + \frac{0.01795}{EI}$$

$$y_p \text{ due to } W_8 = \frac{0.00298 \times 2.32 \times 2.53}{6 \times 5.12\ EI}(2 \times 5.12 - 2.53)$$

$$(5.12 - 2.53) = + \frac{0.01137}{EI}$$

$$y_p \text{ due to } P = \frac{0.1103 \times 2.59^2 \times 2.53^2}{3 \times 5.12\ EI} = - \frac{0.3081}{EI}$$

Total deflection at P = $\Sigma y_P = \frac{1}{EI}$ (0.00935 + 0.01854 - 0.0169 - 0.0178

- 0.01728 - 0.01257 + 0.01795 + 0.01137 - 0.3081)

$= -\frac{0.31544}{187.5} = -0.001682$ inch

W	|y|	|Wy|	|Wy^2|
0.00252	0.0020065	5.056×10^{-6}	1.014×10^{-8}
0.00931	0.0011255	1.047×10^{-5}	1.179×10^{-8}
0.00944	0.00103678	9.788×10^{-6}	1.015×10^{-8}
0.00645	0.0016631	1.075×10^{-5}	1.784×10^{-8}
0.00629	0.0016519	1.040×10^{-5}	1.717×10^{-8}
0.00669	0.00111703	7.471×10^{-6}	8.345×10^{-9}
0.00902	0.0010816	9.763×10^{-6}	1.057×10^{-8}
0.00298	0.002038	6.073×10^{-6}	1.238×10^{-8}
0.1103	0.001682	1.856×10^{-4}	3.120×10^{-7}

$\Sigma|Wy| = 25.537 \times 10^{-5}$

$\Sigma|Wy| = 41.0385 \times 10^{-8}$

$$W = \sqrt{\frac{g\Sigma|Wy|}{\Sigma|Wy^2|}} = \sqrt{\frac{386 \times 25.537 \times 10^{-5}}{41 \times 0385 \times 10^{-8}}} = 490.1 \text{ rad/sec}$$

$$f = \frac{W}{2\pi} = 78.0 \text{ cycles/sec}$$

Note: If only the central load, 0.1103 lb, is considered

$$W = \sqrt{\frac{386EI}{0.3081}} = 496.0 \text{ rad/sec}$$

$$f = \frac{496.0}{2\pi} = 77.1 \text{ cycles/sec}$$

APPENDIX C

VIBRATION ANALYSIS OF ADHESIVE BONDED HONEYCOMB AND NATURAL FREQUENCY DETERMINATION

CONTRACT NAS 8-11733

Appendix C

VIBRATION ANALYSIS OF ADHESIVE BONDED HONEYCOMB AND NATURAL FREQUENCY DETERMINATION

VIBRATION ANALYSIS OF HONEYCOMB COMPOSITES

The acoustic wave propagation in the cells of a honeycomb core cause standing waves to oscillate in two normal modes of vibration. The component of particle velocity normal to the direction of propagation can not be considered zero since the walls are subject to vibration due to conduction of the waves emitted by the acoustically energized face sheet. The cross-sectional dimension of cells can also be large so that waves may travel transversely as well as along the length. Therefore, various normal modes of vibration can be present in the cells. And, since each normal mode has its own characteristic frequencies of vibration, the resonant conditions of the cells are quite complex.

The characteristic frequencies of vibration of various modes in a rigid-walled rectangular enclosure is first considered. The particular solution of the wave equation for sound pressure when applied to this rectangular enclosure Figure C-1 (Ref. 1) is

$$p = \cos\sqrt{\beta}\ x\ \cos\ \sqrt{\alpha - \beta}\ y \cos\sqrt{\frac{w^2}{c^2} - \alpha}\ z \sin wt$$

where c is sound velocity in air and α and β are constants. Application of the boundary conditions at wall surfaces (x = o, a; y = o, b; z = o, d) to the normal derivatives of this particular solution results in three equations

$$\beta = \frac{M\pi}{a},\quad \sqrt{\alpha - \beta} = \frac{n\pi}{b}\ ;\ \text{and}\ \sqrt{\frac{w^2}{c^2} - \alpha} = \frac{\ell\pi}{d}$$

where m, n and ℓ are indices which can be zero or integers. The angular frequency is thus

$$w = \pi c \left[\left(\frac{m}{a}\right)^2 + \left(\frac{n}{b}\right)^2 + \left(\frac{\ell}{d}\right)^2\right]^{1/2}$$

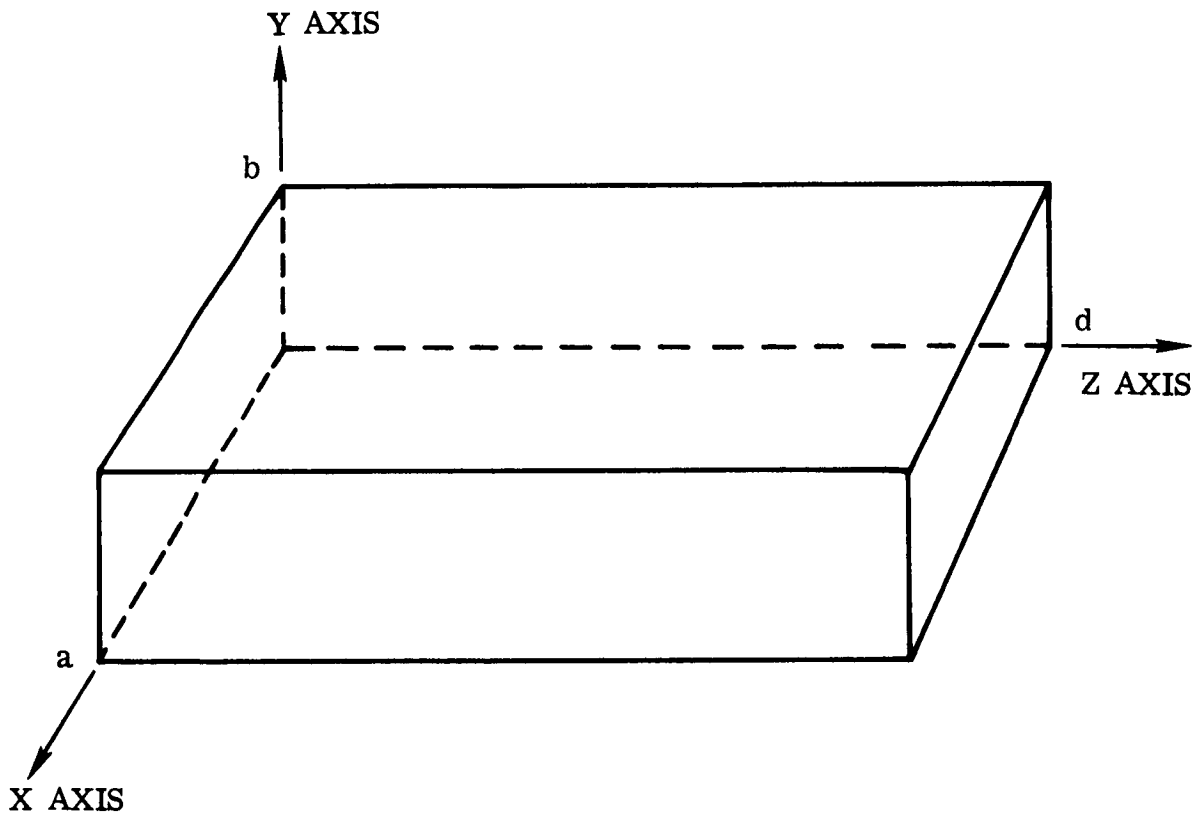

Figure C-1. Honeycomb Represented by a Rectangular Enclosure

and the characteristic frequencies (resonant frequencies) are

$$f = \frac{w}{2} = \frac{c}{2}\left[\left(\frac{m}{a}\right)^2 + \left(\frac{n}{b}\right)^2 + \left(\frac{\ell}{d}\right)^2\right]^{1/2}$$

This frequency equation indicates that there are three types of normal modes of vibration in the enclosure: (a) Axial modes (one-dimensional) in which the component waves travel parallel to an axis when either one of the three indices (m, n and ℓ) is an integer and the other are both zero. (b) Tangential modes (two-dimensional) in which the component waves are tangent to one pair of surfaces but are oblique to the other two pairs when either two of the three indices (m, n and ℓ) are integers and the remaining one is zero. (c) Oblique modes (three-dimensional) in which the component waves are oblique to all three pairs of the walls when all the three indices (m, n and ℓ) are integers.

A particular normal mode of vibration corresponding to any set of values of m, n and ℓ can be produced by starting a wave in the direction given by any combination of the direction cosines $\pm k_x/k$, $\pm k_y/k$ and $\pm k_z/k$ where $k_x k_y$ and k_z are component wavelength constant and $k = (k_x^2 + k_y^2 + k_z^2)^{1/2}$, and letting it be reflected from the various walls until it becomes a standing wave. However, if a wave starts out in a direction not satisfying the above conditions for its direction cosines and frequency, the reflected waves will interfere with each other in a nonperiodic manner and no regular pattern of standing waves will form.

In applying the characteristic frequencies equation to honeycomb cells, the hexagonal cross section is replaced by a square section whose side is assumed equal to the cell size. As an example, characteristic frequencies below 35 kilohertz for a 3/16-inch cell and 4-3/4 inches long are computed below:

m	n	ℓ	f, KHz	m	n	ℓ	f, KHz	m	n	ℓ	f, KHz
0	0	1	1.42	0	0	12	17.04	0	0	23	32.66
0	0	2	2.84	0	0	13	18.46	0	1	24	34.08
0	0	3	4.26	0	0	14	19.88	0	1	0	34.65
0	0	4	5.68	0	0	15	21.30	1	0	0	34.65
0	0	5	7.10	0	0	16	22.72	0	1	1	34.69
0	0	6	8.52	0	0	17	24.14	1	0	1	34.69
0	0	7	9.94	0	0	18	25.56	0	1	2	34.77
0	0	8	11.36	0	0	19	26.98	1	0	2	34.77
0	0	9	12.78	0	0	20	28.40	0	1	3	34.90
0	0	10	14.20	0	0	21	29.82	1	0	3	34.90
0	0	11	15.62	0	0	22	31.24				

If a single, rigid-walled cell of this size were acoustically excited, the normal modes of vibration having frequency below 34.5 kilohertz is seen to be axial and only along the length direction. If the frequency limit is raised to 35 kilohertz, not only other axial modes in the transverse direction but tangential modes of vibration were possible, when they were properly excited. The computation shows that in low frequency range only axial modes of vibration along the length direction can exist in the cells. This is because the cross-sectional dimensions of the cell are small compared to wavelength.

In the above discussion, the walls of the rectangular enclosure are assumed perfectly rigid. Since the walls are not perfectly rigid, the waves can be damped at the surfaces of the walls. An axial wave is damped by the wall surfaces perpendicular to its axis; a tangential wave which travels parallel to the surfaces of one pair of walls is damped by the remaining four walls. Finally, damping of an oblique wave can take place at all six walls. In theory, a damping term can be introduced into the undamped standing wave equation and it should be possible to apply the boundary conditions at the various wall surfaces to solve the damping problem. In practice, however, this problem becomes so involved that solution of a few special cases, such as axial waves, has been attempted.

Solution of a special case of waves traveling along x-axis and with rigid walls perpendicular to y and z axes (Ref. 2) reveals that if the normal specific acoustic impedance of the non-rigid wall perpendicular to the x-axis is such that the resistive component of the impedance is large with respect to both the reactance component and unity, the characteristic frequencies of the damped axial waves are identical with those of the corresponding undamped waves. However, the characteristic frequencies will differ if the resistive component is not large. The presence of flaws in the walls may also change the characteristic frequencies due to possible change of acoustic impedance.. Since it is difficult to compute the characteristic frequency shift due to either presence of flaws or damping, the computed values based on rigid walls will be used in discussion.

Assume the x, y and z coordinate system of a rectangular enclosure. If it is desired to know whether flaws are present in the walls in xy plane (normal to z-axis) x-axial waves will be excited so that one-dimensional standing waves oscillating in x-axis can exist in the enclosure. Values of resonant frequencies can be estimated by applying the characteristic frequencies equation for rigid walls. Due to the change in acoustic impedance of the wall because of the presence of flaws, at the resonant frequencies there can be different indications (between flaw-free walls and defective walls) in the apparatus used for measuring and recording the response to impedance change. With like manner, flaws in the walls in xz plane and in yz plane can be detected by generating one-dimensional standing waves in y-axis and x-axis, respectively. If it is immaterial whether flaws are present in the

side walls in xz plane or yz plane, a tangential mode of vibration parallel to xy plane and oblique to the other two planes may be excited to produce two-dimensional standing waves for flaw detection.

Several limitations will rise when this technique of applying certain particular characteristic frequencies of an enclosure to detect flaws in the walls to a honeycomb composite panel. Though the honeycomb cells can be treated as separate enclosures, it can be difficult to generate certain desired standing waves due to vast difference in magnitudes between cross-sectional dimensions and length dimension. Furthermore, the wave of proper indices m, n and ℓ must propagate in a direction given by any combination of the direction cosines $\pm k_x/k$, $\pm k_y/k$ and $\pm k_z/k$ before thar particular normal mode of vibration can be produced. These conditions may not be easily satisfied when the face sheet vibrates by acoustic waves of nearly normal incidence from a transducer.

NATURAL FREQUENCY DETERMINATION FOR HONEYCOMB COMPOSITES

A classical analysis was made of the Saturn common bulkhead honeycomb to determine the natural frequency. This analysis considers properly and poorly bonded face sheet conditions with two facing sheet thicknesses. The following assumptions were made:

1. The hexagonal cross section of a cell may be replaced by a circular cross section.

2. The honeycomb core does not vibrate, only the face sheet vibrates.

3. The face sheet is well bonded to the core.

4. Vibration of that portion of the face sheet above a single cell is similar to vibration of a circular plate clamped at its boundaries.

The approximate solution by the Rayleigh-Ritz method of the lowest mode of vibration for a circular plate clamped at boundary is:

$$W = \frac{10.21}{r^2}\sqrt{\frac{gD}{\rho h}}$$

where:

W = angular vibration frequency, radians/sec

r = plate radius, in.

$g = 386 \text{ in/sec}^2$

ρ = density of plate material, lb/in^3

h = plate thickness, in

D = flexural rigidity $= \dfrac{E h^3}{12(1-\nu^2)}$

E = Young's modulus of plate material, lb/in^2

ν = Poisson's ratio of plate material

This equation can be reduced to:

$$W = \frac{10.21\, h}{r^2} \sqrt{\frac{386E}{12\rho(1-\nu^2)}}$$

The natural frequency $f = W/2\pi$

As an example, for the honeycomb similar to the test material:

cell size = 3/16 in., therefore $r = 3/32$ in.
aluminum facing sheet, $E = 10 \times 16^6$ psi, $\nu = 0.3$, $\rho = 0.097$ lbs/cu. in.

For $h = 0.032$ in $W = \dfrac{10.21 \times 0.032}{\left(\frac{3}{32}\right)^2} \sqrt{\dfrac{386 \times 10 \times 10^6}{12 \times 0.097(1-0.3^2)}} = 2.244 \times 10^6$ rad/sec

$$f = \frac{W}{2\pi} = \frac{2.244 \times 10^6}{2} = 3.57 \times 10^5 \text{ hertz}$$

For $h = 0.050$ in $W = \dfrac{10.21 \times 0.050}{\left(\frac{3}{32}\right)^2} \sqrt{\dfrac{386 \times 10 \times 10^6}{12 \times 0.097(1-0.3^2)}} = 3.505 \times 10^6$ rad/sec

$$f = \frac{W}{2\pi} = \frac{3.505 \times 10^6}{2\pi} = 5.58 \times 10^5 \text{ hertz}$$

However, if the face sheet is poorly bonded to the honeycomb core the portion of face sheet above a single cell would then vibrate like an unsupported circular plate. The lowest mode of vibration of such plate has two nodal diameters and the angular frequency vibration is:

$$W = \frac{5.25}{r^2} \cdot \sqrt{\frac{gD}{\rho h}}$$

$$= \frac{5.25h}{r^2} \cdot \sqrt{\frac{386\ E}{12\rho(1-\nu^2)}}$$

For $h = 0.032$ in $W = \frac{5.25 \times 0.032}{(3/32)^2} \sqrt{\frac{386 \times 10^7}{12 \times 0.097(1-0.3^2)}} = 1.152 \times 10^6$ rad/sec

$$f = \frac{W}{2\pi} = \frac{1.152 \times 10^6}{2\pi} = 1.83 \times 10^5 \text{ hertz}$$

for $h = 0.050$ in $W = \frac{5.25 \times 0.050}{(3/32)^2} \sqrt{\frac{386 \times 10^7}{12 \times 0.97(1-0.3^2)}} = 1.80 \times 10^6$ rad/sec.

$$f = \frac{W}{2\pi} = \frac{1.80 \times 10^6}{2} = 2.87 \times 10^5 \text{ hertz}$$

REFERENCES

1. G. W. Swenson, Principles of Modern Acoustics, D. Van Nostrand Co., New York, 1953. (Figure 1)

2. L. E. Kinsler and A. R. Frey, Fundamentals of Acoustics, John Wiley & Sons, Inc., New York, 1962.

APPENDIX D

RELAXATION MECHANISM HYPOTHESIS AND ANALYSIS FOR BOND STRENGTH DETERMINATION

CONTRACT NAS 8-11733

Appendix D

RELAXATION MECHANISM HYPOTHESIS AND ANALYSIS FOR BOND STRENGTH DETERMINATION

To illustrate the damping mechanism as applied to the Saturn composites by analytical techniques, let us consider that the amplitude of response $u(x, y, t)$ of the unbonded sheet is described by the equation

$$\rho \frac{\partial^2 u}{\partial t^2} + k \left(\frac{\partial^2 u}{\partial x^2} + \frac{\partial^2 u}{\partial y^2} \right) = F(x, y, t)$$

where ρ is the mass per unit area of sheet, k measures the elastic restoring force of the sheet, and F is the driving force. The solution to this equation for arbitrary F can be written in terms of the Green's function G_O as

$$u(x, y, t) = \int dx' \int dy' \int_{-\infty}^{t} dt' \, G_O (x-x', y-y', t-t') \, F(x', y', t')$$

The Fourier transform of this equation yields for the frequency response of the unbonded sheet to a driver at the origin:

$$\hat{u} (O, O, \omega) = \hat{G}_O (O, O, \omega) \, \hat{F} (\omega)$$

The presence of bonds to the honeycomb will alter the quation for u by the addition of restoring forces along the lines of bonding, e.g.:

$$\rho \frac{\partial^2 u}{\partial y^2} + k \left(\frac{\partial^2 u}{\partial y^2} + \frac{\partial^2 u}{\partial y^2} \right) + \sum_i k_1 (x, y_i) \, \delta (y-y_i) \, u (x, y_i)$$

$$+ \sum_i k_2 (x_j, y) \, \delta (x-x_j) \, u (x_j, y) = F (x, y, t)$$

Here $\delta (x)$ is the Dirac delta-function and $x = x_i$ and $y = y_j$ define the lines of bonding. Damping has been ignored in the interest of simpliticy. The

Green's function G for the bonded sheet can now be written in terms of G_O in the form

$$G(x,y,t) = G_O(x,y,t) - \sum_i \int dx' k_1(x', y_i)\, G_O(x-x',\ y-y_i, t)\, G(x', y_i, t)$$

$$- \sum_j dy' k_2(x_j, y')\, G_O(x-x_j, y-y', t)\, G(x_j, y', t)$$

This equation can be solved numerically for G, and the frequency response of the bonded sheet can then be found by Fourier analyzing G.

As a check on the methods, the above procedure has been carried out analytically for the one-dimensional analog (a string with many springs attached) and results have been obtained for the frequency response.